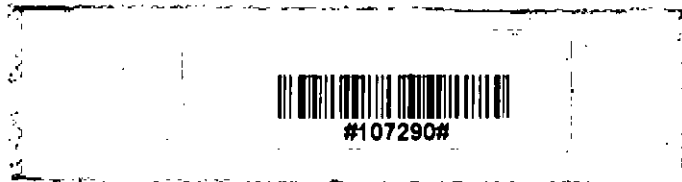
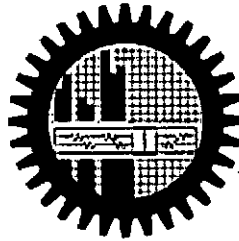
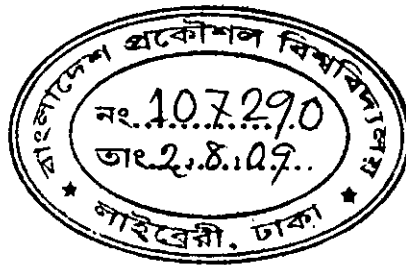


**ELASTIC PROPERTIES OF CARBON NANOTUBE BUNDLE  
BASED POLYMER COMPOSITE**

**Shahla Chowdhury**



**MASTER OF SCIENCE IN MECHANICAL ENGINEERING**

Department of Mechanical Engineering

**BANGLADESH UNIVERSITY OF ENGINEERING AND TECHNOLOGY**

Dhaka – 1000, Bangladesh

July 2009

**ELASTIC PROPERTIES OF CARBON NANOTUBE BUNDLE  
BASED POLYMER COMPOSITE**

A thesis submitted to the Department of Mechanical Engineering  
Bangladesh University of Engineering and Technology (BUET)

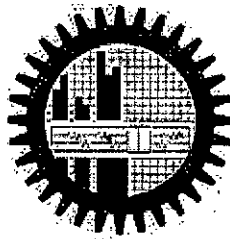
In partial fulfillment for the requirement of the degree of  
Master of Science in Mechanical Engineering

Submitted by

**Shahla Chowdhury**

Roll No: 100710061 P

Session: October 2007



**BANGLADESH UNIVERSITY OF ENGINEERING AND TECHNOLOGY**

Dhaka – 1000, Bangladesh

July 2009

The thesis titled “Elastic Properties of Carbon Nanotube Bundle Based Polymer Composite”, submitted by **Shahla Chowdhury**, Roll No: 100710061 P, Session: October 2007 has been accepted as satisfactory in partial fulfillment of the requirement for the degree of MASTER OF SCIENCE IN MECHANICAL ENGINEERING on July 26, 2009.

### BOARD OF EXAMINERS



**Dr. Sanjib Chandra Chowdhury**  
Assistant Professor  
Department of Mechanical Engineering  
BUET, Dhaka, Bangladesh

Chairman



**Dr. Abu Rayhan Md. Ali**  
Professor  
Department of Mechanical Engineering  
BUET, Dhaka, Bangladesh

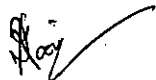
Member  
(Ex-officio)



**Dr. Sheikh Reaz Ahmed**  
Professor  
Department of Mechanical Engineering  
BUET, Dhaka, Bangladesh

Member

Member  
(External)



**Dr. Syed Md. Ihsanul Karim**  
Additional Director  
BITAC  
Tejgaon Industrial Area, Dhaka, Bangladesh

## **Declaration**

It is hereby declared that the thesis titled “**Elastic Properties of Carbon Nanotube Bundle Based Polymer Composite**” is author’s original work and has not been submitted for the award of any other degree or diploma.



---

Author

**Shahla Chowdhury**

## **DEDICATIONS**

**This work is dedicated to my beloved parents**

**Mrs. Jannatun Nayeem**

**&**

**Md. Khorshed Alam Chowdhury**

## **ACKNOWLEDGEMENT**

The author would like to take the opportunity of expressing her heartiest gratitude to her thesis supervisor Dr. Sanjib Chandra Chowdhury, Assistant Professor, Department of Mechanical Engineering, Bangladesh University of Engineering and Technology (BUET), Dhaka, Bangladesh, for his cordial support and advice. His advice helped the author at every step of this work. Without his proper supervision this report could not be finished.

The author is grateful to Dr. Abu Rayhan Md. Ali, Professor, Department of Mechanical Engineering, Bangladesh University of Engineering and Technology (BUET), Dhaka, Bangladesh, for his valuable support from time to time.

The author expresses indebtedness to Dr. Sheikh Reaz Ahmed, Professor, Department of Mechanical Engineering, Bangladesh University of Engineering and Technology (BUET), Dhaka, Bangladesh, for his important suggestions.

The author also expresses gratitude to Dr. Syed Md. Ihsanul Karim, Additional Director, BITAC, Tejgaon Industrial Area, Dhaka, Bangladesh, for his co-operations.

Finally the author thanks his colleagues, family members, friends and other relatives who supported a lot for completion of this thesis work.

# CONTENTS

---

	Page No.
Title Page	i
Board of Examiners	ii
Declaration	iii
Dedication	iv
Acknowledgement	v
Contents	vi
Abstract	ix
List of Figures	x
List of Tables	xvi

## Chapter 01

### INTRODUCTION

1.1	Introduction	1
1.2	Carbon Nanotube Structure	2
1.2.1	Single-Walled Nanotube (SWNT)	2
1.2.2	Multi-Walled Nanotube (MWNT)	7
1.2.3	CNT Bundle	8
1.3	Properties of Carbon Nanotube	10
1.4	Layout of the Thesis	11

## Chapter 02

### LITERATURE REVIEWS

2.1	Introduction	12
2.2	Literature Review	12
2.3	Motivation of the Present Work	16
2.4	Objectives	16

## Chapter 03

## FINITE ELEMENT MODELLING

3.1	Introduction	18
3.2	Finite Element Method	18
3.2.1	Finite Element Used in the Analysis	19
3.3	Representative Volume Element (RVE)	22
3.3.1	RVE for Long CNT Based Composite	25
3.3.2	RVE for Long CNT Bundle Based Composite	26
3.3.3	RVE for Short CNT Based Composite	26
3.3.4	RVE for Short CNT Bundle Based Composite	28
3.4	Elastic Properties Evaluation	29
3.4.1	RVE under Axial Loading	29
3.4.2	RVE under Lateral Loading	31
3.4.3	Volume Fraction of CNT in CNT-Matrix Composite	32
3.5	Equivalent Single Solid Fiber	33
3.6	Interface Properties	35
3.6.1	Interface with Van Der Waals Interaction	36
3.6.2	Interface with Cross-Link	37

## Chapter 04

## RESULTS AND DISCUSSION

4.1	Introduction	38
4.2	Interface Stiffness/ Young's Modulus	39
4.2.1	Interface Strength between CNT-CNT	39
4.2.2	Interface Strength between CNT- Matrix	41
4.3	Validation of Finite Element Model	42



4.3.1	Validation for Single CNT Based Composite	42
4.3.2	Validation for CNT Bundle Based Composite	43
4.4	Results and Discussion	44
4.4.1	Effect of CNT Diameter on Composite Elastic Properties	45
4.4.2	Effect of CNT Length on Composite Elastic Properties	58
4.4.3	Effect of Cross-Link Between CNT-CNT in the Bundle	63
4.4.4	Effect of Cross-Link Between CNT-Matrix	65
4.5	Equivalent Single Solid Fiber as a Substitute of CNT Bundle	67
<b>Chapter 05</b>	<b>CONCLUSIONS AND RECOMMENDATIONS</b>	
5.1	Introduction	74
5.2	Conclusion	74
5.3	Recommendation	76
<b>REFERENCES</b>		<b>77</b>
<b>APPENDIX</b>		<b>81</b>

## ABSTRACT

Carbon nanotubes (CNTs) demonstrate unusually high stiffness, strength and resilience, and may become an ideal reinforcing material for nano-composites. CNTs have a propensity to aggregate to bundle or wrap together due to high surface energy and surface area. Therefore, manipulating single CNT or dispersing bundle CNTs is very difficult, and this is the bottleneck for their potential commercial applications. Evaluating the effective material properties of such CNT bundle based polymer composite is very important at present. In the present research work, a suitable finite element model is developed to investigate the effects of bundle diameter, bundle length and interfacial bonding (i.e. cross-link) between the CNT-CNT and CNT-matrix on the elastic properties of CNT bundle based polymer composites, using representative volume elements. CNT bundle consisted of four single walled nanotubes is considered here. Diameter of the CNT bundle is varied by varying the diameter of the constituent CNTs of the bundle. Regarding the length of the CNT bundle, both short and long bundles are considered. Short bundle remains within the matrix (i.e. bundle length is smaller than the matrix length) whereas long bundle remains through the length of the matrix. Interface stiffness for the nonbonded van der Waals interaction is determined from the nonlinear cohesive law. The cross-links effect is incorporated in this research by introducing interface with different stiffness between the CNT-CNT within the bundle and between the CNT and the polymer matrix. For all cases, volume fraction of the CNTs is considered 5%. Then a suitable analytical formula is developed for calculating elastic properties of the equivalent solid fiber as a substitute of the CNT bundle. FEM software is used to determine the elastic properties of the CNT bundle based composites. FEM results of the composites considering the CNT bundle as it is and considering the CNT bundle as an equivalent solid fiber are compared. Present investigation demonstrates that the elastic properties of the CNT bundle based polymer composite are significantly affected by the morphology of the CNT bundle.

## LIST OF FIGURES

Figure 1.1	The unrolled honeycomb lattice of a carbon-nanotube	ix
Figure 1.2	SWCN structure and example of nanotubes.	5
Figure 1.3	All possible structures of SWNT	6
Figure 1.4	Multiwalled Carbon Nanotube (Approximate diagram)	7
Figure 1.5	Multiwalled Carbon Nanotube (by Atomic Force Microscope)	7
Figure 1.6	Typical nanotube bundle	8
Figure 1.7	CNT bundles after pullout from the composite	8
Figure 1.8	Nanotube bundle of (a) Three, (b) Four, (c) Seven, (e) Nineteen SWNTs	9
Figure 3.1	The tetrahedral SOLID92 Geometry having 10 nodes (I, J, K....P).	19
Figure 3.2	(a) CNT based composite and (b) its square RVE	23
Figure 3.3	(a) CNT-bundle based composite, (b) a segment of it, (c) its square RVE	24
Figure 3.4	RVE for long CNT based composite	25
Figure 3.5	RVE for long CNT bundle based composite	26
Figure 3.6	RVE for short CNT composite, (a) total view, (b) half sectional view	27
Figure 3.7	Wire frame view of the RVE for short CNT bundle based composite	28

Figure 3.8	Cross sectional view of the RVE for short CNT bundle based composite	28
Figure 3.9	RVEs under axial loading (a) long CNT composite (b) short CNT composite	30
Figure 3.10	RVE under lateral loading of, (a) long CNT composite, (b) short CNT composite	32
Figure 3.11	Cross section of the CNT bundle	34
Figure 3.12	A bridge involving carbon atoms formed through an interstitial carbon atom	37
Figure 3.13	Crosslink formed by chemical reaction between carboxyl functional groups attached to neighboring nanotubes.	37
Figure 4.1	Cohesive stress versus interface opening curve for CNT-CNT interface	40
Figure 4.2	Stiffness versus interface opening curve for CNT-CNT interface	40
Figure 4.3	Cohesive stress versus interface opening curve for CNT-polymer matrix interface	41
Figure 4.4	Stiffness versus interface opening curve for CNT-polymer matrix interface	42
Figure 4.5	$E_z/E_m$ versus CNT diameter for single CNT based composite	46
Figure 4.6	$E_x/E_m$ versus CNT diameter for single CNT based composite	46

Figure 4.7	Composite's Poisson's ratio versus CNT diameter for single CNT based composite	47
Figure 4.8	Plot of first principle stress (Z-axis) for long single CNT based composite (for, axial stretch, $\Delta L = 1$ nm)	47
Figure 4.9	Plot of second principle stress (X-axis) for long single CNT based composite (for lateral stretch $\Delta a = 0.3$ nm)	48
Figure 4.10	Plot of strain on Z-axis for long single CNT based composite (for, $\Delta L = 1$ nm)	48
Figure 4.11	Plot of strain on X-axis for long single CNT based composite (for, $\Delta L = 1$ nm)	49
Figure 4.12	Plot of first principle stress (Z-axis) for short single CNT based composite (for, $\Delta L = 1$ nm)	49
Figure 4.13	Plot of first principle stress on the cut-plane (for, $\Delta L = 1$ nm)	50
Figure 4.14	Plot of second principle stress (X-axis) for short single CNT based composite (for, $\Delta a = 0.3$ nm)	50
Figure 4.15	Plot of second principle stress on the cut-plane (for, $\Delta a = 0.3$ nm)	51
Figure 4.16	Plot of strain on Z-axis for short single CNT based composite (for, $\Delta L = 1$ nm)	51
Figure 4.17	Plot strain on X-axis for short single CNT based composite (for, $\Delta L = 1$ nm)	52
Figure 4.18	$E_z/E_m$ versus CNT diameter for CNT bundle composite	53
Figure 4.19	$E_x/E_m$ versus CNT diameter for CNT bundle composite	54

Figure 4.20	Composite's Poisson's ratio versus CNT diameter for CNT bundle composite	54
Figure 4.21	Long CNT bundle composite with cut-plane	55
Figure 4.22	Plot of first principle stress (Z-axis) for long CNT bundle composite (for axial stretch, $\Delta L = 1$ nm)	55
Figure 4.23	Plot of second principle stress (X-axis) for long CNT bundle composite (for lateral stretch, $\Delta a = 0.3$ nm)	56
Figure 4.24	Short CNT bundle composite with cut-plane	56
Figure 4.25	Total strain intensity for short CNT bundle composite (for, $\Delta L = 1$ nm)	57
Figure 4.26	Plot of first principle stress (Z-axis) for short CNT bundle composite (for, $\Delta L = 1$ nm)	57
Figure 4.27	Plot of second principle stress (X-axis) for short CNT bundle composite (for, $\Delta a = 1$ nm)	58
Figure 4.28	$E_z/E_m$ versus CNT aspect ratio ( $L_c/D$ ) for single CNT based composite	59
Figure 4.29	$E_x/E_m$ versus CNT aspect ratio ( $L_c/D$ ) for single CNT based composite	59
Figure 4.30	Composite's Poisson's ratio versus CNT aspect ratio ( $L_c/D$ ) for single CNT based composite	60
Figure 4.31	$E_z/E_m$ versus CNT aspect ratio ( $L_c/D$ ) for CNT bundle based composite	61

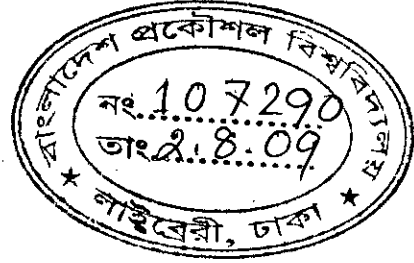
Figure 4.32	Ex/Em versus CNT aspect ratio ( $L_c/D$ ) for CNT bundle based composite	62
Figure 4.33	Composite's Poisson's ratio versus CNT aspect ratio ( $L_c/D$ ) for CNT bundle based composite	62
Figure 4.34	Ez/Em versus CNT radius for CNT bundle based composite	64
Figure 4.35	Ex/Em versus CNT radius for CNT bundle based composite	64
Figure 4.36	Composite's Poisson's ratio versus CNT radius for CNT bundle based composite	63
Figure 4.37	Ez/Em versus CNT radius for CNT bundle based composite	66
Figure 4.38	Ex/Em versus CNT radius for CNT bundle based composite	66
Figure 4.39	Composite's Poisson's ratio versus CNT radius for CNT bundle based composite	67
Figure 4.40	Young's modulus of the CNT bundle and equivalent solid fiber for different radii of them	68
Figure 4.41	Longitudinal Young's modulus ratio ( $E_z/E_m$ ) of the long CNT bundle composite and equivalent long solid fiber composite for different radii of CNT bundle/ equivalent solid fiber	69

Figure 4.42	Longitudinal Young's modulus ratio ( $E_z/E_m$ ) of the short CNT bundle composite and equivalent short solid fiber composite for different radii of CNT bundle/ equivalent solid fiber	69
Figure 4.43	Transverse Young's modulus ratio ( $E_z/E_m$ ) of the long CNT bundle composite and equivalent long solid fiber composite for different radii of CNT bundle/ equivalent solid fiber	70
Figure 4.42	Transverse Young's modulus ratio ( $E_z/E_m$ ) of the short CNT bundle composite and equivalent short solid fiber composite for different radii of CNT bundle/ equivalent solid fiber	70
Figure 4.43	Composite containing a single fiber having equivalent strength of CNT-bundle of four	71
Figure 4.44	Plot of first principal stress (Z-axis) for long equivalent solid-fiber composite	71
Figure 4.45	Plot of first principal stress on cut-plane for long fiber composite	72
Figure 4.46	The equivalent short solid-fiber composite under axial stretch of 1 nm (i.e. $\epsilon_z = 0.1$ )	72
Figure 4.47	Plot of first principal stress on the cut-plane for The equivalent short solid-fiber composite; [(a) The cross section is 15 nm apart from the origin, (b) The cross section is 24.5 nm apart from the origin]	73
Figure 4.48	Plot of second principal stress on the cut plane for equivalent solid-fiber composite	73



## LIST OF TABLES

Table 1.1	Parameters of Carbon Nanotube	3
Table 1.2	Types of Nanotube based on Chiral Indices	6
Table 3.1	Properties for interfaces between CNT-Polymer and CNT-CNT	36
Table 4.1	The radii of CNT for different CNT index	39
Table 4.2	Dimension and Properties of CNT and Matrix	43
Table 4.3	Dimension and Properties of CNT, Matrix and Interface	44
Table 4.4	Properties of CNT, Matrix and their Interfaces	45



## CHAPTER 01

---

---

# INTRODUCTION

## 1.1 INTRODUCTION

The discovery of carbon nanotubes (CNTs) can be traced back to the origin of fullerene chemistry (buckyball, C<sub>60</sub>) in 1985 [1]. Fullerenes have provided an exciting new insight into carbon nanostructures built from sp<sup>2</sup> carbon units based on geometric architectures. In 1991, Iijima [2] discovered carbon nanotubes CNTs that are elongated fullerenes where the walls of the tubes are hexagonal carbon and often capped at each end. Since then CNTs have grown from a material of dreams to a real world material that has already found its application fields. The production capability for CNTs is growing every year in an exponential degree. It is now being used in the fields of electronics, field emission devices, nano-electro-mechanical (NEMS) devices, sensors, medical appliances, nano robotics and of course in light weight structural composites. CNTs have physical characteristics of solids and are micro-crystals with high aspect ratios of 1000 or more, although their diameter is close to molecular dimensions [3]. The CNTs have unique mechanical, electrical, magnetic, optical and thermal properties. In some special applications, such as space explorations, high-performance lightweight structural materials are required, and they can be developed by adding CNTs to polymers or other matrix materials. Moreover, although graphite is a semi-metal, CNTs can be either metallic or semi-conducting due to the topological defects from the fullerene-like end caps in CNTs (pentagons in a hexagonal lattice). Thus, the physico-mechanical properties of CNTs are dependent upon their dimensions, helicity or chirality. The syntheses, structures, properties and applications of CNTs have been discussed in several books [3-4]. The superior properties of CNTs offer exciting opportunities for new composites. NASA has invested large sums of money to develop CNT-based composites for applications such as the Mars mission. Recently, polymer/CNT composites have attracted considerable attention owing to their unique mechanical, surface and multi-functional properties, and strong interactions with the matrix resulting from the nano-scale microstructure and extremely large interfacial area.

## 1.2 CARBON NANOTUBE STRUCTURE

Since the discovery of CNTs in 1991 [2], much research has been focused on their mechanical and electrical properties. A single-walled nanotube (SWNT) is a hollow structure formed by covalently bonded carbon atoms. It can be imagined as a rectangular graphene sheet rolled from one side of its longest edge to form a cylindrical tube. Hemispherical caps seal both ends of the tube. For multi-walled nanotubes (MWNT), a number of graphene layers are co-axially rolled together to form a cylindrical tube. The spacing between graphene layers is about 0.34 nm [3]. Another form of the CNTs is the bundled CNTs. During the production due to van der Waals (vdW) interaction the SWNTs agglomerate and form CNT bundles. Theoretically, the tensile modulus and strength of a graphene layer reach up to 1 TPa and 200 GPa, respectively [3]. These values have been widely used to interpret the mechanical properties of single-walled and multi-walled nanotubes.

### 1.2.1 Single-Walled Nanotube (SWNT)

SWNT can be of three types: zigzag, armchair and chiral. The size, mechanical strength, and electrical properties of nanotubes are highly dependent on their atomic architectures. Armchair nanotubes exhibit better ductility and electrical conductivity than zigzag nanotubes [2]. In recent years, CNTs have been utilized as nano-fillers to enhance the mechanical strength of polymeric matrices. An important increase of the tensile modulus and yield strength of polymers has been reported [5] after the random dispersion of SWNTs.

The direction along which the graphene sheet is rolled up to form the nanotube determines its chirality and also affects whether the nanotube is metallic or behaves like a semiconductor (Fig. 1.1 – 1.3). The ‘chiral vector’,  $C_h$  can be expressed as a linear combination of unit vectors in hexagonal lattice can be found from the following equation [6].

$$C_h = na_1 + ma_2 \quad (1.1)$$

Here  $n$  and  $m$  are integer numbers. The circumference,  $L$  of carbon nanotube is found from the following equation [6].

$$L = |C_h| = a\sqrt{n^2 + m^2 + mn} \quad (1.2)$$

The important parameters of CNT are given in the Table 1.1. After determining 'unit vectors' we can calculate  $C_h$  and  $L$ .

Table 1.1: Parameters of carbon nanotube

Symbol	Name	Formula	Value
$a_{c-c}$	Carbon-carbon distance	-	0.1421 (nm)
$a$	Length of unit vector	$\sqrt{3}a_{c-c}$	0.246 (nm)
$a_1$	Unit vector	$\left(\frac{\sqrt{3}}{2}, \frac{1}{2}\right)a$	In (x, y) coordinates
$a_2$	Unit vector	$\left(\frac{\sqrt{3}}{2}, -\frac{1}{2}\right)a$	In (x, y) coordinates

The angle between  $C_h$  and  $a_1$  is known as the chiral angle,  $\theta$  and can be calculated from the following equation [6].

$$\sin \theta = \frac{\sqrt{3}m}{2\sqrt{n^2 + m^2 + mn}} \quad (1.3)$$

The diameter of any nanotube can be calculated from the following equation [6].

$$d_t = \frac{L}{\pi} = \frac{\sqrt{n^2 + m^2 + mn}}{\pi} a \quad (1.4)$$

The variation of the chiral indices ( $m, n$ ) and chiral angle,  $\theta$ , occurs in different types of nanotubes. Table 1.2 summarizes three major categories of nanotube, which could be formed depending on chiral indices ( $m, n$ ). The diameter/radius of the CNT can be determined according to these chiral indices.

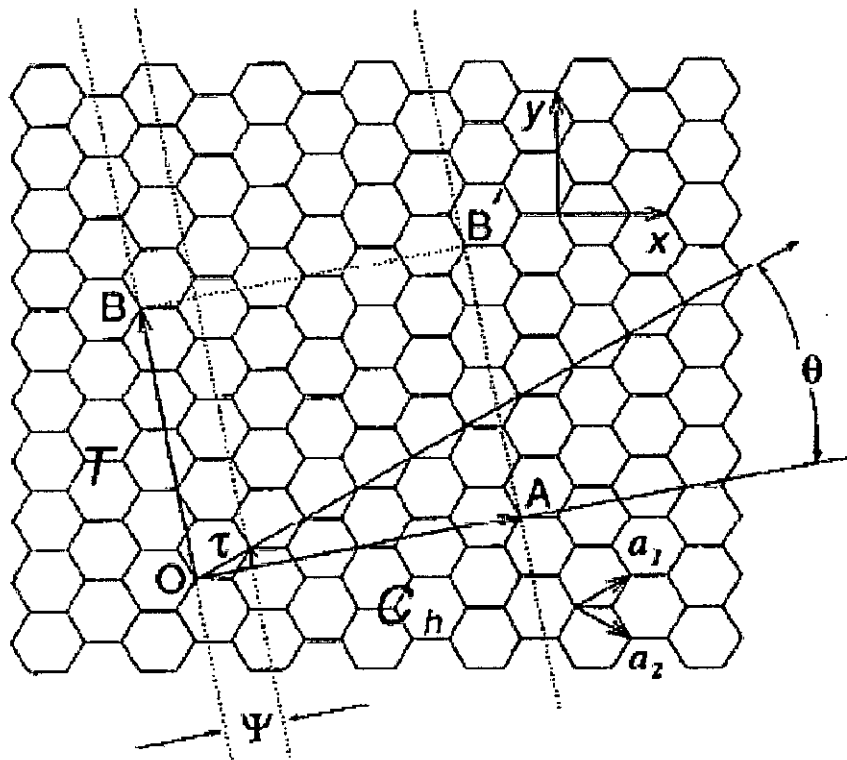
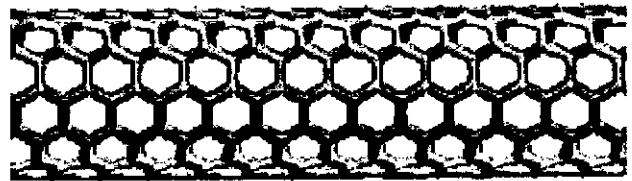
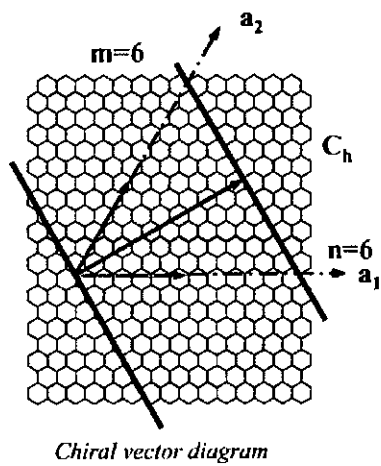
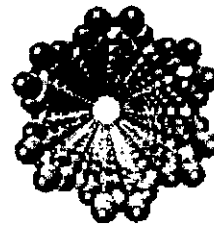


Fig. 1.1: The unrolled honeycomb lattice of a carbon-nanotube [6]

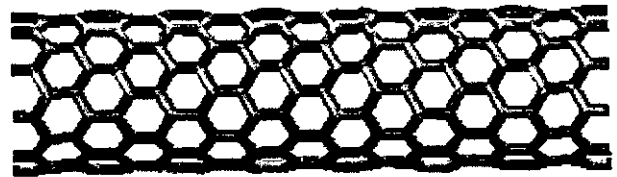
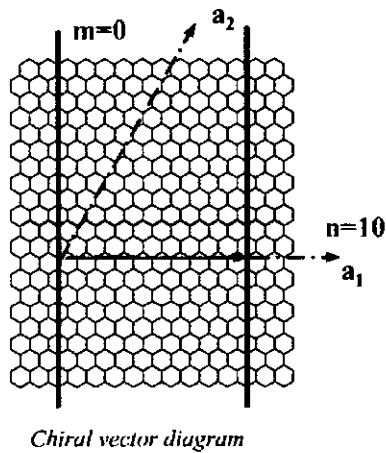


Side view

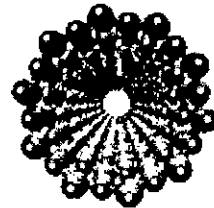


Front view

**a) Armchair nanotube (6,6)**

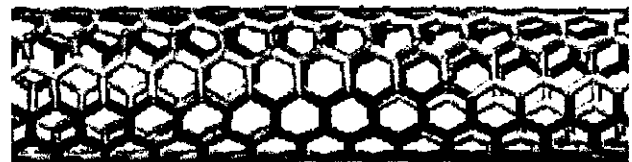
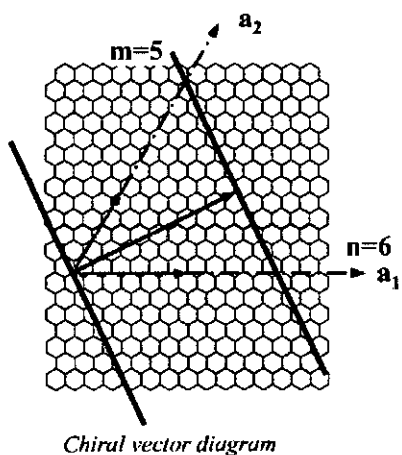


Side view



Front view

**b) Zig zag nanotube (10,0)**



Side view



Front view

**c) Chiral nanotube (6,5)**

Fig. 1.2: SWNT structure and example of nanotubes.

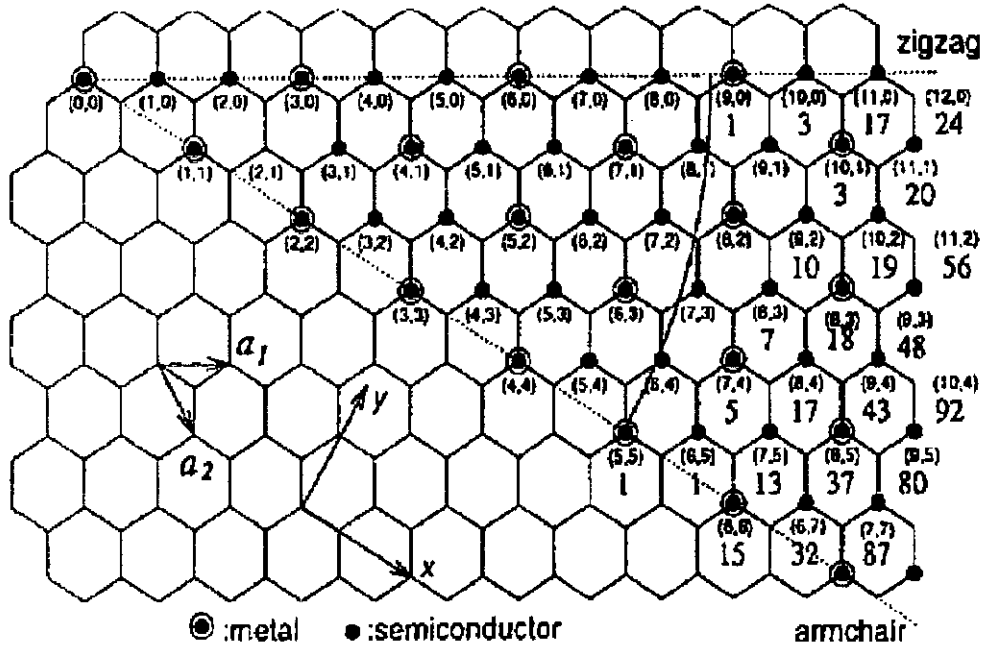


Fig. 1.3: All possible structures of SWNT [6]

Table 1.2: Types of nanotube based on chiral indices

Types of CNT	Chiral indices, (m, n)	Chiral angle, $\theta$	CNT diameter, $d_t$
Zigzag	(m, 0)	0	$\frac{a_o m}{\pi}$
Armchair	(m, m)	30°	$\frac{\sqrt{3}a_o m}{\pi}$
Chiral	(m, n); $m \neq n \neq 0$	$0 < \theta < 30^\circ$	$\frac{a_o \sqrt{m^2 + mn + n^2}}{\pi}$



### 1.2.2 Multi-Walled Nanotube (MWNT)

MWNT comprises of several layers of grapheme cylinders that are concentrically nested like rings of a tree trunk with an interlayer spacing of 0.34 nm). The diameter of MWNT can be up to several hundred nanometers. In MWNT a number of concentric SWNTs are held together (Fig. 1.4- 1.5) with relatively weak vdW forces. For MWNT, the individual graphene cylinders tend to slide with respect to each other. This characteristic of the MWNT lowers the stiffness.

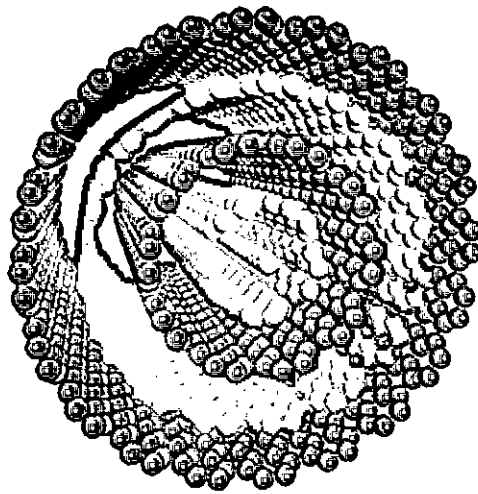


Fig. 1.4: Multiwalled Carbon Nanotube

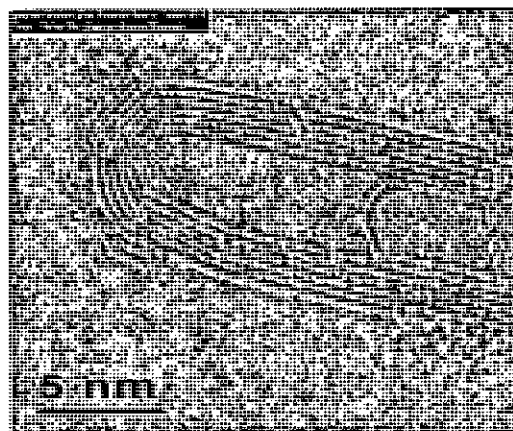


Fig. 1.5: Multiwalled Carbon Nanotube (by Atomic Force Microscope) [7]

### 1.2.3 CNT BUNDLE

During the production, CNTs form crystalline bundles (Fig. 1.6). And they can remain in this bundle form in the composite (Fig. 1.7). Owing to the weak vdW interaction that holds them together in the bundle, the tubes can easily slide on each other, resulting in a shear modulus comparable to that of graphite. This low shear modulus is also a major obstacle in the fabrication of macroscopic fibers composed of CNTs. However this obstacle can be overcome by making cross-links between the CNT-CNT within the bundle. CNT bundle can be made of different numbers of CNTs. CNT bundles of three, four, seven and nineteen SWNTs are shown in Fig. 1.8.

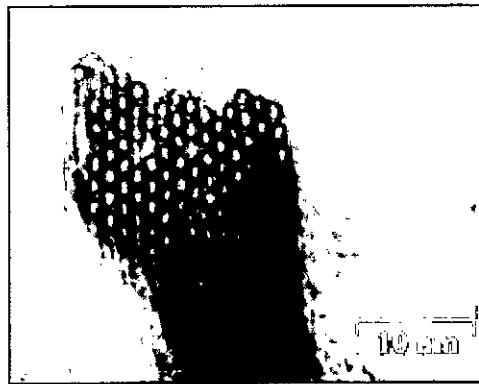


Fig. 1.6: Typical nanotube bundle [7]

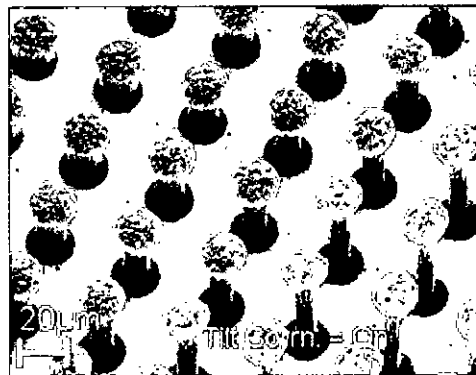


Fig. 1.7: CNT bundles after pullout from the composite [7]

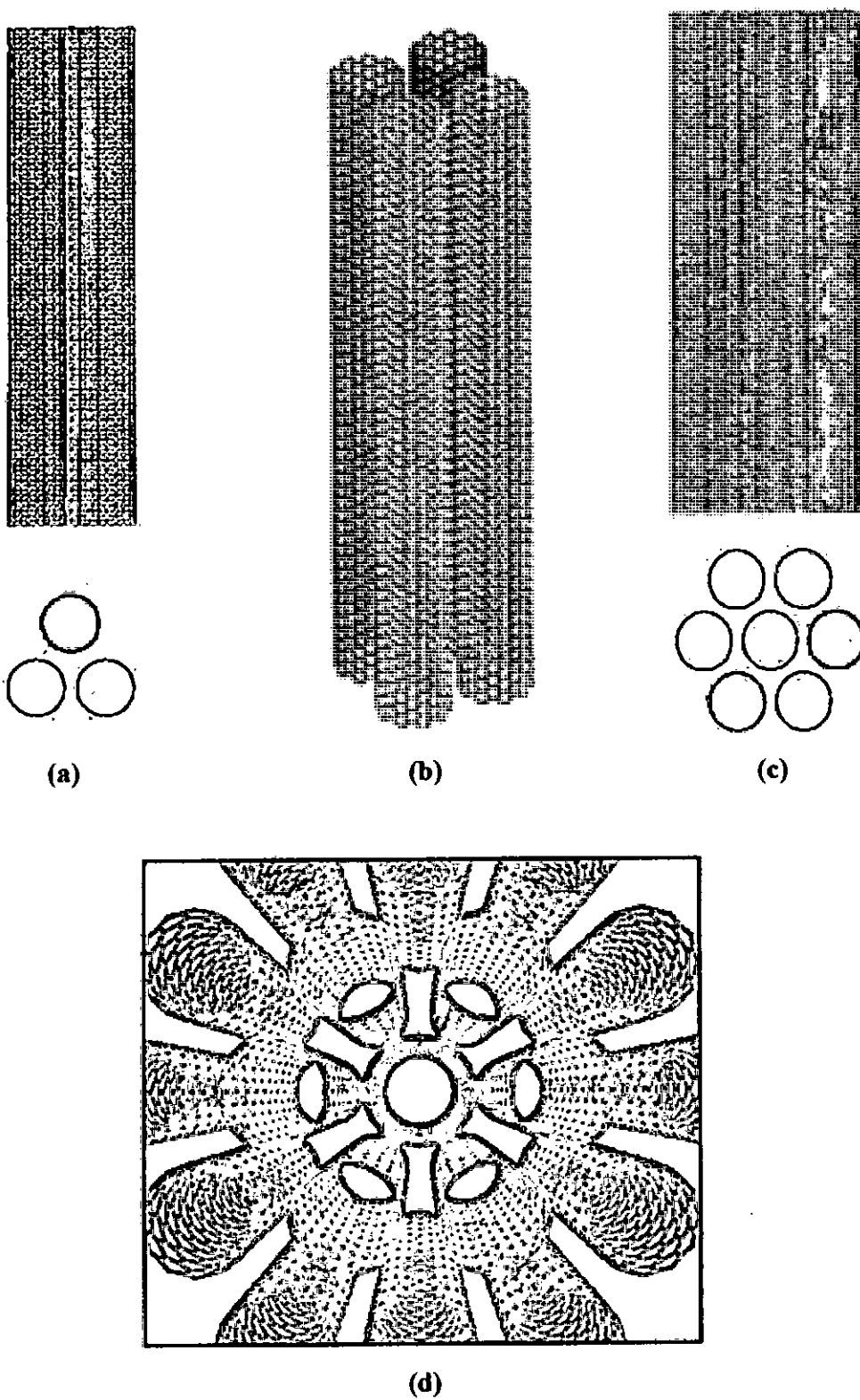


Fig. 1.8: Nanotube bundle of (a) Three, (b) Four, (c) Seven, (e) Nineteen SWNTs.

### 1.3 PROPERTIES OF CARBON NANOTUBE

CNTs have remarkable mechanical, thermal and electrical properties. The properties of CNTs depend on atomic arrangement (how the sheets of graphite are rolled), the diameter and length of the tubes and morphology of nanostructure. Mechanically, they are the stiffest known materials along with a predicted strength of about 100 times that of steel at only one-sixth of the weight. Recent theoretical calculations and direct experimental measurements showed that the elastic modulus of a SWNT is in the range of 1-5 TPa [8, 9], which is significantly higher than the elastic modulus of a carbon fiber (0.1-0.8 TPa) [10]. It has a breaking strength of about 37 GPa [11].

The MWNT are reported to have lower mechanical performance than the SWNTs [3]. Owing to the weak vdW interaction that holds the individual CNTs together in the MWNT, the tubes can easily slide on each other, resulting in a low shear modulus. Again the CNT bundle also possesses lower stiffness than SWNT. These different geometry definitions have led to reported axial moduli ranging from 1.25 TPa [12] for SWNT to 67 GPa [13] in CNT arrays.

With regards to their thermal properties, CNTs are thermally stable up to 2800 °C (in vacuum), exhibit a thermal conductivity about twice as high as diamond [14], and may exhibit a capacity to carry electric current a thousand times better than copper wires [15].

Furthermore, the chirality of the CNT has significant implications on the material properties. In particular tube chirality is known to have a strong impact on the electronic properties of CNT. CNTs can behave either as a metal or semiconductor depending on the arrangement of the carbon atoms [16]. In addition to their elastic and thermal properties, the bending of some CNTs has been found to be fully reversible.

#### **1.4 LAYOUT OF THE THEIS**

For convenience of presentation, the contents of this thesis are divided into five chapters. Chapter-1 contains the brief discussion about CNTs along with its typical types: SWNT, MWNT and CNT bundle. Chapter-2 contains brief discussion on the available literature related to the present investigation, justification and objectives of this research. Chapter-3 contains a concise discussion on finite element method and representative volume element used in the present work. Chapter-4 contains results and discussion of present investigation. Conclusion and recommendation are presented in Chapter-5.

## **CHAPTER 02**

---

---

# **LITERATURE REVIEWS**

## **2.1 INTRODUCTION**

Carbon nanotubes (CNTs) have exceptional mechanical properties [17–23]. However, the nanotube dimensions of the order of a few nanometers in diameter and a few hundreds of microns in length have put huge unsolved challenges before researchers. Perhaps, the most common challenging aspect is the CNT dispersion into the polymer matrix since CNTs tend to agglomerate because of van der Waals (vdW) forces. Most experimental investigations of CNT/polymer composites involve CNT bundles or ropes instead of individual nanotubes because of vdW interactions between tubes.

## **2.2 LITERATURE REVIEW**

Future nanostructured composite materials are expected to incorporate CNT reinforcement either dispersed individually or as nanofilamentary bundles or ropes yielding unprecedented mechanical properties. Many believe that CNTs may provide the ultimate reinforcing materials for the development of a new class of nanocomposites [24]. The elastic properties and load carrying capacities of CNTs in nanocomposites have been demonstrated in several research works. Some of these investigations show that the load-carrying capacity of CNTs in a matrix as well as the improvement of the elastic properties of the composites is significant and the CNT-based composites have the potential to provide extremely strong and ultralight new materials.

Qian et al. [25] have reported that adding 1% of nanotubes to polystyrene matrix increases the overall tensile modulus (strength) by 42% (25%), indicating significant load transfer across the CNT-matrix interface. They have also observed via transmission-electron-microscope (TEM) graphs that the nanotubes were able to bridge the cracked surface of the composite once a crack was initiated. The crack was nucleated at an area of low nanotube density and propagated towards a region with relatively low nanotube density. Pull-out of the nanotubes was observed at a relatively large crack-opening displacement. Wagner et al. [26] have reported single nanotube fragmentation, under

tensile stress, using nanotube-containing thin polymeric films. They have found that the interfacial shear strength (ISS) between the nanotubes and polymer could reach as high as 500 MPa, which is at least one order of magnitude higher than that of conventional fiber-based composites. Cooper et al. [27] have experimentally investigated the adhesion of CNTs to a polymer matrix. CNTs bridging across holes in an epoxy matrix were drawn out using the tip of a scanning-probe microscope while recording the forces involved. Based on the experiment, an approximate calculation of the ISS of the CNT-polymer composite was performed. Their ISS values for MWNTs vary from 76-416 MPa for different interfacial area indicating that ISS of the CNT-polymer could be significantly higher than that of a conventional fiber-polymer interface. In another study, Barber et al. [28] have conducted a similar pull-out test of nanotubes from a polymer and calculated the interface fracture energy from the measured pull-out force and embedded length. They have concluded that for smaller diameter nanotubes there exists a strong interface. This strong interface with high ISS indicates that more loads will be transferred from the matrix to the nanotubes through the interface and as a result reinforcement will be better.

All of the above experimental observations indicate that the CNT-polymer interfacial strength is high and significant load transfer occurs through the interface. However, some experimental observations indicate poor load transfer through a CNT-polymer interface. Schadler et al. [29] have studied MWNT with epoxy polymer in both tension and compression. They observed a  $6 \text{ cm}^{-1}$  shift in compression and no shift in tension, implying that in tension load transfer to the MWNTs is negligible. This is attributed to two factors, the sliding of inner tubes within the outer tubes that prevents the load from being effectively transferred to all MWNT layers and the extremely low interfacial shear stress between the tubes and the matrix arising from poor interfacial bonding. Barber et al. [30] have conducted MWNT pull-out from a polymer matrix using atomic force microscope. They have conducted several pull-out tests and calculated average ISS from the slope of the linear fit of the forces and corresponding interfacial areas data. They have found separation stress of 47 MPa indicating that CNTs do not significantly reinforce the polymer.



The molecular dynamics (MD) approach has provided abundant simulation results for evaluating the mechanical properties of the CNT based polymer composites [31-33.]. However, MD simulations are limited to very small length and time scales and cannot deal with the larger length scales in studying nanocomposites. Nanocomposites for engineering applications must expand from nano to micro, and eventually to macrolength scales. Therefore, continuum mechanics models can be applied initially for simulating the mechanical responses of the CNTs in a matrix for studying the overall responses of CNT composites, before efficient large multiscale models are established.

Odegard et al. [34] used an equivalent continuum modeling method to model the nanotube, the local polymer near the nanotube and polymer/nanotube interaction. A suitable representative volume element (RVE) was chosen for the model. Molecular dynamics (MD) was used to simulate the interaction between the polymer (LaRC-SI) and a (6,6) single-walled carbon nanotube. In this work, the atomic lattice has been viewed as discrete masses assembled together with atomic forces that resemble elastic springs. The mechanical analogy of this model was a pin-jointed truss model in which each truss represents either a bonded or nonbonded atomic interaction. Next, the total strain energy of both truss model and the continuum model put equal under identical loading conditions. By applying proper loading conditions, it was possible to calculate all elastic constants (five sets of boundary conditions to determine five stiffness constants). Finally, traditional micromechanics models were utilized to determine the elastic properties of a polymer film reinforced by these fibers. Berhan et al. [35] presented a model to predict the upperbound moduli of “bucky paper” or nanotube sheet containing nanotube ropes with an emphasis on the effect of joint morphology. They obtained a sheet Young’s modulus ranging from 1% to 10% of the rope Young’s modulus depending on the area fraction of the nanotube while their experimental results are fairly below these range (around 0.2% of the rope Young’s modulus).

Chen et al. [36] has proposed a 3-D continuum elasticity models for modeling the CNTs embedded in a matrix, in order to ensure the accuracy and compatibility between the models for the CNTs and matrix. There is a method based on the elasticity theory for

evaluating effective material properties of CNT-based composites using the RVE is established and cylindrical RVE are investigated. Formulas to extract the effective material properties from numerical solutions for the cylindrical RVEs under three loading cases are derived. Analytical results (extended rule of mixtures) based on the strength of materials theory to estimate the effective Young's modulus in the axial direction, which can help validate the numerical solutions, are also derived for both long and short CNT cases in. Numerical results using the finite element method (FEM) for the cylindrical RVEs show significant increases of the stiffness in the CNT direction of the nanocomposites under various combinations of the CNT and matrix material properties. However, although cylindrical RVEs are easy to use, for which analytical solutions can be derived and efficient 2-D axisymmetric FEM models can be applied, they are the most primitive models and can lead to errors due to ignoring materials not covered by the cylindrical cells.

In the production processes, it is difficult to get isolated CNT. CNTs have a propensity to aggregate to bundle or wrap together due to high surface energy and surface area and they are used in composite in this bundled form. Compared to the researches done on isolated CNT based composites, there are not much works on CNT bundle based composites. However, there are few studies regarding the mechanical characterization of the CNT bundle based polymer composites.

Lourie et al. [37] have studied nanotube-polymer systems using TEM. Well-aligned bundles of SWNTs under tensile stress were observed to fracture in real time by TEM. The expansion of elliptical holes in the polymer matrix results in a tensile force in bridging nanotubes. The polymer matrix at both ends of the bundles deforms extensively under the tension force. The nanotubes fracture in tension within the polymer-hole region rather than in shear within the gripping region at the ends of the bundles. Direct observation of nanotube fracture in such a tensile test implies that stress is transferred from the surrounding matrix to the nanotubes through the nanotube-polymer interface, which is quite strong. Ajayan et al. [38] have also experimentally investigated the mechanical properties of CNT bundle based composite and they have reported that

slipping of the tubes in the nanotube bundle limits load transfer from the polymer to the nanotubes. Ashrafi et al. [39] have investigated the elastic properties of twisted arrays of CNT based polymer composites using FEM. The elastic properties of the polymer composites reinforced by twisted CNT array are also determined by using traditional micromechanics at low concentrations of CNT, and the effects of different parameters such as the degree of the alignment, the twist angle and the volume fraction of the CNT on the polymer composite are examined.

### **2.3 MOTIVATION OF THE PRESENT WORK**

From the above literature review it is seen that there are contradictory results regarding the reinforcement of the polymer matrix with the incorporation of CNTs. Moreover, in the literature on the CNTs based polymer composites, there is also a wide variation in the reported elastic properties [40]. Reported improvements in the elastic moduli are lower than the expected if the CNTs are assumed to act as reinforcing elements with an elastic modulus of 1 TPa. Discrepancies in the reported elastic moduli as well as in the strength of the CNT based polymer composites may be due to the insufficient load transfer through the interface between the CNT and the polymer matrix of the composites. Load transfer through the interface is affected by several factors. One of the vital factors is the morphology of the CNT bundle (i.e., agglomerated CNTs). Therefore it is necessary to investigate the effect of the morphology of the CNT bundle on the mechanical behavior of the CNT bundle based composites to fully realize the potentials of the CNT-based composites in real engineering applications

### **2.4 OBJECTIVES**

The main objective of this research work is to evaluate elastic properties of CNT bundle based polymer composite. In doing so, several investigations are done. They are as follow:

- (a) To develop a suitable FEM model for CNT bundle reinforced polymer composite.
- (b) To investigate the effect of bundle diameter on the elastic properties of the CNT bundle reinforced polymer composite using FEM.
- (c) To investigate the effect of bundle length on the elastic properties of the CNT bundle reinforced polymer composite using FEM.
- (d) To investigate the effect of cross-link between CNT-CNT (within the bundle) and between the CNT-matrix on the elastic properties of the CNT bundle reinforced polymer composite using FEM.
- (e) To develop approximate analytical formula to get an equivalent single solid fiber, which can replace the CNT bundle. Then compare the elastic properties of the equivalent solid fiber composite with the CNT bundle based composite.

## **CHAPTER 03**

---

---

# **FINITE ELEMENT MODELLING**

### **3.1 INTRODUCTION**

In this chapter detail of finite element method (FEM) and representative volume element (RVE) are discussed. The square RVE used in this research is discussed in brief. Also the fundamental equations and analytical formulas of the current research work are given.

### **3.2 FINITE ELEMENT METHOD**

In the field of engineering design we come across many complex problems, the mathematical formulation of which is tedious and usually not possible by analytical methods. At such instants we resort to the use of numerical techniques. Here lies the importance of FEM, which is a very powerful tool for getting the numerical solution of a wide range of engineering problems. The basic concept is that a body or structure may be divided into smaller elements of finite dimensions called as “finite elements”. The original body or structure is then considered as an assemblage of these elements connected at a finite number of joints called as “nodes” or “nodal points”. The properties of the elements are formulated and combined to obtain the properties of the entire body.

The equations of equilibrium for the entire structure or body are then obtained by combining the equilibrium equation of each element such that the continuity is ensured at each node. The necessary boundary conditions are then imposed and the equations of equilibrium are solved to obtain the required variables such as stress, strain, temperature distribution or velocity flow depending on the application.

Thus instead of solving the problem for the entire structure or body in one operation, in the method attention is mainly devoted to the formulation of properties of the constituent elements. A common procedure is adopted for

combining the elements, solution of equations and evaluation of the required variables in all fields. Thus the modular structure of the method is well exploited in various disciplines of engineering.

### 3.2.1 Finite Element Used in the Analysis

In the analysis of finite element in this research the Solid 92 type of element is used. It is a tetrahedral three-dimensional element which consists of 10 nodes in each volume element. The geometry, node locations, and the coordinate system for this element are shown in Fig. 3.1 "SOLID92 Geometry". Beside the nodes, the element input data includes the orthotropic material properties. Orthotropic material directions correspond to the element coordinate directions. Element Loadings are defined to be of two types: nodal and element. Nodal loads are defined at the nodes and are not directly related to the elements. These nodal loads are associated with the degrees of freedom at the node. Element loads are surface loads, body loads, and inertia loads. Element loads are always associated with a particular element (even if the input is at the nodes). Pressures may be input as surface loads on the element faces as shown by the circled numbers on Fig. 3.1 "SOLID92 Geometry". Positive pressures act into the element.

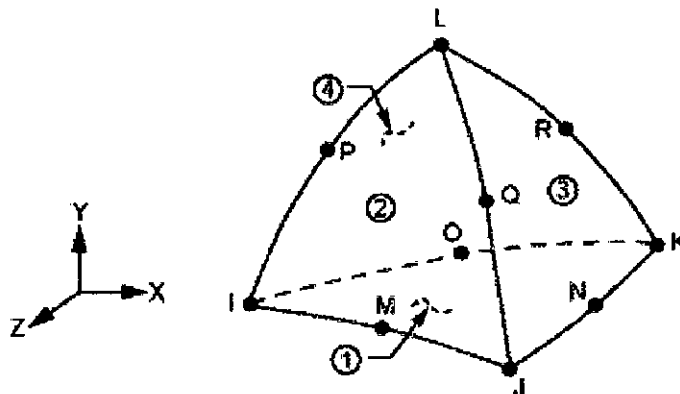


Fig. 3.1: The tetrahedral SOLID92 Geometry having 10 nodes (I, J, K...P).

The models dealt in present research work are three dimensional as explained above. So the fundamental equations contain Cartesian axes X, Y, Z (i.e. X, Y, Z Coordinates). If  $u$ ,  $v$  and  $w$  are the displacements in X, Y and Z coordinates respectively, then the displacement vector can be expressed as the following equation.

$$U = [u \ v \ w]^T \quad (3.1)$$

The stresses and strains are given by the following equations respectively.

$$\sigma = [\sigma_x \ \sigma_y \ \sigma_z \ \tau_{xy} \ \tau_{yz} \ \tau_{xz}]^T \quad (3.2)$$

$$\varepsilon = [\varepsilon_x \ \varepsilon_y \ \varepsilon_z \ \gamma_{xy} \ \gamma_{yz} \ \gamma_{xz}]^T \quad (3.3)$$

The strain displacement relation is given by the following equation [41].

$$\varepsilon = \begin{bmatrix} \varepsilon_x \\ \varepsilon_y \\ \varepsilon_z \\ \gamma_{xy} \\ \gamma_{yz} \\ \gamma_{xz} \end{bmatrix} = \begin{bmatrix} \frac{\partial u}{\partial x} \\ \frac{\partial v}{\partial y} \\ \frac{\partial w}{\partial z} \\ \frac{\partial u}{\partial y} + \frac{\partial v}{\partial x} \\ \frac{\partial w}{\partial y} + \frac{\partial v}{\partial z} \\ \frac{\partial u}{\partial z} + \frac{\partial w}{\partial x} \end{bmatrix} \quad (3.4)$$

For isotropic materials, the two material properties are Young's modulus (or modulus of elasticity),  $E$  and Poisson's ratio,  $\nu$ . If X, Y and Z are the three Cartesian coordinates of a point; then the generalized Hooke's law is given by the following equation [41].



$$\begin{aligned}
\sigma_x &= E\{\varepsilon_x - \nu(\varepsilon_y + \varepsilon_z)\} \\
\sigma_y &= E\{\varepsilon_y - \nu(\varepsilon_x + \varepsilon_z)\} \\
\sigma_z &= E\{\varepsilon_z - \nu(\varepsilon_x + \varepsilon_y)\} \\
\tau_{xy} &= G\gamma_{xy} \\
\tau_{yz} &= G\gamma_{yz} \\
\tau_{zx} &= G\gamma_{zx}
\end{aligned} \tag{3.5}$$

And the modulus of rigidity can be found from the following equation.

$$G = \frac{E}{2(1+\nu)} \tag{3.6}$$

For linear elastic materials, the stress strain relations can come from the generalized Hooke's law by the following equation.

$$\sigma = \begin{bmatrix} \sigma_x \\ \sigma_y \\ \sigma_z \\ \tau_{xy} \\ \tau_{yz} \\ \tau_{zx} \end{bmatrix} = D\varepsilon \tag{3.7}$$

Now solving for the stresses the elasticity matrix,  $D$  becomes a symmetric (6×6) material matrix as follows [41].

$$D = \frac{E}{(1+\nu)(1-2\nu)} \begin{bmatrix} 1-\nu & \nu & \nu & 0 & 0 & 0 \\ \nu & 1-\nu & \nu & 0 & 0 & 0 \\ \nu & \nu & 1-\nu & 0 & 0 & 0 \\ 0 & 0 & 0 & 0.5-\nu & 0 & 0 \\ 0 & 0 & 0 & 0 & 0.5-\nu & 0 \\ 0 & 0 & 0 & 0 & 0 & 0.5-\nu \end{bmatrix} \tag{3.8}$$

For  $F_x$ ,  $F_y$  and  $F_z$  being the body force in X, Y and Z axis, the equilibrium equations for Cartesian coordinate can be expressed as the following equations [41].

$$\begin{aligned}
 \frac{\partial \sigma_x}{\partial x} + \frac{\partial \tau_{xy}}{\partial y} + \frac{\partial \tau_{xz}}{\partial z} + F_x &= 0 \\
 \frac{\partial \tau_{yx}}{\partial x} + \frac{\partial \sigma_y}{\partial y} + \frac{\partial \tau_{yz}}{\partial z} + F_y &= 0 \\
 \frac{\partial \tau_{zx}}{\partial x} + \frac{\partial \tau_{zy}}{\partial y} + \frac{\partial \sigma_z}{\partial z} + F_z &= 0
 \end{aligned} \tag{3.9}$$

Thus the stresses and strains are considered as a function of displacements ( $u$ ,  $v$ ,  $w$ ). Thus all the parameters can be evaluated from them.

### 3.3 REPRESENTATIVE VOLUME ELEMENT (RVE)

CNTs remain in different sizes and forms when they are dispersed in a matrix to make a nanocomposite. They can be single-walled or multi-walled, again both can be in individual or in bundle form. The CNT bundle can consist different numbers of SWNTs, but in this research CNT bundle with four SWNTs is considered. Length of the CNT can be from few nanometers or a few micrometers and can be straight, twisted or curled, or in the form of ropes [42]. Their distribution and orientation in the matrix can be uniform and unidirectional (which may be the ultimate goal) or random. All these factors make the simulations of CNT-based composites extremely difficult. The concept of unit cells or representative volume elements (RVEs) which have been applied successfully in the studies of conventional fiber-reinforced composites at the microscale, can be extended to study the CNT-based composites at the nanoscale. In the present study 3D nanoscale square RVEs are employed to investigate the various effects on the elastic properties of nanocomposites. The RVEs of single CNT based composite (Fig. 3.2) and CNT bundle based composite (Fig. 3.3) are shown below.

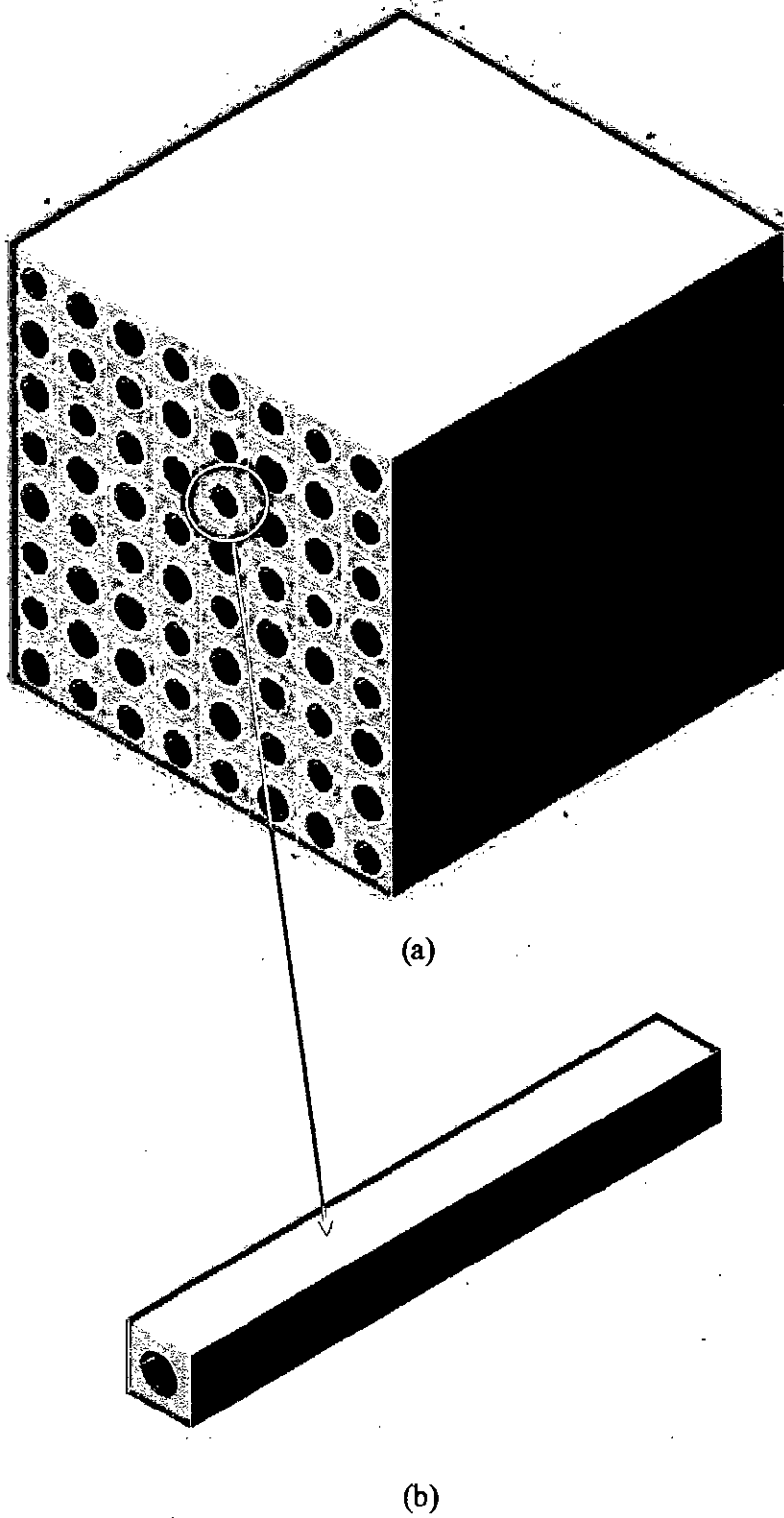


Fig. 3.2: (a) CNT based composite and (b) its square RVE

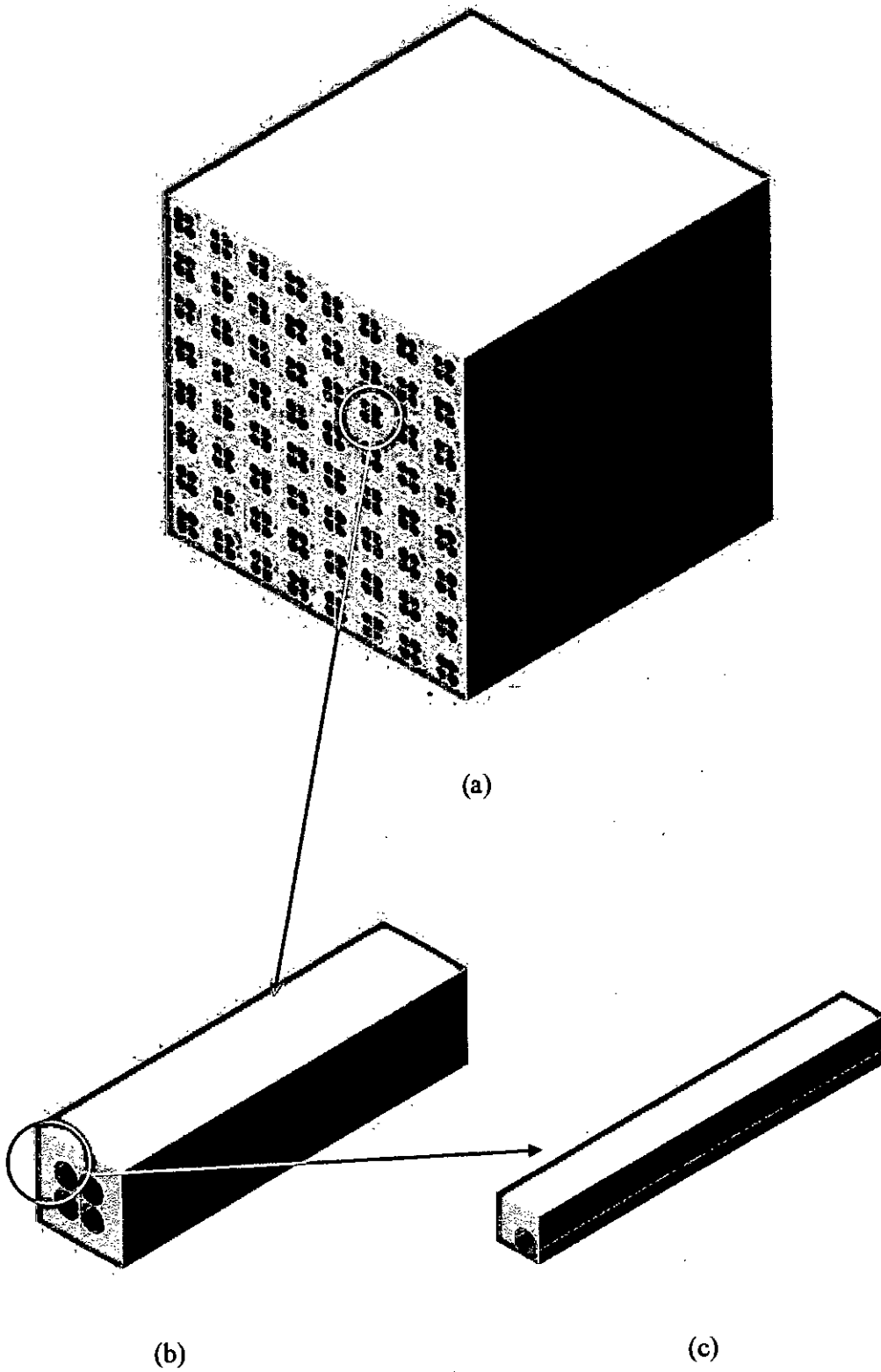


Fig. 3.3: (a) CNT-bundle based composite, (b) a segment of it, (c) its square RVE

### 3.3.1 RVE for Long CNT Based Composite

The RVE used for analyzing long CNT-polymer composite has a length,  $L = 100$  nm (Fig. 3.4). The CNT is embedded through out the length in the mid position. The diameter ( $d_t$ ) of the CNT is varied (according to the chiral indices (10, 10), (50, 50), (80, 80), (110, 110)) and so is the square cross section of the composite (width =  $a$ ) accordingly to keep the CNT volume fraction to 5%. The volume fraction of CNT is considered arbitrarily but it is kept constant to evaluate other effects of CNT morphology on the elastic properties of CNT based composite.

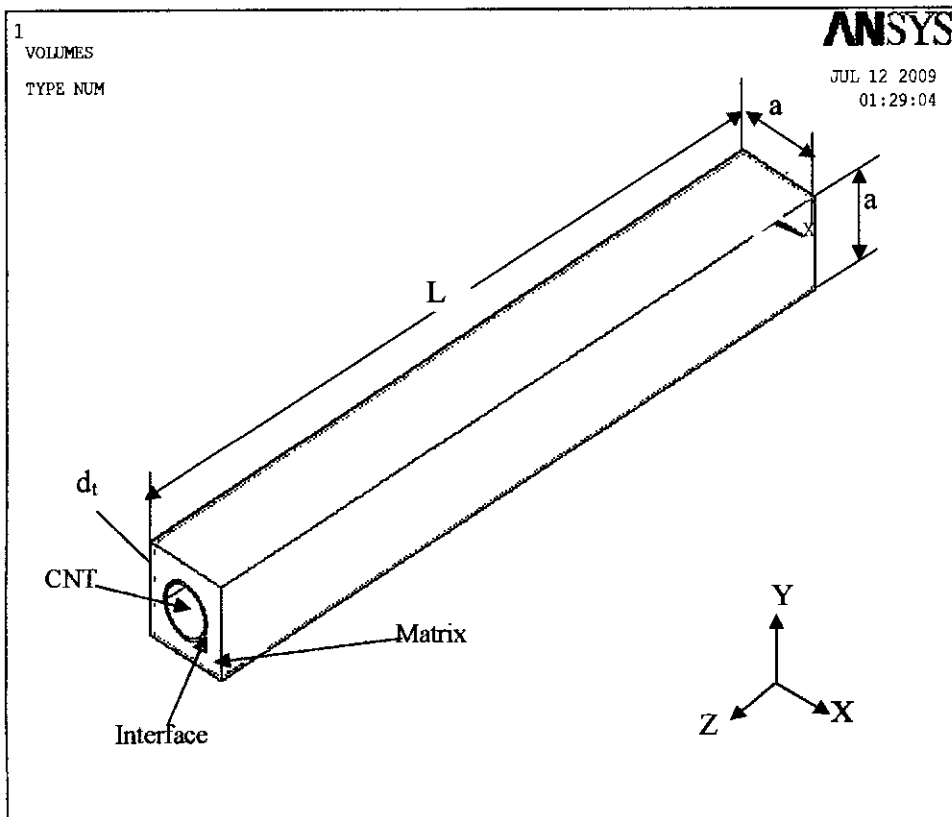


Fig. 3.4: RVE for long CNT based composite

### 3.3.2 RVE for Long CNT Bundle Based Composite

The RVE used for analyzing long CNT bundle based composite has a length,  $L = 100$  nm (Fig. 3.5). The CNT is embedded through out the length in one of the corners. The diameter ( $d_t$ ) of the CNT is varied [according to the chiral indices (10, 10), (50, 50), (80, 80), (110, 110)] and so is the cross section of the composite (width =  $a$ ) to keep the CNT volume fraction to 5%.

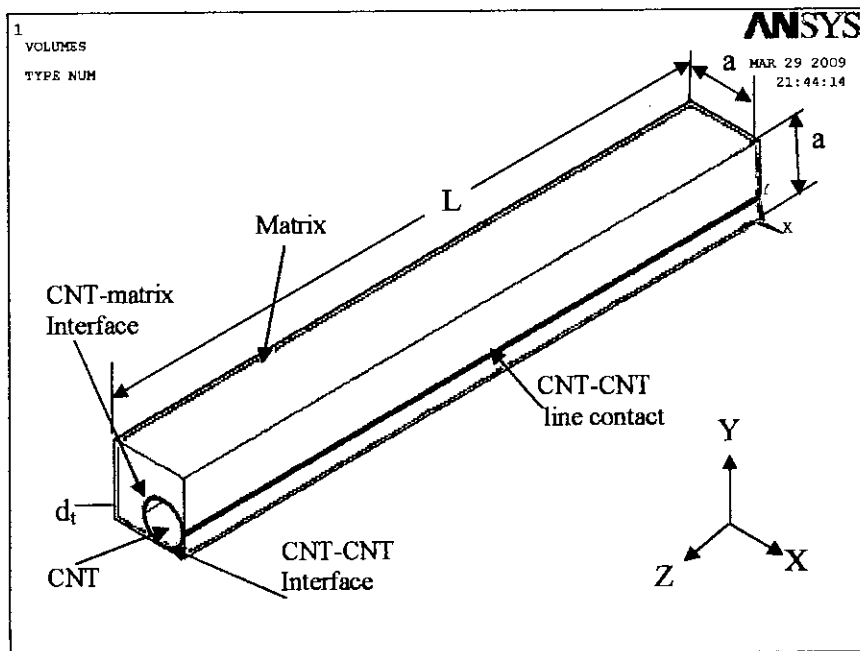
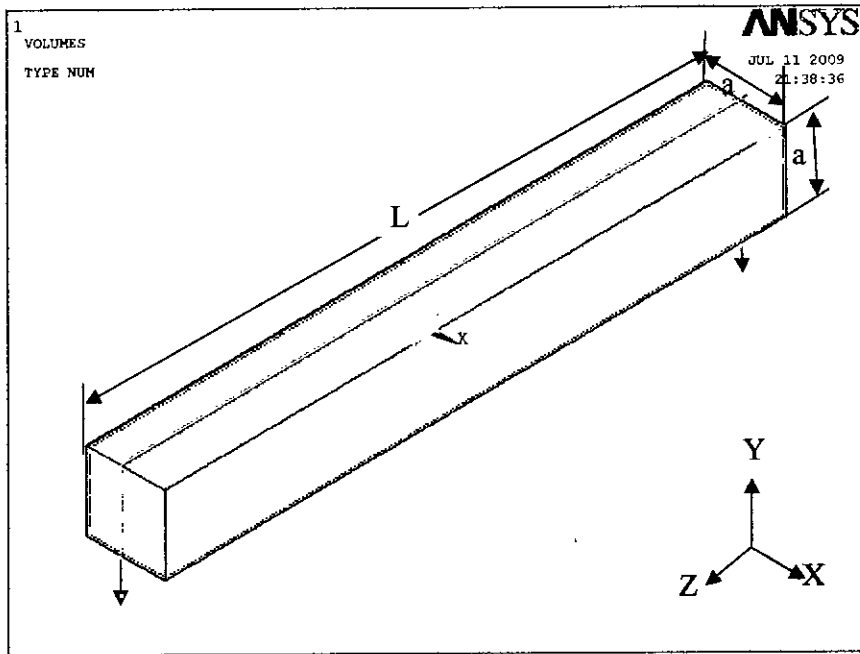


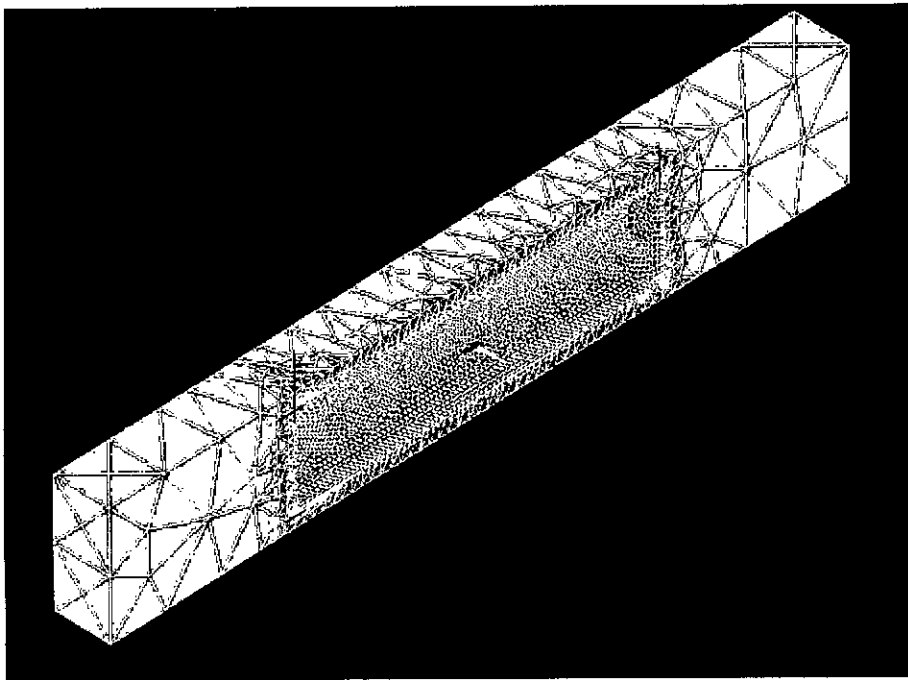
Fig. 3.5: RVE for long CNT bundle based composite

### 3.3.3 RVE for Short CNT Based Composite

The RVE used for analyzing short CNT based composite (Fig. 3.6) also has a length,  $L = 100$  nm, but the CNT is embedded inside the RVE. The length of the CNT,  $L_c$  is varied (36.4, 50 and 80 nm) and the diameter ( $d_t$ ) of the CNT is varied according to the chiral indices (50, 50), (80, 80), (110, 110). The cross section ( $a$ ) is chosen so to keep the CNT volume fraction to 5%.



(a)



(b)

Fig. 3.6: RVE for short CNT composite, (a) total view, (b) half sectional view

### 3.3.4 RVE for Short CNT Bundle Based Composite

The RVE used for analyzing long CNT-bundle composite (Fig. 3.7 and 3.8) has a length ( $L$ ) of 100 nm, but the CNT is embedded inside the RVE. The length of the CNT ( $L_c$ ) is varied (36.4, 50 and 80 nm) and the diameter ( $d_t$ ) of the CNT is varied according to the chiral indices (50, 50), (80, 80), (110, 110). The cross section of the composite is chosen so to keep the CNT volume fraction to 5%.

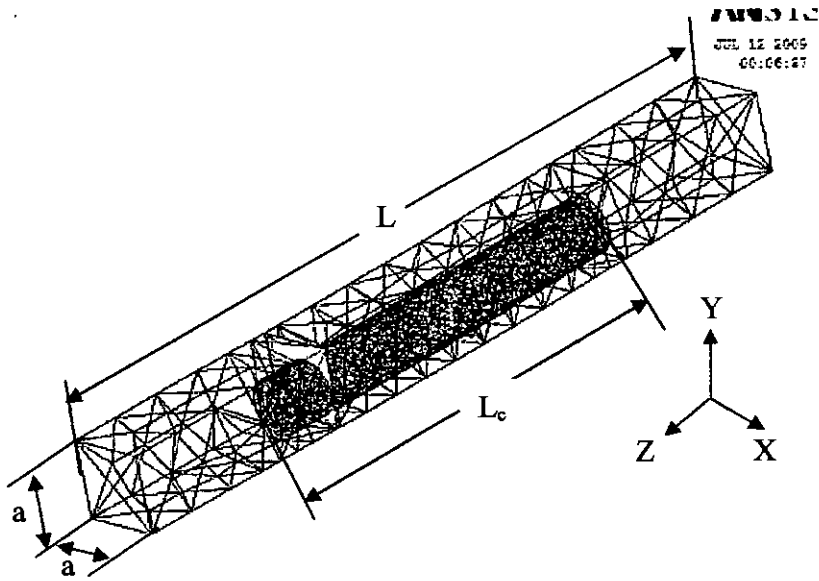


Fig. 3.7: Wire frame view of the RVE for short CNT bundle based composite

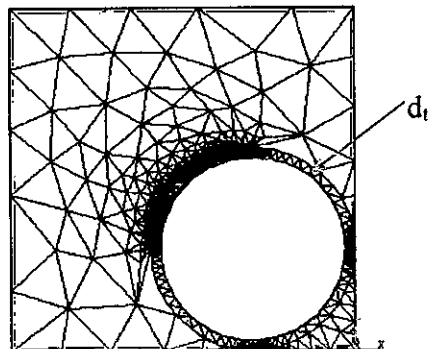


Fig. 3.8: Cross sectional view of the RVE for short CNT bundle based composite



### 3.4 ELASTIC PROPERTIES EVALUATION

The square RVEs described above are given longitudinal and transverse load (applied in the form of displacement) to evaluate longitudinal and transverse Young's modulus and major Poisson's ratio.

#### 3.4.1 RVE under Axial Loading

Square RVE under an axial stretch  $\Delta L$  is shown in Fig. 3.9. In this load case the stress and strain components on the lateral surface are given in the following equations:

$$\begin{aligned}\varepsilon_x &= \frac{\Delta a}{a} \\ \varepsilon_z &= \frac{\Delta L}{L} \\ \sigma_x &= \sigma_y\end{aligned}\tag{3.11}$$

Where  $\Delta a$  is the change of dimension, 'a' of the cross-section under the stretch  $\Delta L$  in the z-direction ( $\Delta a < 0$ , if  $\Delta L > 0$ ). The longitudinal Young's modulus can be found from the following equation.

$$E_z = \frac{\sigma_{ave}}{\varepsilon_z} = \frac{L}{\Delta L} \sigma_{ave}\tag{3.12}$$

Where the averaged value of stress  $\sigma_{ave}$  is given by the following equation [36].

$$\sigma_{ave} = \frac{1}{A} \int_A \sigma_z(x, y, L/2) dx dy\tag{3.13}$$

With 'A' being the area of the end surface the value of  $\sigma_{ave}$  is evaluated for the RVE using the FEM results.

From the fundamental rules, Poisson's ratio can be found as the following equation.

$$\nu_x = -\frac{\varepsilon_x}{\varepsilon_z} \quad (3.14)$$

Thus, one obtains an expression for the Poisson's ratio as the following equation.

$$\nu_x = -\left(\frac{\Delta a}{a}\right) / \left(\frac{\Delta L}{L}\right) \quad (3.15)$$

Eqs. 3.12 and 3.15 can be applied to estimate the effective Young's modulus,  $E_z$  and Poisson's ratio,  $\nu_{zx}$ , once the contraction  $\Delta a$  and the stress  $\sigma_{ave}$  are obtained.

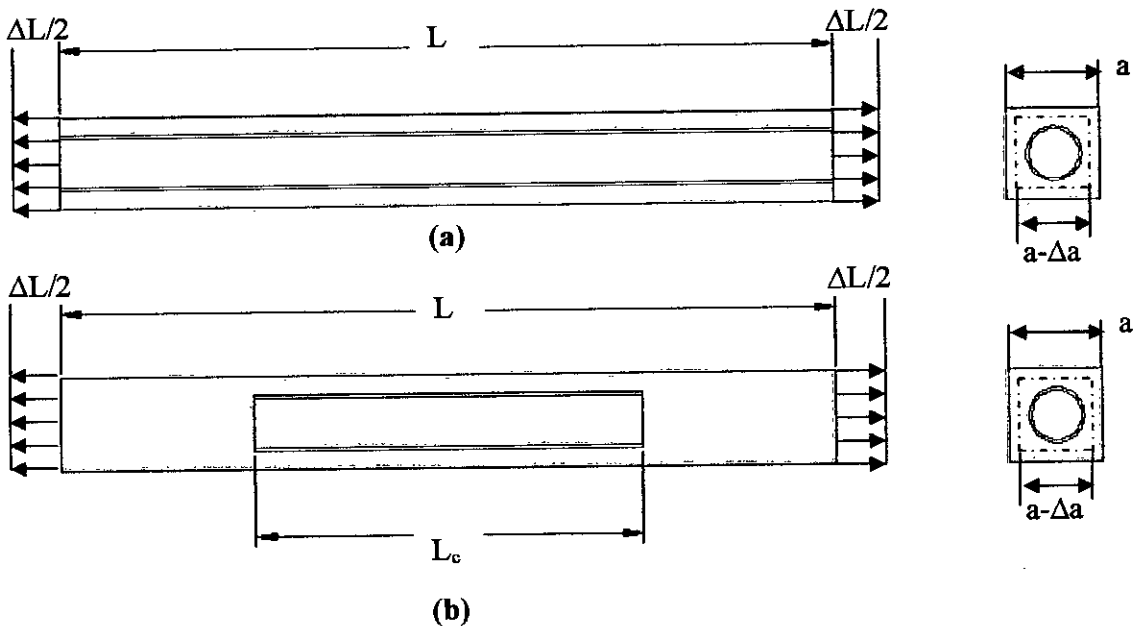


Fig. 3.9: RVEs under axial loading (a) long CNT composite (b) short CNT composite

### 3.4.2 RVE under Lateral Loading

Square RVE under a lateral stretch  $\Delta a$  is shown in Fig. 3.10, in this load case the stress and strain components are:

$$\begin{aligned}\varepsilon_x &= \frac{\Delta a}{a} \\ \varepsilon_z &= \frac{\Delta L}{L} \\ \sigma_x &= \sigma_y\end{aligned}\tag{3.16}$$

Where for  $\Delta a$ , the change of dimension, 'a' of the cross-section under the lateral stretch; in the axial direction,  $\Delta L$  change occurs ( $\Delta a > 0$ , if  $\Delta L < 0$ ). Integrating and averaging the third equation one has immediately the following equation.

$$E_x = \frac{\sigma_{ave}}{\varepsilon_x} = \frac{a}{\Delta a} \sigma_{ave}\tag{3.17}$$

Where the averaged value of stress  $\sigma_{ave}$  is given by the following equation [36].

$$\sigma_{ave} = \frac{1}{A} \int_A \sigma_x(x, y, L/2) dx dy\tag{3.18}$$

With 'A' being the area of the side surface the value of  $\sigma_{ave}$  is evaluated for the RVE using the FEM results.

Eq. 3.17 can be applied to estimate the effective transverse Young's modulus,  $E_x$ ; once the contraction  $\Delta a$  and the stress  $\sigma_{ave}$  in case (a) are obtained.

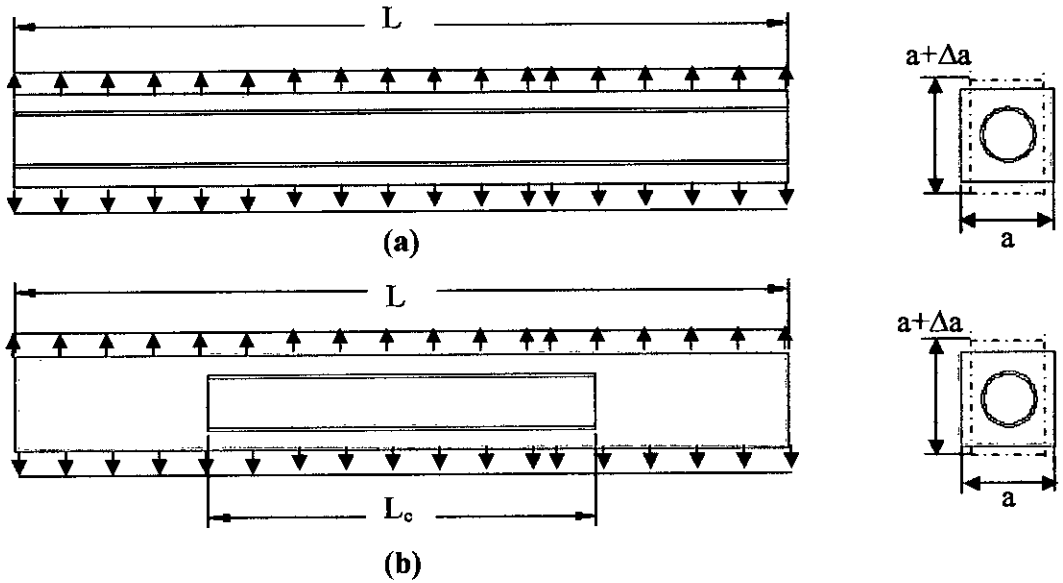


Fig. 3.10: RVE under lateral loading of, (a) long CNT composite, (b) short CNT composite

### 3.4.3 Volume Fraction of CNT in CNT-matrix composite

In case of long CNT based composite, the CNT is relatively long (with large aspect ratio) and it is through out the RVE. For the square RVE, the volume fraction of the CNT (a tube) (Fig. 3.9 (a)) is defined by the following equation [36].

$$V^t = \frac{A_f L}{A_c L}$$

$$V^t = \frac{\pi(r_o^2 - r_i^2)}{a^2 - \pi r_i^2} \quad (3.19)$$

In case of short CNT based composite, the CNT is embedded inside the RVE. For the square RVE, the volume fraction of the CNT (a tube) (Fig. 3.13(b)) is defined by the following equation [36].

$$V^t = \frac{A_f L_c}{(A_c L_c + a^2 L_e)} \quad (3.20)$$

Where,  $A_f = \pi(r_o^2 - r_i^2)$

And  $L = L_c + L_e$

Here,

$V^t$	CNT volume fraction
$A_f$	Cross sectional area of the fiber
$r_o$	CNT outer radius
$r_i$	CNT inner radius
$L$	Length of the RVE
$L_c$	Length of the CNT

### 3.5 EQUIVALENT SINGLE SOLID FIBER

The equivalent single solid fiber may replace the CNT bundle based composite without hampering the effective mechanical properties of the CNT bundle based composite. The radius of the solid fiber,  $R_{eq}$  (Fig. 3.1) is found from the following equation.

$$R_{bundle} = \sqrt{r_o^2 + r_o^2} + r_o = (\sqrt{2}+1)r_o = R_{eq} \quad (3.21)$$

Where  $r_o$  is the outer radius of the CNT. In both cases the fiber will experience same strain under same amount of force. Therefore,

$$\varepsilon_{eqv} = \varepsilon_{bl}$$

so, 
$$\frac{F_{eq}}{A_{eq} E l_{eq}} = \frac{F_{bl}}{A_{bl} E_{bl}}$$

$$\text{Thus, } E_{eq} = \frac{A_{bl} E_{bl}}{A_{eq}} \quad (3.22)$$

$$\text{Where, } A_{eq} = \pi(2.414r_o)^2$$

$$A_{bl} = (3\pi + 4)r_o^2 - 4\pi r_o^2$$

So from the Eq. 3.22, effective Young's modulus,  $E_{eq}$  of the equivalent single solid fiber can be found.

Here,

$R_{bundle}$	Radius of the CNT-bundle
$R_{eqv}$	Radius of the equivalent solid fiber
$A_{bl}$	Cross sectional area of the CNT-bundle
$A_{eqv}$	Cross sectional area of the equivalent solid fiber
$A_{c-c}$	Cross sectional area of the CNT-CNT interface
$E_{bl}$	Young's modulus of the CNT-bundle
$E_{eq}$	Young's modulus of the equivalent solid fiber
$E_{c-c}$	Young's modulus of the CNT-CNT interface

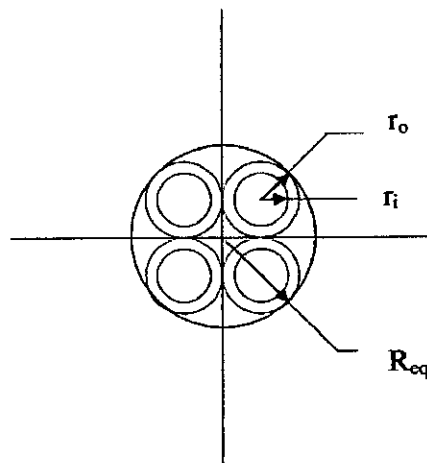


Fig. 3.11: Cross section of the CNT bundle

### 3.6 INTERFACE PROPERTIES

Nanocomposites possess a large amount of interfaces due to the small size (nanometer) of reinforcements. The interface behavior can significantly affect the mechanical properties of nanocomposites, since load from the matrix to the fibers is transferred through this interface. For example, CNTs in general do not bond well to polymers [43] and their interactions result mainly from the vdW forces [44]. Consequently CNTs may slide inside the matrix and may not provide much reinforcing effect. It is however, important to assess whether the poor interface behavior is indeed responsible for the short fall of CNT-reinforced composites in order to reach their expected properties.

It is difficult to account for the vdW interactions in the continuum modeling of nanocomposites. Jiang et al. [45] established a nonlinear cohesive law (Eq. 3.23) for the CNT-Matrix polymer interfaces directly from the Lennard-Jones (LJ) potential for the vdW interactions. The cohesive law gives analytically the normal cohesive stress at the CNT-Polymer interface,  $\sigma^{int}$ , in terms of the interface opening displacement,  $u$ . The normal cohesive stress,  $\sigma^{int}$  displays nonlinear hardening, peak strength and softening as the opening displacement,  $u$  increases. All cohesive law properties (e.g. cohesive strength, cohesive energy) are obtained analytically in terms of the parameters in the LJ potential. The properties used for CNT-CNT and CNT- Matrix bond strength evaluation are shown in the Table 3.1.

$$\sigma^{int} = 3.07\sigma_{max} \left[ \left( 1 + 0.682 \frac{\sigma_{max}}{\phi_{total}} [u] \right)^{-4} - \left( 1 + 0.682 \frac{\sigma_{max}}{\phi_{total}} [u] \right)^{-10} \right] \quad (3.23)$$

$$\text{Here,} \quad \sigma_{max} = \frac{6\pi}{5} \rho_1 \rho_2 \epsilon \sigma^2 \quad (3.24)$$

$$\text{And,} \quad \phi_{total} = \frac{4\pi}{9} \sqrt{\frac{5}{2}} \rho_1 \rho_2 \epsilon \sigma^3 \quad (3.25)$$

Table 3.1: Properties for interfaces between CNT-Polymer and CNT-CNT [45]

Properties for interfaces	CNT-CNT	CNT-Polymer
CNT area density, $\rho_1$ (/m <sup>2</sup> )	$3.82 \times 10^{19}$	$3.82 \times 10^{19}$
CNT/ Polymer volume density, $\rho_2$ (/m <sup>3</sup> )	$1.1 \times 10^{29}$	$3.1 \times 10^{28}$
Bond energy, $\epsilon$ (ev)	0.00286	0.004656
Bond energy, $\epsilon$ (J)	$4.58 \times 10^{-22}$	$7.46 \times 10^{-22}$
Distance potential, $\sigma$ (nm)	0.3468	0.3825
Maximum stress, $\sigma_{max}$ (MPa)	892	487
Total energy per unit area, $\Phi_{Total}$ (J/m <sup>2</sup> )	0.181092	0.109139

### 3.6.1 Interface with Van Der Waals (vdW) Interaction

The cohesive stress,  $\sigma^{int}$  for interface opening,  $u$  for the CNT-CNT and CNT-matrix interface with only vdW interaction can be found from equations 3.23 to 3.25 [45]. The change of stress,  $\Delta\sigma$  for change of opening distance,  $\Delta u$  can also be found from the plot of above equations. Now considering unit change of opening distance ( $\Delta u/u$ ) as strain we can evaluate the strain imposed. Thus from this stress strain plot we can appraise the stiffness (i.e. Young's modulus) of the interface.

The interface between CNT-matrix is considered to be 0.04 nm thickness. But the interface between CNT-CNT is varied according to the diameter of the CNTs.



### 3.6.2 Interface with Cross-Link

The CNT bundles can slide on each other due to weak vdW interaction. To improve this cross-link is incorporated. By introducing cross-links higher stiffness (i.e. Young's modulus) of the interface can be obtained [46]. Cross-links can be formed between two neighboring CNTs also between CNT and Matrix. Fig. 3.12 and 3.13 shows different cross-links in the CNT-CNT interface.

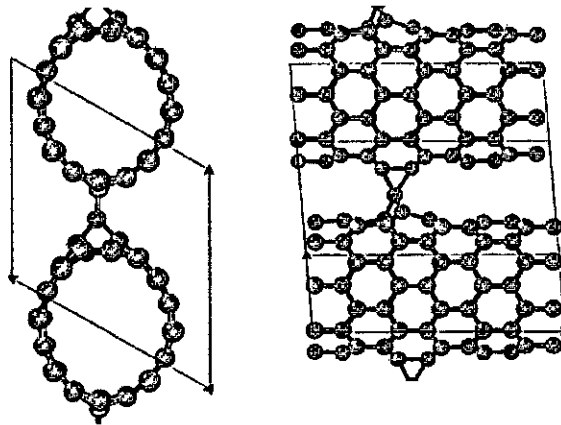


Fig. 3.12: A bridge involving carbon atoms formed through an interstitial carbon atom [46].

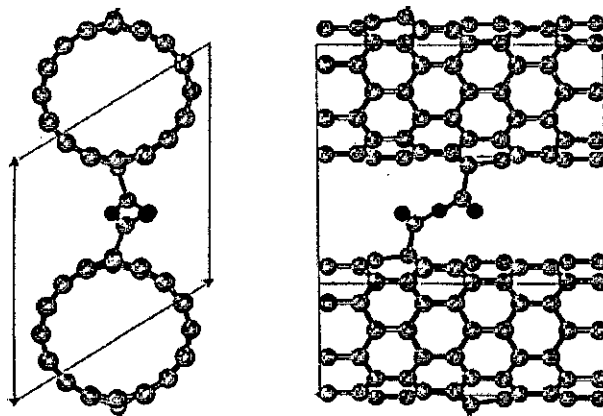


Fig. 3.13: Cross-link formed by chemical reaction between carboxyl functional groups attached to neighboring nanotubes. Oxygen atoms are shown in black [46].

# **CHAPTER 04**

---

## **RESULTS AND DISCUSSION**

## 4.1 INTRODUCTION

In the preceding chapter, FEM used for evaluating effective material properties of representative volume element (RVE) is discussed. There are two cases: single CNT embedded in the RVE and CNT bundle embedded in the RVE. CNT bundle is consisted of four SWNTs. However, in case of CNT bundle the RVE is selected with one CNT due to symmetry of axis. Both cases again have two distinguished types of models with long CNT (through out the model) and short CNT (inside the model).

It is mentioned in chapter one, the nanotubes are of three types based on chiral indices  $(m, n)$ . They are zigzag, armchair and chrial type nanotubes. In the present research work, armchair CNT is taken into consideration. It is specified by chiral indices  $(m,m)$ . The radii of armchair CNTs are calculated using Eq. 1.4 (from chapter 1). The indices which are considered in this research are  $(10, 10)$ ,  $(50, 50)$ ,  $(80, 80)$  and  $(110, 110)$ . The CNT wall thickness is considered 0.34 nm. The radii of different CNTs are tabulated in the Table 4.1. For all the cases as mentioned earlier, the volume fraction of CNT in the composite is taken to be 5%.

In this work first the interface stiffness between CNT-CNT and CNT-Matrix is evaluated. The effect of bundle diameter, length and cross-link among the CNTs within the bundle on the elastic properties of CNT bundle reinforced composite are evaluated using FEM. At last an approximate analytical formula is developed for evaluating the elastic properties of composite with an equivalent single solid fiber replacing the CNT bundle.

In the following sections, the results of all these investigations are shown graphically with detail description and also compared with analytical results. The contour plots of stress and strain are also shown in this chapter.

Table 4.1: The radii of CNT for different CNT index

<b>CNT Index</b>	<b>CNT Mean Radius R (nm)</b>	<b>CNT Outer Radius <math>R_o</math> (nm)</b>	<b>CNT Inner Radius <math>R_i</math> (nm)</b>
(10, 10)	0.68	0.85	0.51
(50, 50)	3.39	3.56	3.22
(80, 80)	5.43	5.60	5.26
(110, 110)	7.46	7.63	7.29

## 4.2 INTERFACE STIFFNESS/ YOUNG'S MODULUS

The fundamental of evaluating vdW interaction in the interface is discussed in Chapter 3 elaborately. Here it is employed in determining interface stiffness/ Young's modulus between CNT-CNT and CNT-Matrix.

### 4.2.1 Interface Properties between CNT-CNT

Variation of cohesive stress with the interface opening for the CNT-CNT interface with only vdW interaction is shown in Fig. 4.1. The cohesive stress increases at small opening displacement, reaches the maximum value at opening displacement of 0.05 nm and then gradually decreases as opening displacement increases. Variation of the tangent modulus of stress-displacement at small opening displacement is shown in Fig. 4.2. It should be mentioned here that this tangent modulus indicates the stiffness of the interface. It is seen that at small opening displacement, the tangent modulus is almost constant and its value is 5.35 MPa.

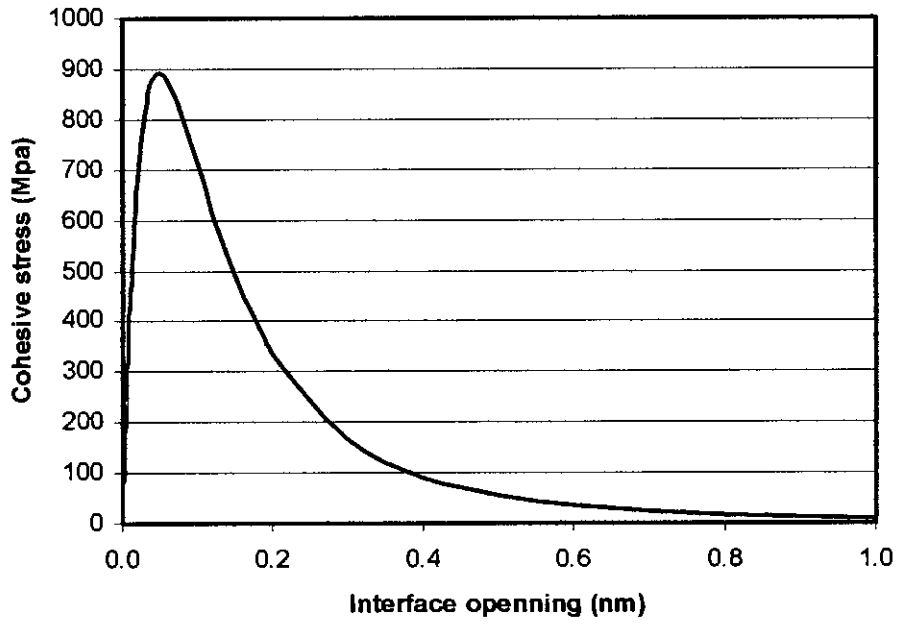


Fig. 4.1: Cohesive stress versus interface opening curve for CNT-CNT interface

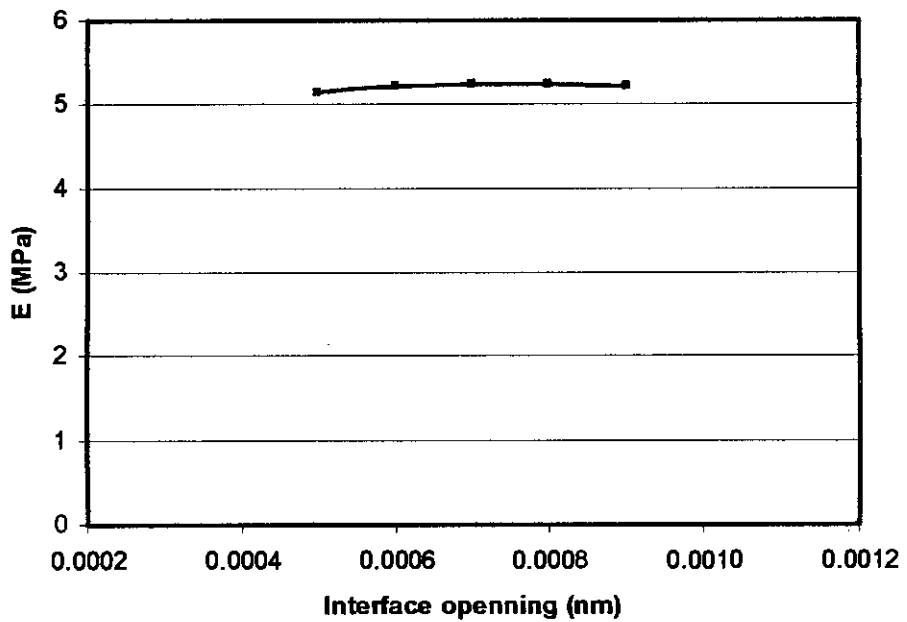


Fig. 4.2: Stiffness versus interface opening curve for CNT-CNT interface

#### 4.2.2 Interface Properties between CNT-Matrix

Variation of cohesive stress with the interface opening for the CNT-polythene interface with only vdW interaction is shown in Fig. 4.3. The cohesive stress increases at small opening displacement, reaches the maximum value at opening displacement of 0.0542 nm and then gradually decreases as opening displacement increases. Variation of the tangent modulus of stress-displacement at small opening displacement is shown in Fig. 4.2. It should be mentioned here that this tangent modulus indicates the stiffness of the interface. It is seen that at small opening displacement, the tangent modulus is almost constant and its value is 2.70 MPa.

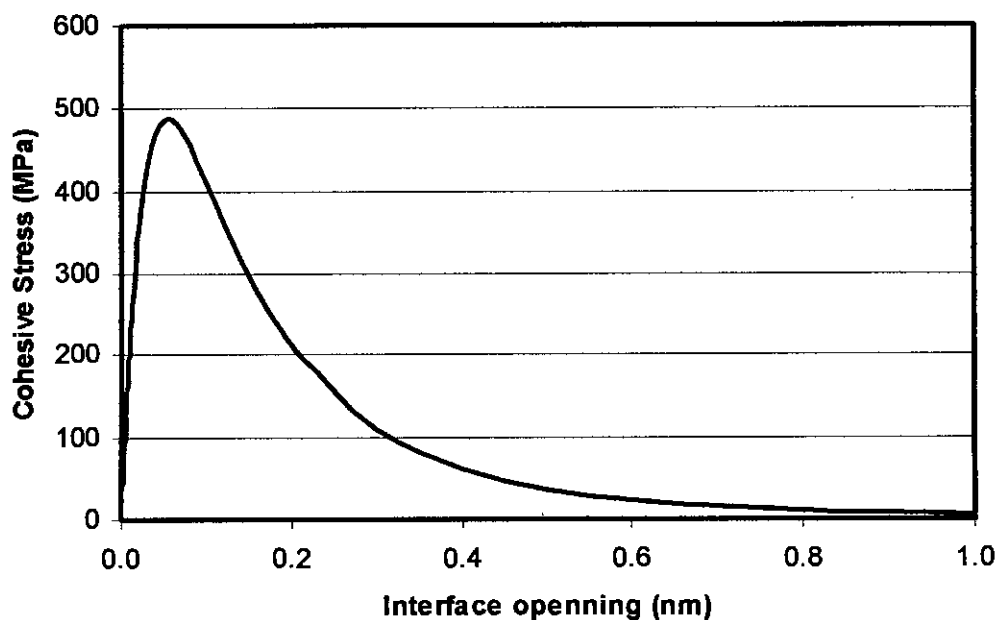


Fig. 4.3: Cohesive stress versus interface opening curve for CNT-polymer matrix interface

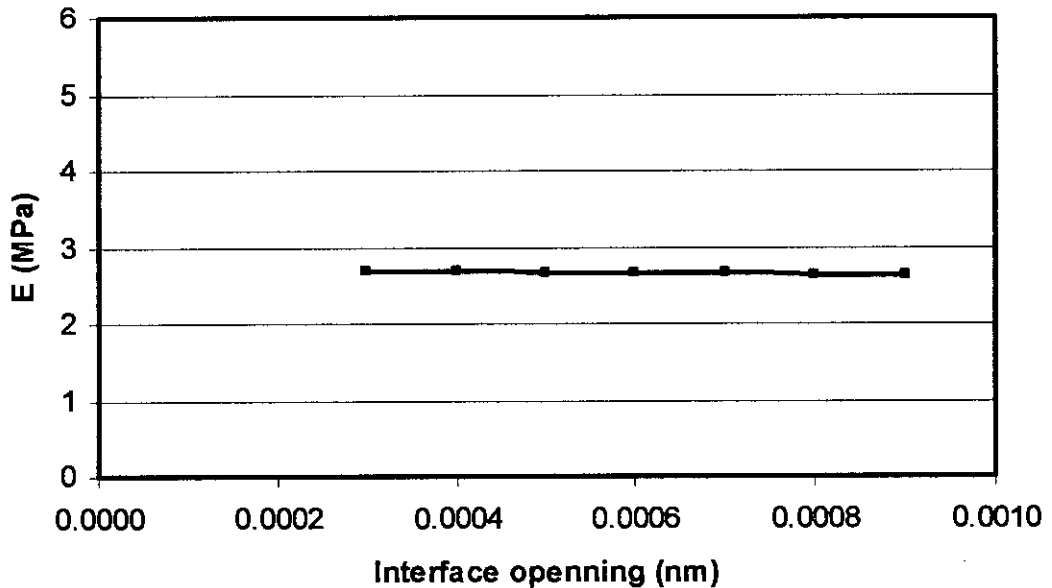


Fig. 4.4: Stiffness versus interface opening curve for CNT-polymer matrix interface

### 4.3 VALIDATION OF FINITE ELEMENT MODEL

To validate the finite element model, models for single CNT based composites and CNT bundle based composites are considered here.

#### 4.3.1 Validation for Single CNT Based Composite

To validate the present finite element model for single CNT based composite, FEM results are compared with those of Chen et al. [36]. Model size and properties of CNT and matrix are tabulated in Table 4.2, which are exactly the same as those considered by Chen et al. [36]. Volume fraction of CNT is considered to be 3.62%. According to present model, longitudinal Young's modulus,  $E_z$  of the composite is found to be 132.55 GPa. Thus  $E_z/E_m = 1.326$

which exactly matches with the result found by Chen et al. [36]. Thus it ensures the validation of the present model for single CNT based polymer composite.

Table 4.2: Dimension and Properties of CNT and Matrix

<b>Dimension and properties of CNT and matrix</b>	<b>Value</b>
Length of the model, L	100 nm
Width of the square area, 2a	20 nm
CNT index	(5, 5)
Outer radius of the CNT, $r_o$	5 nm
Inner radius of the CNT, $r_i$	4.6 nm
Young's modulus of CNT, $E^t$	1000 GPa
Poisson's ratio of CNT, $\nu^t$	0.3
Young's modulus of Matrix, $E^m$	100 GPa
Poisson's ratio of Matrix, $\nu^m$	0.3

#### 4.3.2 Validation for CNT Bundle Based Composite

To validate the present finite element model for CNT bundle based composite present simulated FEM results are compared with those of Ashrafi et al. [39]. Model size, properties of CNT and matrix used are tabulated in Table 4.3. The stiffness of CNT bundle is found to be 610.5 GPa by present FEM and by Ashrafi et al. [39] it is 580 GPa. The simulated longitudinal Young's modulus is found to be 9.57 GPa, which is quite close to that found (9 GPa) by Ashrafi et al. [39]. The slight variation in the present result, with that of Ashrafi et al. [39] is due the difference between models used. As in this research interface is considered with vdW but in Ashrafi et al. [39] the CNT bundle and the matrix is considered to be perfectly bonded.



Table 4.3: Dimension and Properties of CNT, Matrix and Interface

<b>Dimension and Properties of CNT, Matrix and Interface</b>	<b>Value</b>
Length of the model	100 nm
Length of the bundle	50 nm
CNT index	(5,5)
CNT Young's modulus	1 TPa
CNT Poisson's ratio	0.4
Matrix Young's modulus	3.8 GPa
Matrix Poisson's ratio	0.4
CNT-CNT interface stiffness	5.35 MPa (with only vdW interaction)
CNT-Matrix stiffness	2.70 MPa (with only vdW interaction)

#### 4.4 RESULTS AND DISCUSSION

The FEM analysis has been carried out with both long and short CNTs in single (i.e. isolated) and bundle form. The tetrahedral 10 node (solid 92) element is used to mesh all the RVEs. All the models are of 100 nm length. The cross section is varied according to the requirement to maintain CNT volume fraction to 5%.

Finite element analysis is done on the basis of model specification depicted earlier in chapter 3. The properties used in this research for CNT, matrix and interfaces are given in the Table 4.4.

Table 4.4: Properties of CNT, Matrix and their Interfaces

	CNT	Matrix	CNT-Matrix Interface (with only vdW interaction)	CNT-CNT Interface (with only vdW interaction)
Young's Modulus, E	1 TPa	5 GPa	2.7 MPa	5.35 MPa
Poisson's Ratio, $\nu$	0.3	0.3	0.3	0.3

#### 4.4.1 EFFECT OF CNT DIAMETER ON COMPOSITE ELASTIC PROPERTIES

##### 4.4.1.1 SINGLE CNT

The volume fraction of CNT is kept 5% in all the analysis. The CNT chiral indices (50, 50), (80, 80) and (110, 110) are considered for diameter effect determination. The variations of longitudinal and transverse Young's modulus are shown in Fig. 4.5 and 4.6. From these figures, we can see that for same length of CNT the change of diameter does not affect much the longitudinal or transverse young's modulus. This is so as though the CNT diameter is changed but the volume fraction of CNT in composite is constant, thus effective reinforcement is same. The longitudinal Young's modulus ratio ( $E_z/E_m$ ) for long CNT based composite is about 10.95 and for short CNT it is about 1.9. In case of transverse Young's modulus for both long and short CNT- composite the  $E_x/E_m$  is nearly 1. It indicates that CNT reinforcement in transverse direction is negligible. As the materials of both CNT and matrix are taken isotropic with Poisson's of 0.3, the change of diameter does not have any effect on the major Poisson's ratio of the CNT based composite (Fig. 4.7). The plot of first (Z-axis) and second principal stress (X-axis) and strain on Z and X axis for long and short single CNT-composite are shown in Fig. 4.8 to 4.17.

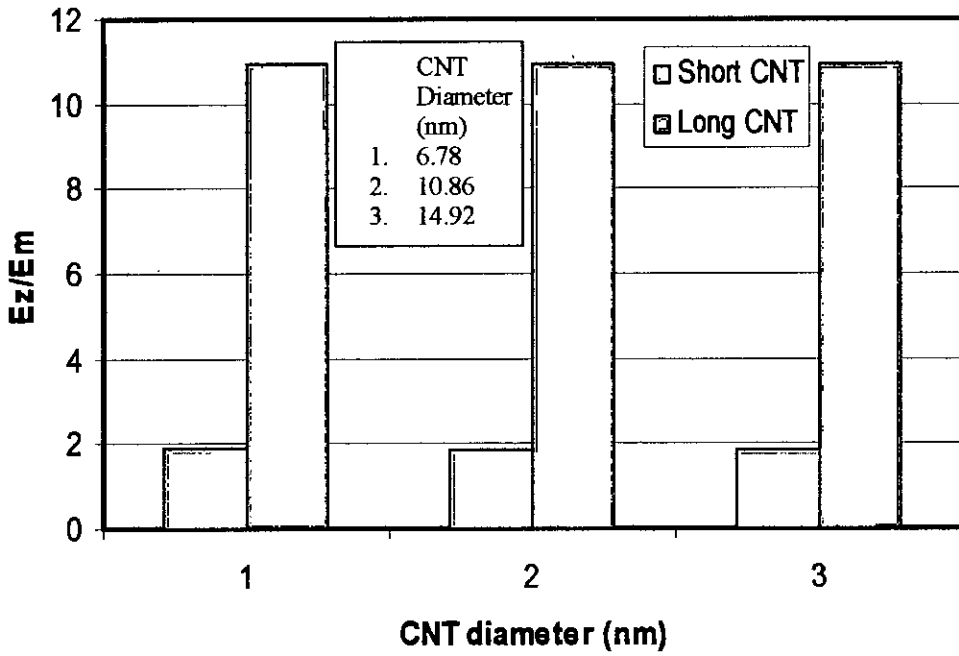


Fig. 4.5:  $E_z/E_m$  versus CNT diameter for single CNT based composite

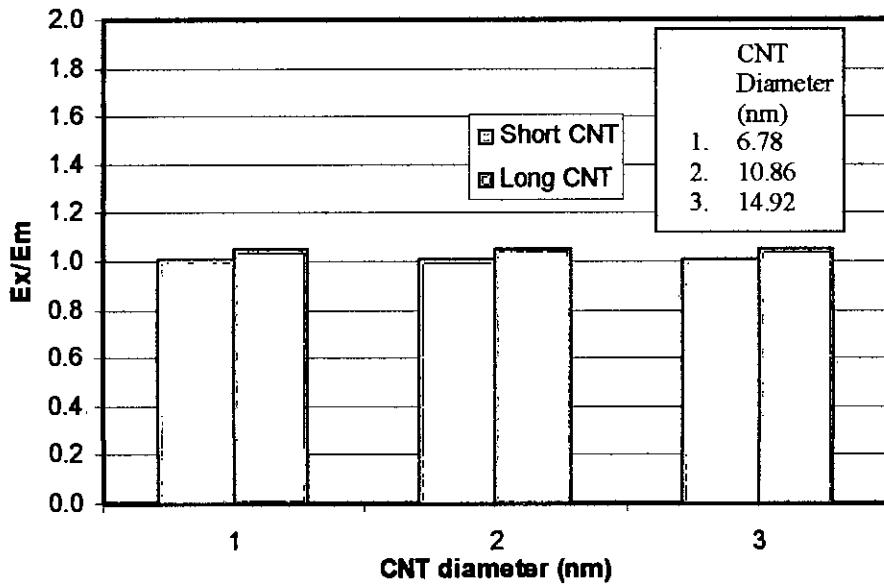


Fig. 4.6:  $E_x/E_m$  versus CNT diameter for single CNT based composite

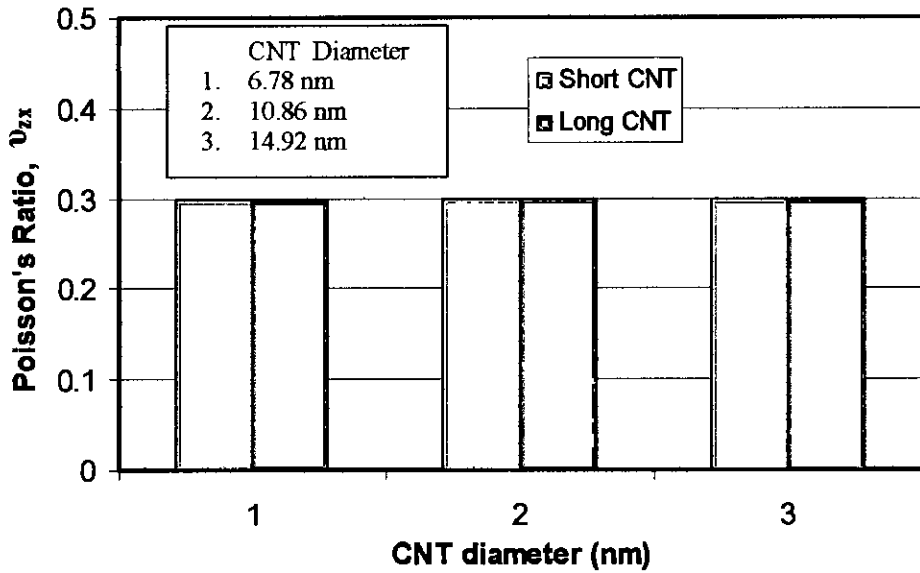


Fig. 4.7: Composite's Poisson's ratio versus CNT diameter for single CNT based composite

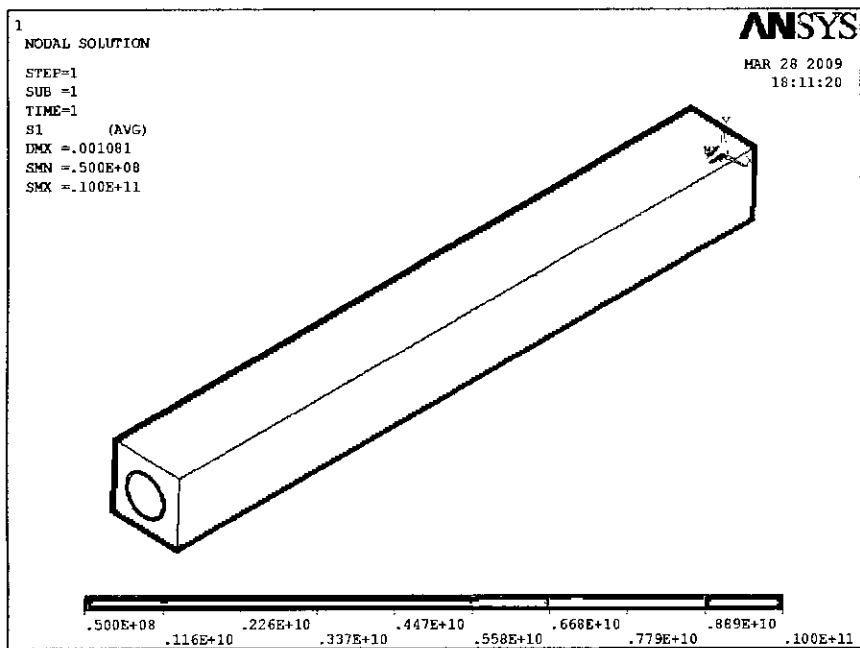


Fig. 4.8: Plot of first principle stress (Z-axis) for long single CNT based composite (for, axial stretch,  $\Delta L = 1$  nm)

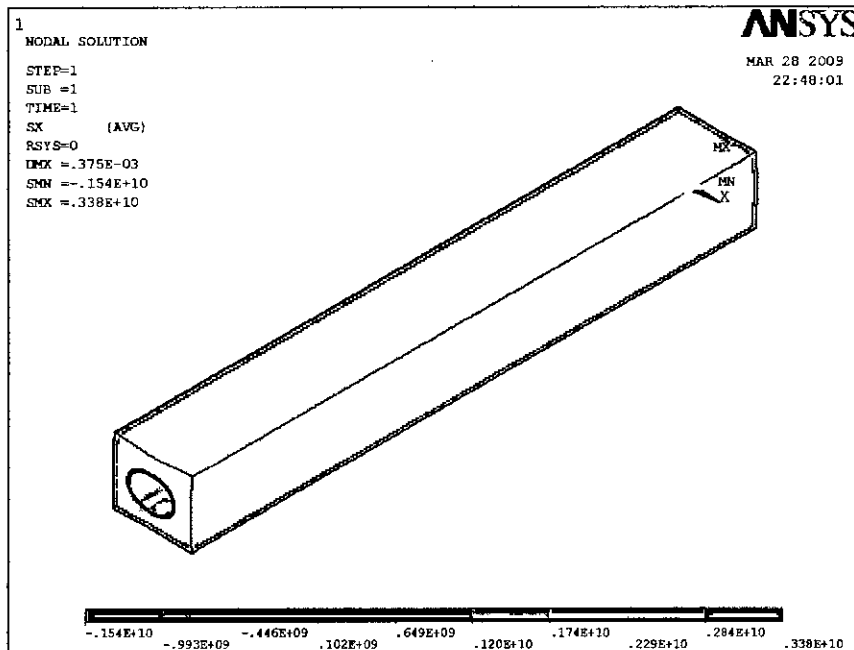


Fig. 4.9: Plot of second principle stress (X-axis) for long single CNT based composite (for lateral stretch  $\Delta a = 0.3$  nm)

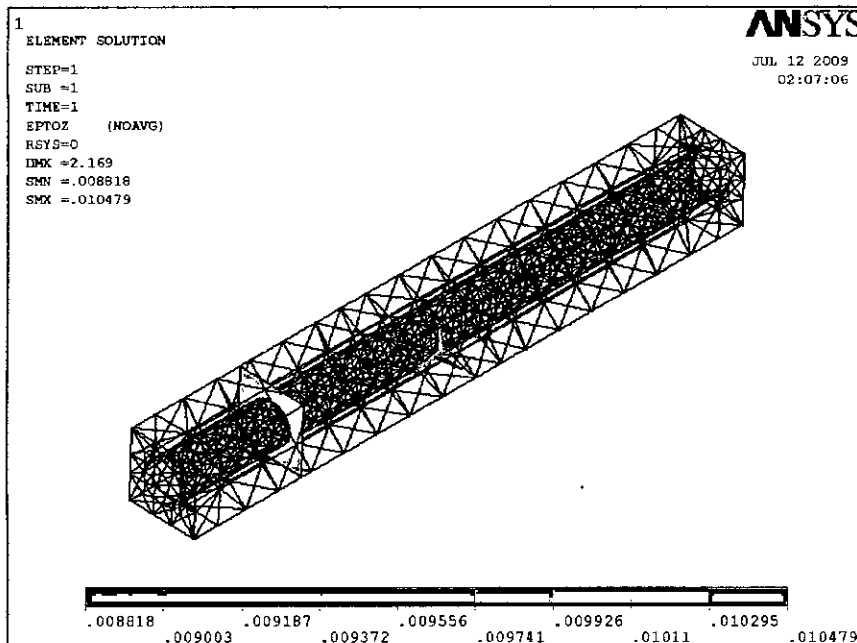


Fig. 4.10: Plot of strain on Z-axis for long single CNT based composite (for,  $\Delta L = 1$  nm)

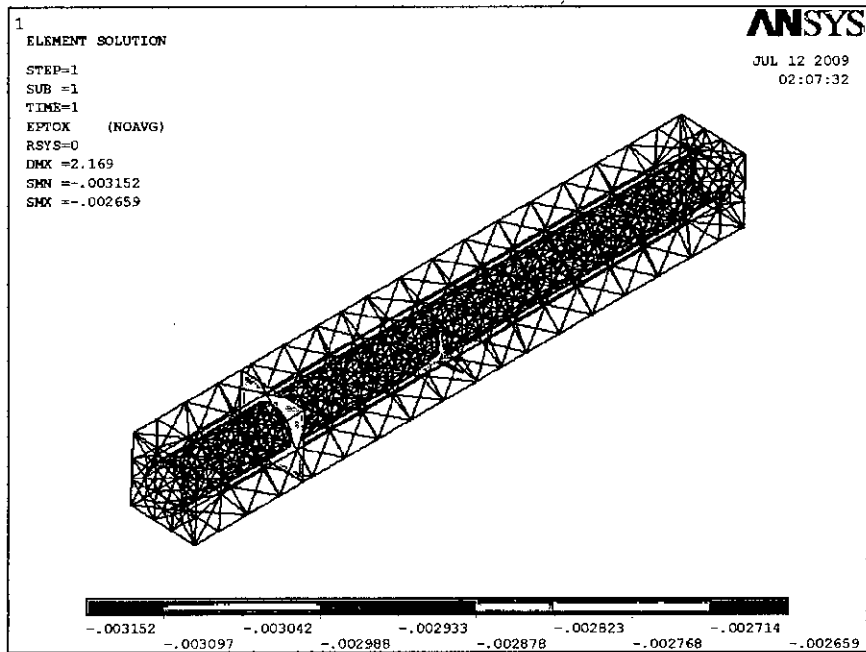


Fig. 4.11: Plot of strain on X-axis for long single CNT based composite (for,  $\Delta L = 1$  nm)

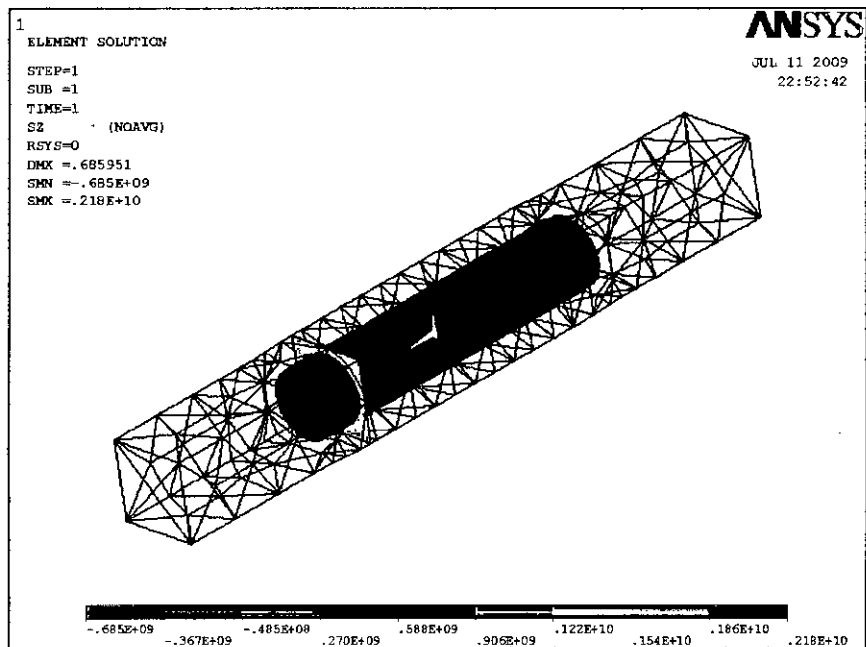


Fig. 4.12: Plot of first principle stress (Z-axis) for short single CNT based composite (for,  $\Delta L = 1$  nm)

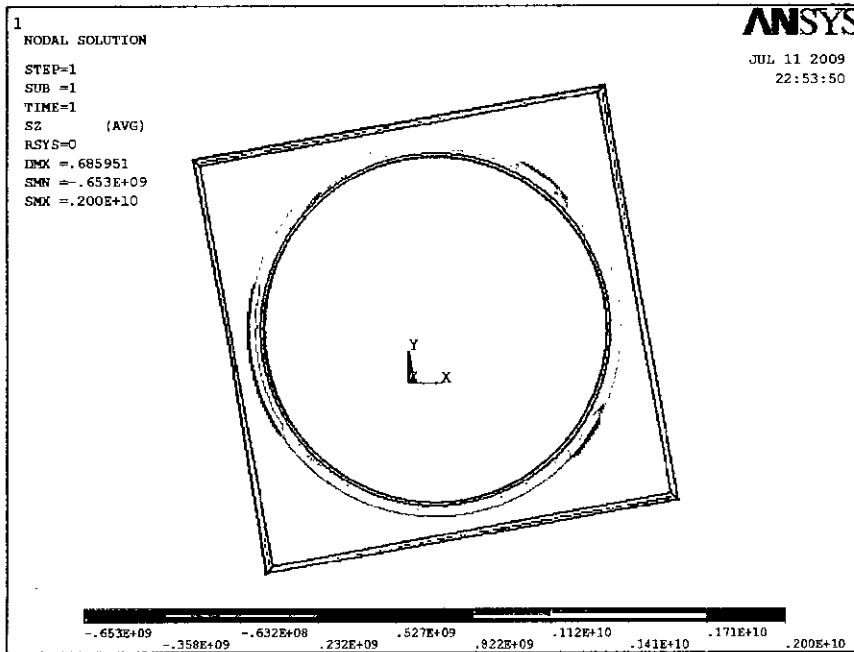


Fig. 4.13: Plot of first principle stress on the cut-plane (for,  $\Delta L = 1$  nm)

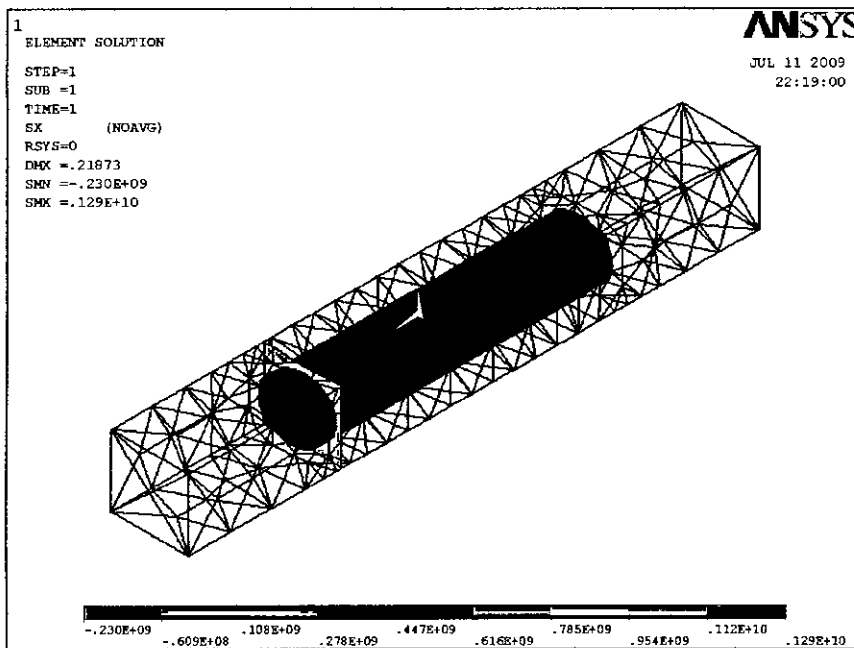


Fig. 4.14: Plot of second principle stress (X-axis) for short single CNT based composite (for,  $\Delta a = 0.3$  nm)

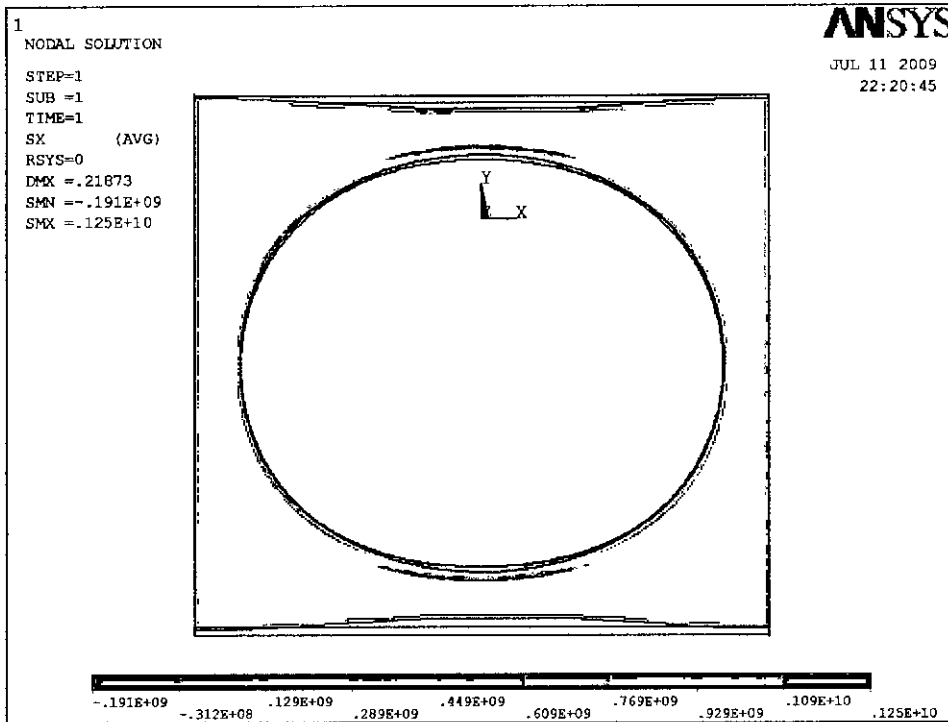


Fig. 4.15: Plot of second principle stress on the cut-plane (for,  $\Delta a = 0.3 \text{ nm}$ )

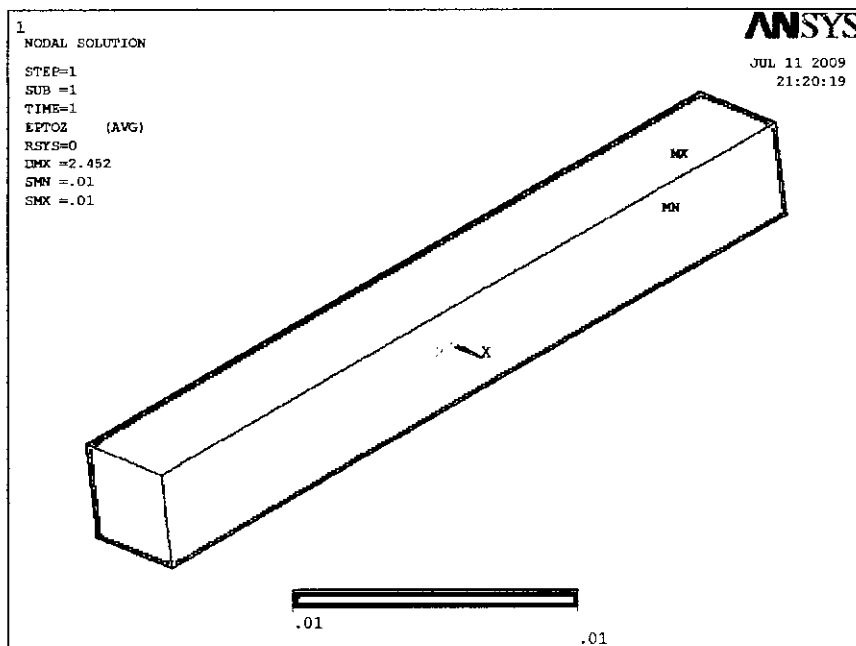


Fig. 4.16: Plot of strain on Z-axis for short single CNT based composite (for,  $\Delta L = 1 \text{ nm}$ )



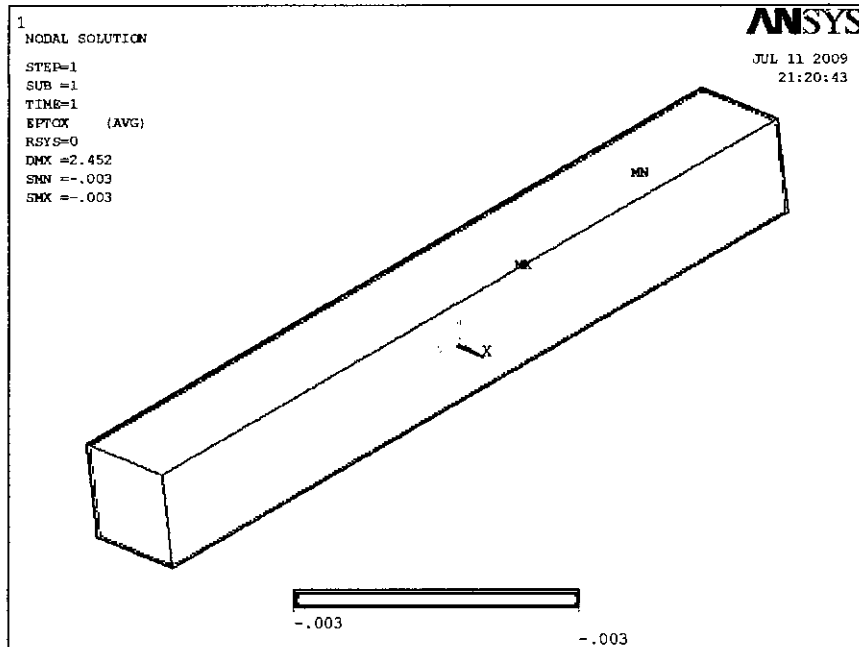


Fig. 4.17: Plot strain on X-axis for short single CNT based composite  
 (for,  $\Delta L = 1 \text{ nm}$ )

#### 4.4.1.2 CNT BUNDLE

The volume fraction of CNT is kept 5% in all the analysis. The CNT chiral indices (50, 50), (80, 80) and (110, 110) are considered for bundle's diameter effect determination. From the Fig. 4.18, 4.19 and 4.20 we can see the effect of the change of CNT bundle diameter on the longitudinal, transverse Young's moduli and on the major Poisson's ratio respectively.

The longitudinal Young's modulus ratio ( $E_z/E_m$ ) for long CNT bundle composite is 10.906 to 10.927 but for short CNT bundle composite it is 1.61 to 1.83. With the increase of CNT bundle diameter the  $E_z/E_m$  decreases for CNT bundle composite. In case of transverse Young's modulus for short CNT-bundle composite the  $E_x/E_m$  is 0.5 but for long CNT-bundle composite it is 0.022 to

0.037. Here with the increase of CNT-bundle diameter the  $E_x/E_m$  decreases for long CNT-bundle composite. As the interface stiffness of CNT-CNT is considered with only vdW interaction, the stiffness is quite low in comparison to CNT or Matrix material (Table 4.5). With the increase of CNT bundle diameter this region increases which results in decrement of composite stiffness.

As the materials of both CNT bundle and matrix are taken isotropic with Poisson's of 0.3, the change of diameter does not have any effect on the major Poisson's ratio of the CNT bundle composite.

During conducting FEM solution, first a cut-plane (cross-sectional area at one end) is selected then all the plots of stress and strain are done on this plane (Fig. 4.21 shows it for long CNT bundle and Fig. 4.24 for short CNT-bundle). The plot of first and second principal stresses and strains for long single CNT bundle composite are shown in Fig. 4.22 and 4.23 and for short CNT bundle composite these are in Fig. 4.25 to 4.27.

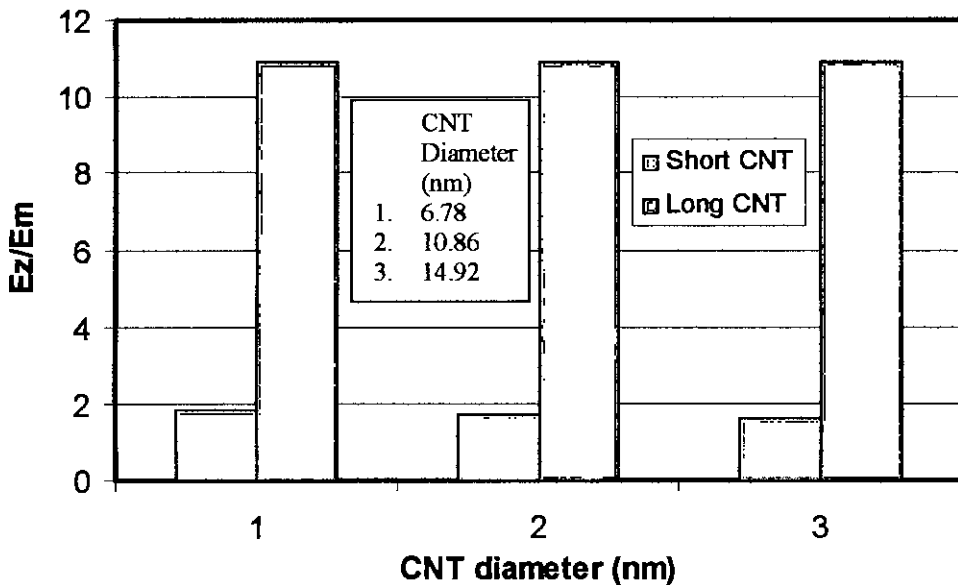


Fig. 4.18:  $E_z/E_m$  versus CNT diameter for CNT bundle composite

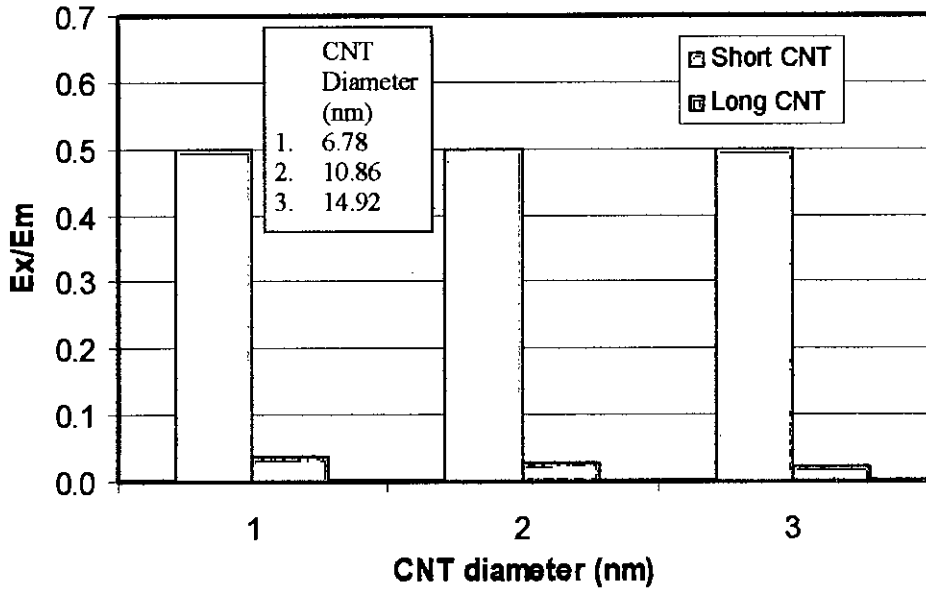


Fig. 4.19:  $E_x/E_m$  versus CNT diameter for CNT bundle composite

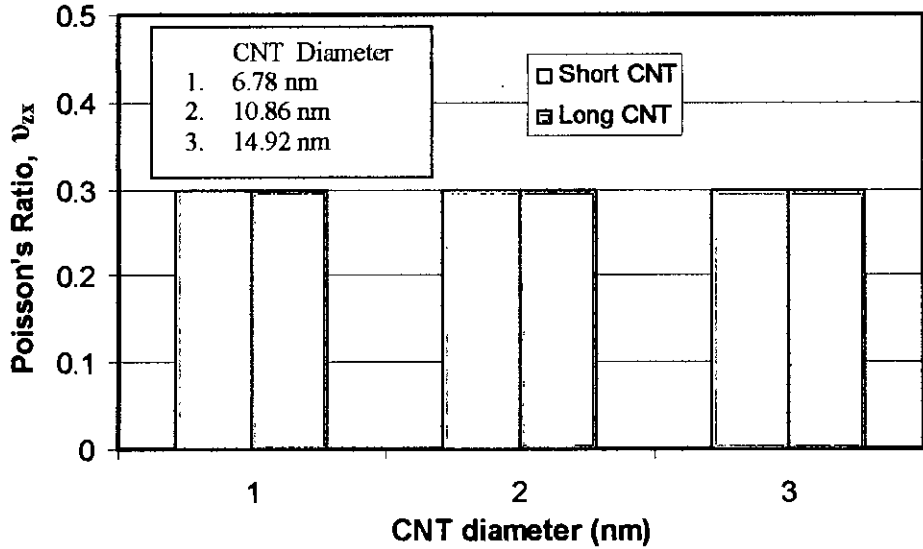


Fig. 4.20: Composite's Poisson's ratio versus CNT diameter for CNT bundle composite

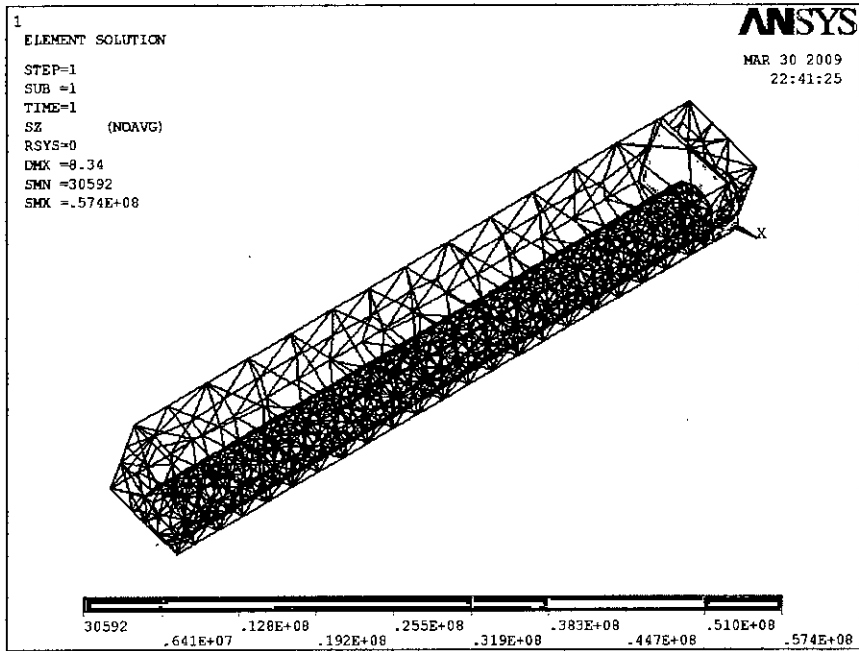


Fig. 4.21: Long CNT bundle composite with cut-plane

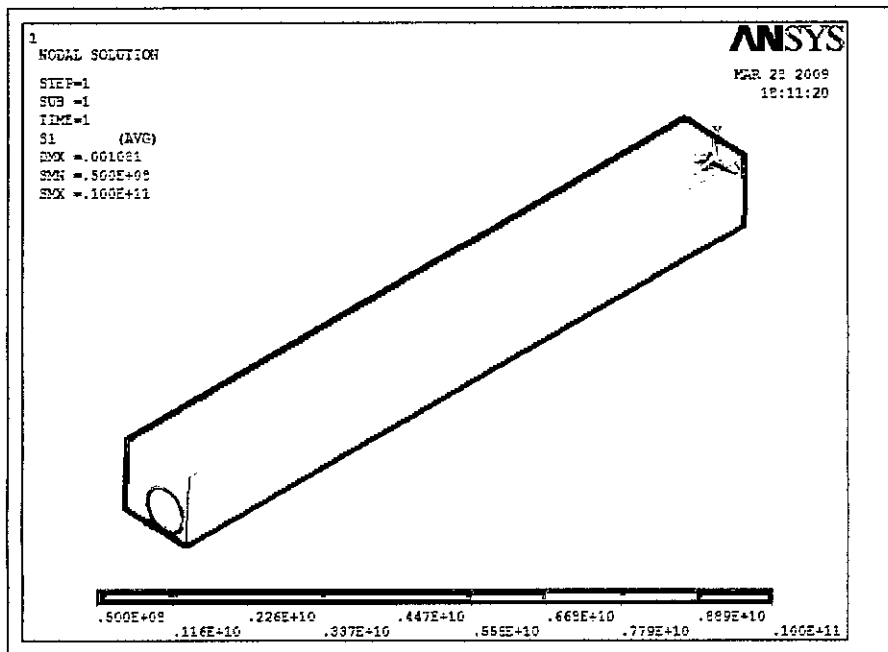


Fig. 4.22: Plot of first principle stress (Z-axis) for long CNT bundle composite  
(for axial stretch,  $\Delta L = 1$  nm)

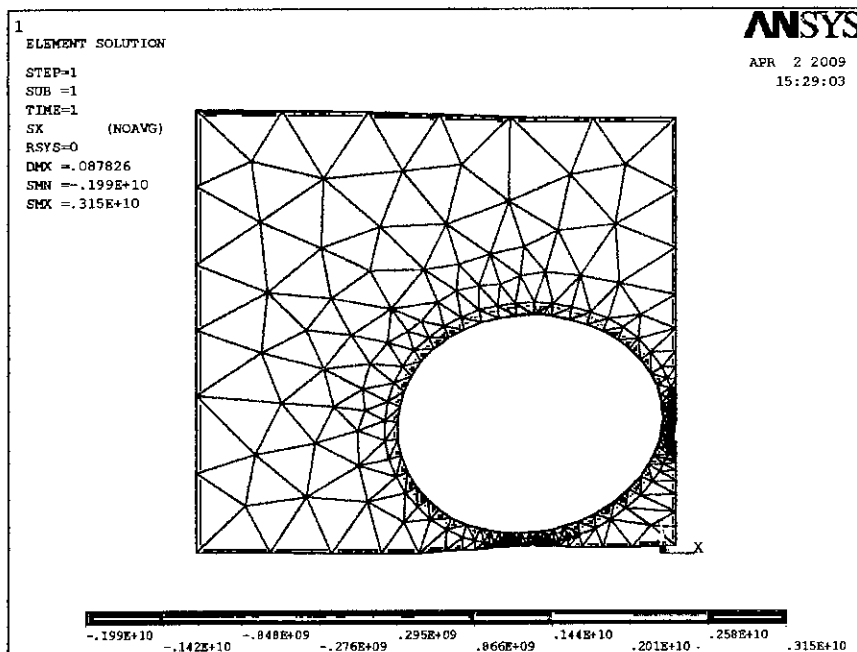


Fig. 4.23: Plot of second principle stress (X-axis) for long CNT bundle composite (for lateral stretch,  $\Delta a = 0.3$  nm)

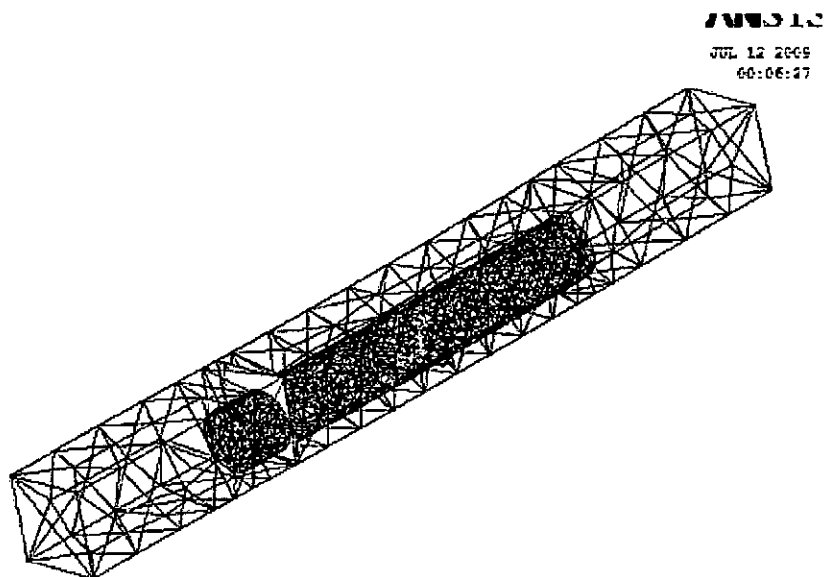


Fig. 4.24: Short CNT bundle composite with cut-plane

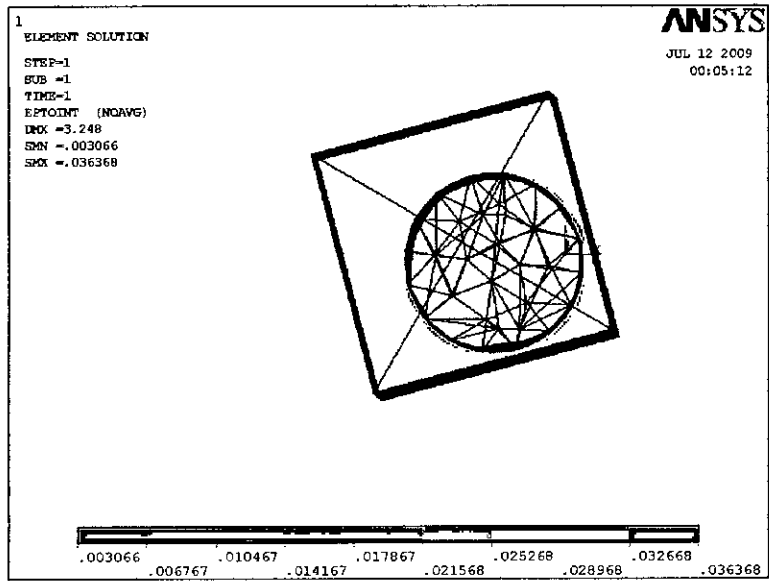


Fig. 4.25: Total strain intensity for short CNT bundle composite (for,  $\Delta L = 1$  nm)

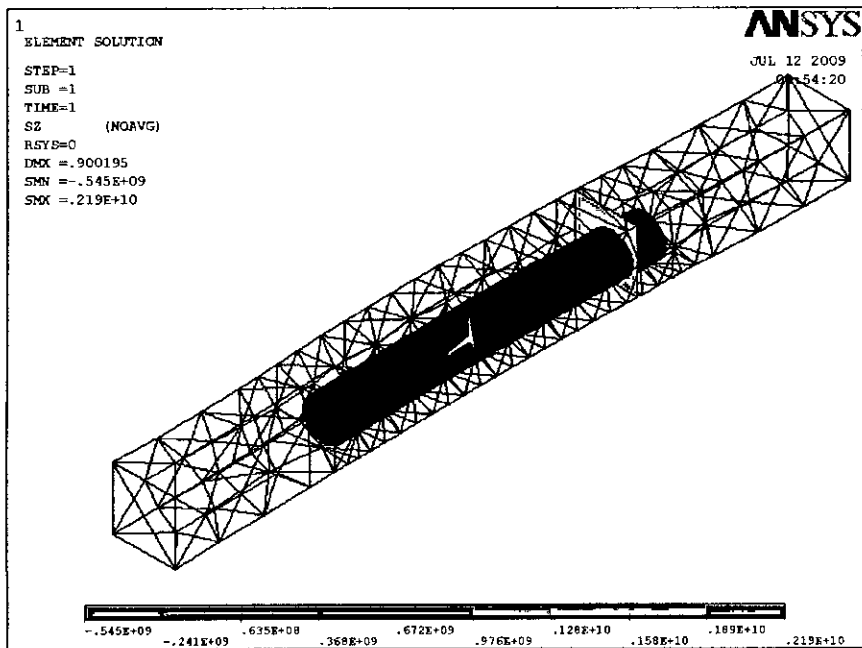


Fig. 4.26: Plot of first principle stress (Z-axis) for short CNT bundle composite (for,  $\Delta L = 1$  nm)

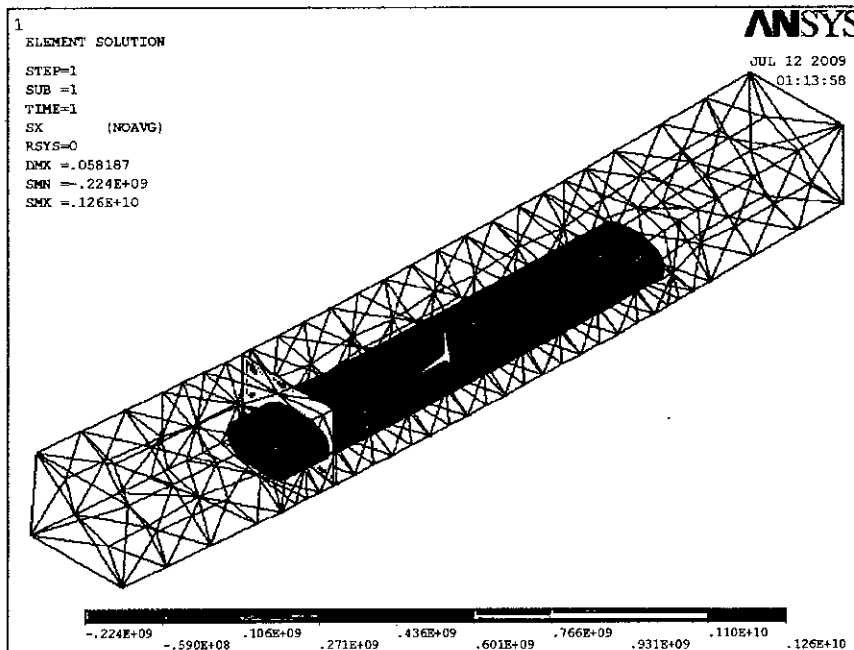


Fig. 4.27: Plot of second principle stress (X-axis) for short CNT bundle composite (for,  $\Delta a = 0.3$  nm)

#### 4.4.2 EFFECT OF CNT LENGTH ON COMPOSITE ELASTIC PROPERTIES

##### 4.4.2.1 SINGLE CNT

The volume fraction of CNT is kept 5% and diameter of the CNT is considered 10.86 nm in all the analysis (both long and short CNT). In case of short CNT consideration the CNT aspect ratio ( $L_c/D$ ) 7.36, 4.61 and 3.35 are considered for length effect determination. From the Fig. 4.28 we can see that for the increase of CNT length, the longitudinal Young's modulus ratio ( $E_z/E_m$ ) for CNT based composite also increases. Even if CNT length increases from 80nm ( $L_c/D = 7.36$ ) to 100 nm (long CNT) the increment of  $E_z/E_m$  is very high (3.54 to 10.94). Thus it indicates that to get better reinforcement the CNTs need to be as long as

possible. In case of transverse Young's modulus, for both long and short CNT based composite the  $E_x/E_m$  is nearly 1 (Fig. 4.29). It indicates that CNT reinforcement in transverse direction is negligible. As the materials of both CNT and matrix are taken isotropic with Poisson's of 0.3, the change of length does not have any effect on the major Poisson's ratio of the CNT based composite (Fig. 4.30).

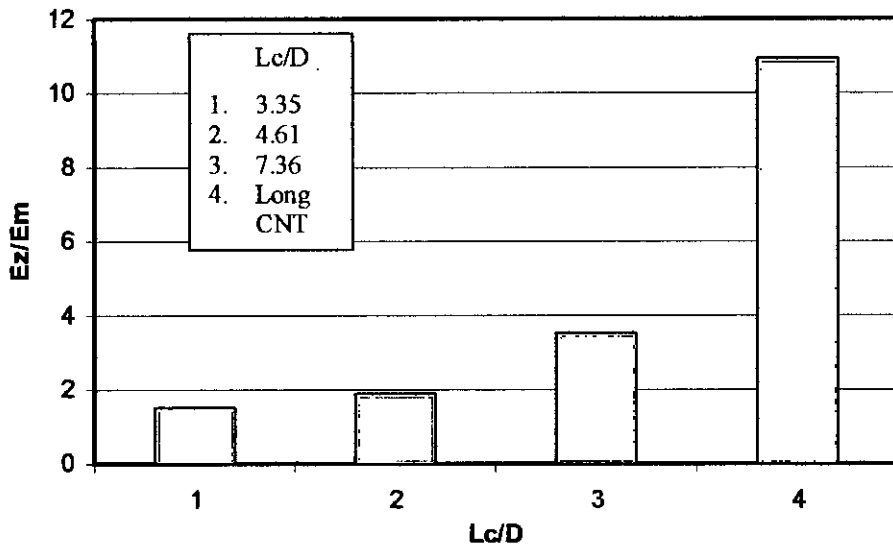


Fig. 4.28:  $E_z/E_m$  versus CNT aspect ratio ( $L_c/D$ ) for single CNT based composite

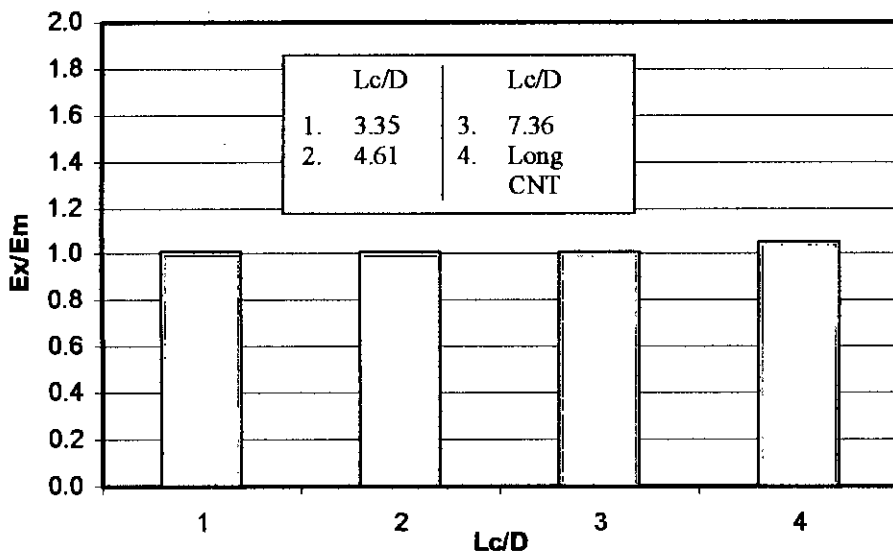


Fig. 4.29:  $E_x/E_m$  versus CNT aspect ratio ( $L_c/D$ ) for single CNT based composite



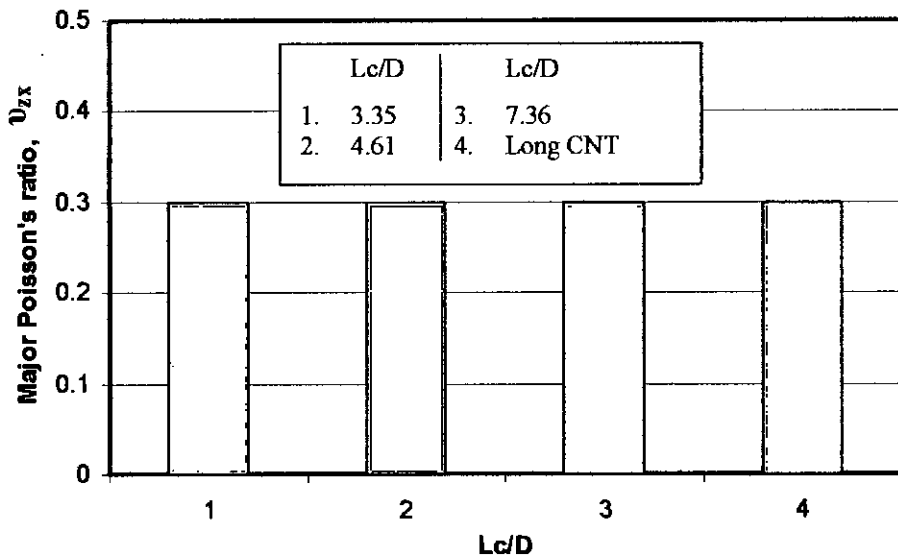


Fig. 4.30: Composite's Poisson's ratio versus CNT aspect ratio ( $Lc/D$ ) for single CNT based composite

#### 4.4.2.2 CNT BUNDLE

The volume fraction of CNT is kept 5% and diameter of the CNT is considered 10.86 nm in all the analysis (for both long and short CNT-bundle). In case of short CNT bundle the CNT aspect ratio ( $Lc/D$ ) of 7.36, 4.61 and 3.35 are considered for length effect determination. From the Fig. 4.31, 4.32 and 4.33 we can see the effect of the change of CNT bundle diameter on the longitudinal and transverse Young's modulus and on the major Poisson's ratio respectively.

The longitudinal Young's modulus ratio ( $E_z/E_m$ ) for long CNT bundle composite is 10.916 but for short CNT bundle composite it is 1.364 to 3.552. Thus with the increment of CNT bundle length better reinforcement is achieved in longitudinal direction.

In case of transverse Young's modulus ratio for short CNT bundle composite the  $E_x/E_m$  is 0.2 to 0.64 but for long CNT-bundle composite it is only 0.027. Here with the increase of CNT bundle length the  $E_x/E_m$  decreases for CNT bundle composite. As the interface stiffness of CNT-CNT is considered with only vdW interaction, the stiffness is quite low in comparison to CNT or matrix material (Table 4.3). With the increase of CNT bundle length this region increases which results in decrement of composite stiffness in transverse direction.

As the materials of both CNT bundle and matrix are taken isotropic with Poisson's of 0.3, the change of length does not have any effect on the major Poisson's ratio of the CNT-bundle composite.

Thus although the stiffness of CNT bundle composite increases in longitudinal direction with the increase of CNT bundle length, it can not be said that the reinforcement is better with the increase of length. As at the same time in the transverse direction, stiffness decreases with the increase of CNT-bundle length.

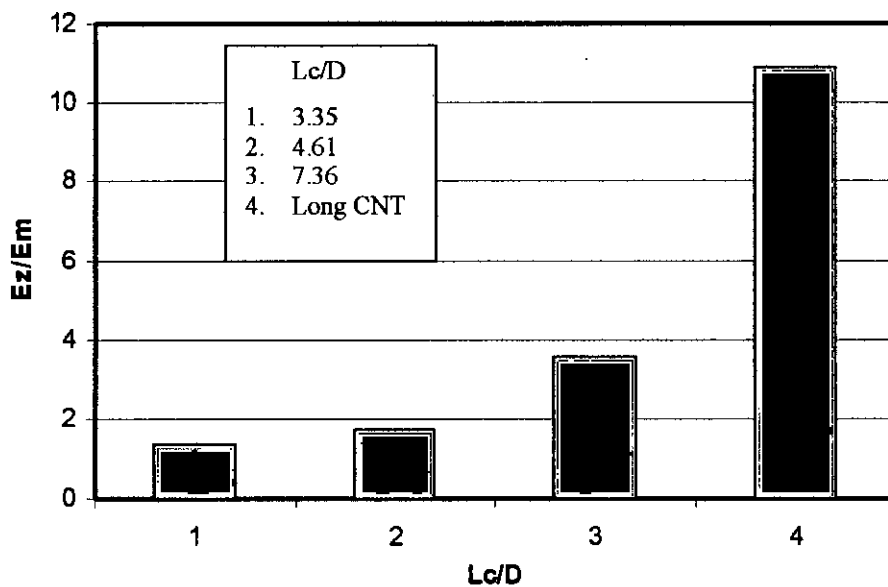


Fig. 4.31:  $E_z/E_m$  versus CNT aspect ratio ( $L_c/D$ ) for CNT bundle based composite

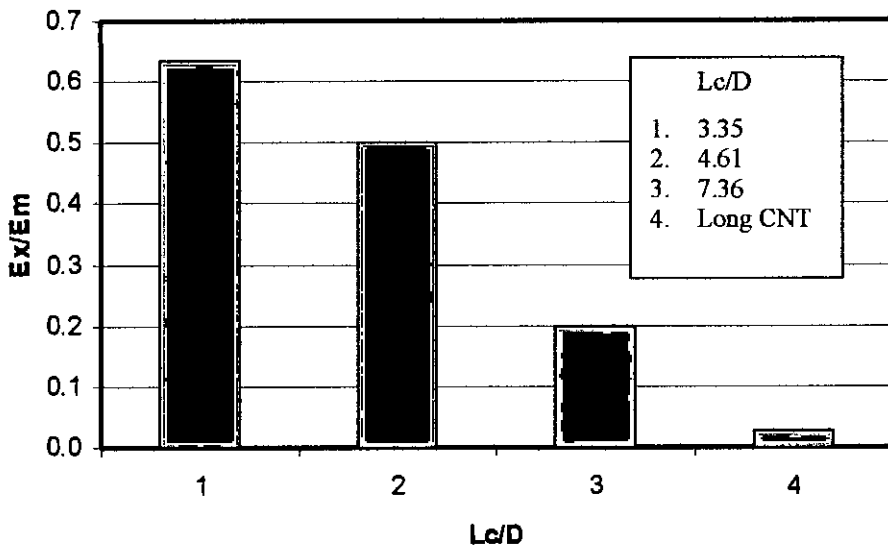


Fig. 4.32:  $E_x/E_m$  versus CNT aspect ratio ( $L_c/D$ ) for CNT bundle based composite

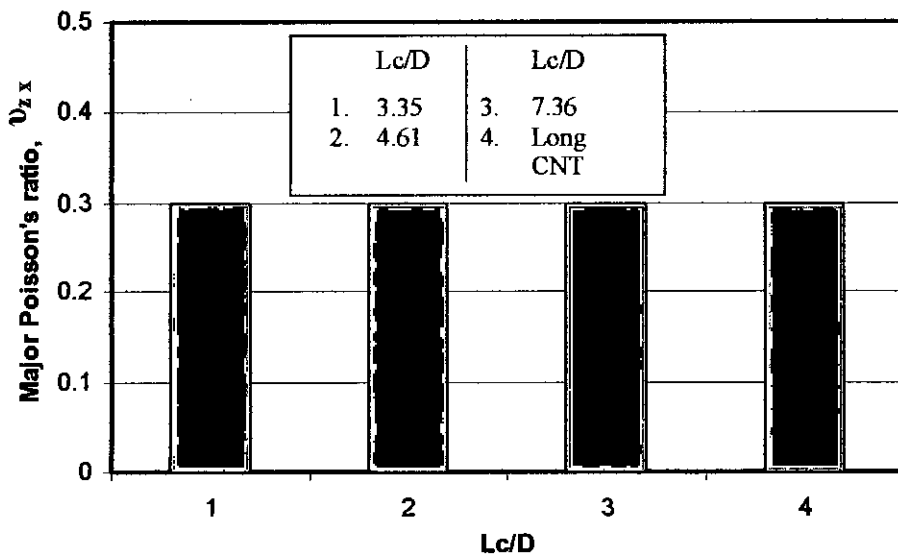


Fig. 4.33: Composite's Poisson's ratio versus CNT aspect ratio ( $L_c/D$ ) for CNT bundle based composite

#### 4.4.3 EFFECT OF CROSS-LINK BETWEEN CNT-CNT IN THE BUNDLE

The stiffness of interface present within the CNT-bundle can be improved by incorporating cross-link among CNT atoms. Addition of cross-link increases the interface stiffness. In the present research the Young's modulus of the interface of CNT-CNT is considered to be 5.35 MPa (only vdW interaction), 50 MPa, 50 MPa, 500 MPa, 50 GPa, 500 GPa and 1 TPa. The volume fraction of CNT is consistently 5% in all the cases.

With the increase of cross-link between CNT-CNT, the longitudinal Young's modulus ratio,  $E_z/E_m$  (Fig. 4.34) increases quite significantly. Effect of cross-link between CNT-CNT for transverse Young's modulus ratio  $E_x/E_m$  (Fig. 4.35) is even higher. As it stiffens the soft interface part which was previously (only vdW interaction) reducing the transverse stiffness of the CNT-bundle composite. For higher bundle diameter (i.e. higher individual CNT radius or diameter) the increment is higher. This is so as the bundle diameter is higher the CNT-CNT interface zone increase comprehensively.

Since the materials of CNT, matrix and CNT-CNT interface are taken isotropic with Poisson's of 0.3, the incorporation of cross-link between two adjacent CNTs does not have any effect on the major Poisson's ratio of the CNT-bundle composite (Fig. 4.36).

Thus the cross-link incorporation between CNT-CNT appreciably increases the stiffness of the CNT bundle based polymer composite.

107290

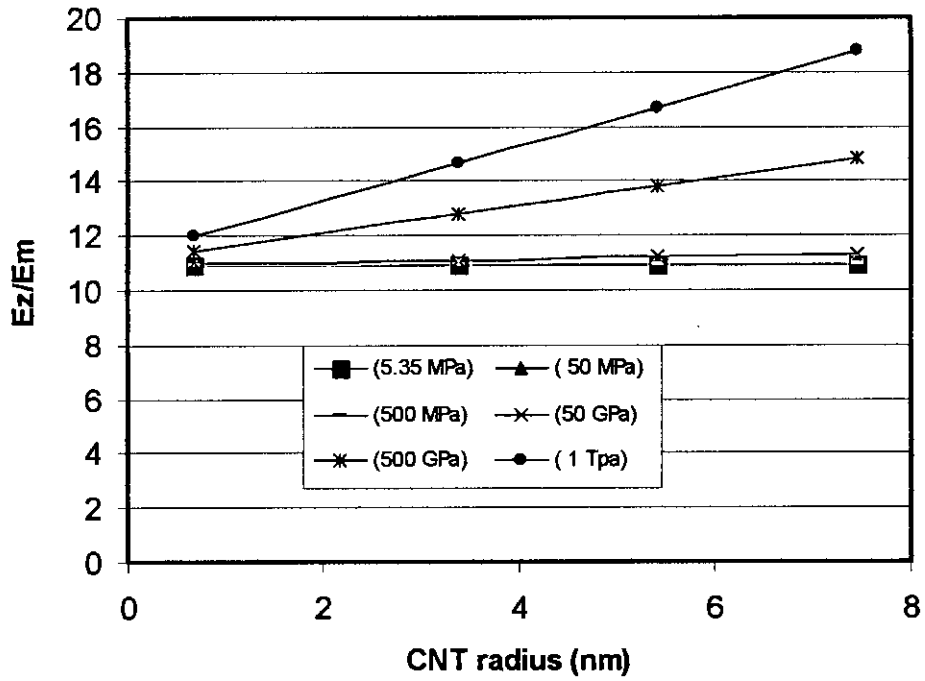


Fig. 4.34:  $E_z/E_m$  versus CNT radius for CNT bundle based composite

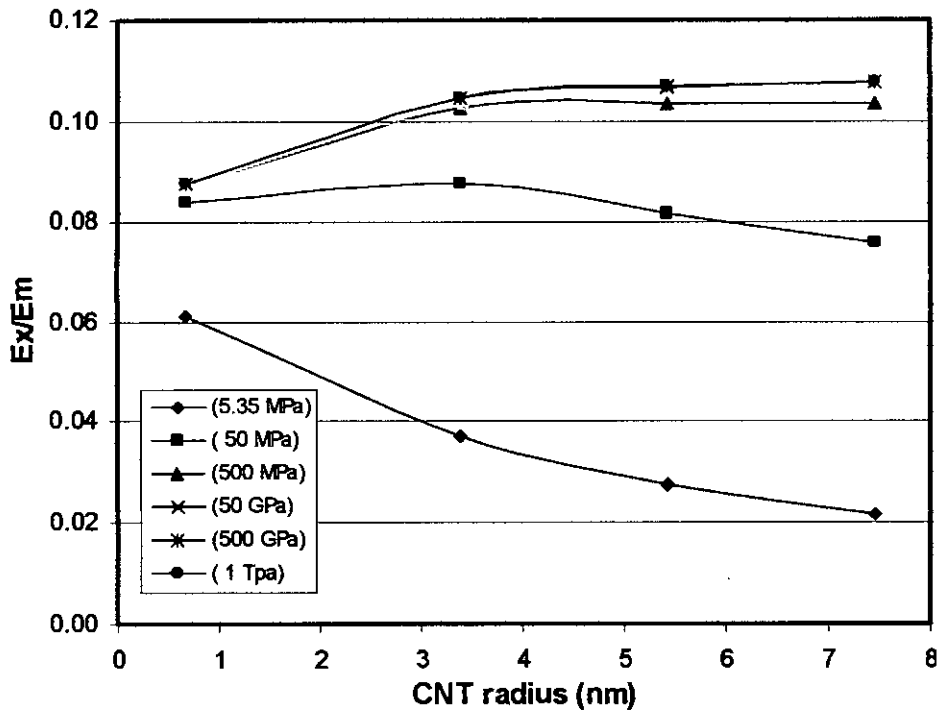


Fig. 4.35:  $E_x/E_m$  versus CNT radius for CNT bundle based composite

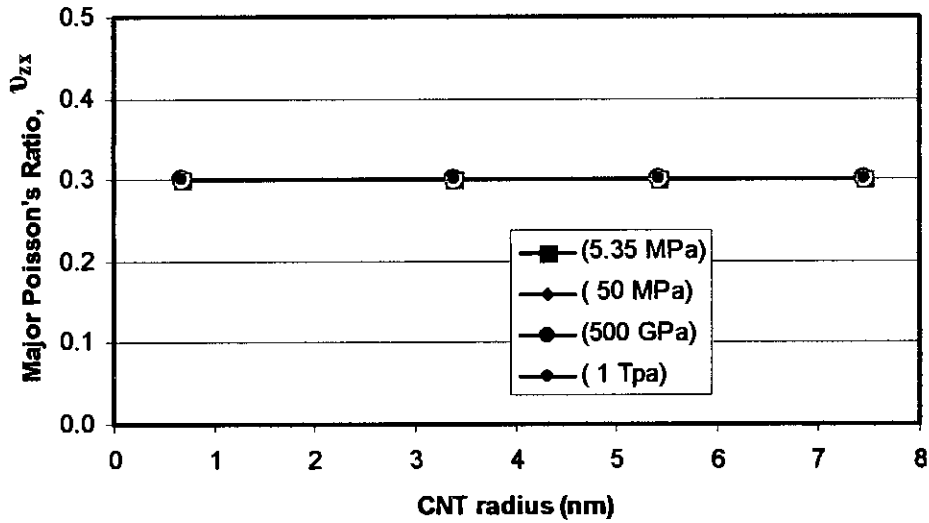


Fig. 4.36: Composite's Poisson's ratio versus CNT radius for CNT bundle based composite

#### 4.4.4 EFFECT OF CROSS-LINK BETWEEN CNT-MATRIX

The stiffness of interface between CNT and matrix can be improved by incorporating cross-link between CNT atom and matrix atom. Addition of cross-link increases the interface stiffness. In the present research the Young's modulus of the interface of CNT-matrix is considered to be 2.7 MPa (only vdW interaction), 27 MPa, 270 MPa and 2.7 GPa. The volume fraction of CNT is consistently 5% in all the cases. Even for the interface with stiffness of 2.7 GPa the longitudinal Young's modulus ratio,  $E_z/E_m$  (Fig. 4.37) increases only 0.02%. As the interface thickness is too low the cross-link effect on longitudinal Young's modulus is negligible. With the increase of cross-link the transverse Young's modulus ratio,  $E_x/E_m$  increases significantly (Fig. 4.38). Though the interface thickness is negligible but by incorporating cross-link it stiffens the soft part; which was previously (with only vdW interaction) reducing the transverse stiffness of the CNT-bundle composite. As all the materials are isotropic with Poisson's ratio of 0.3, the incorporation of cross-link between CNT and matrix

does not have any effect on the major Poisson's ratio of the CNT-bundle composite (Fig. 4.39).

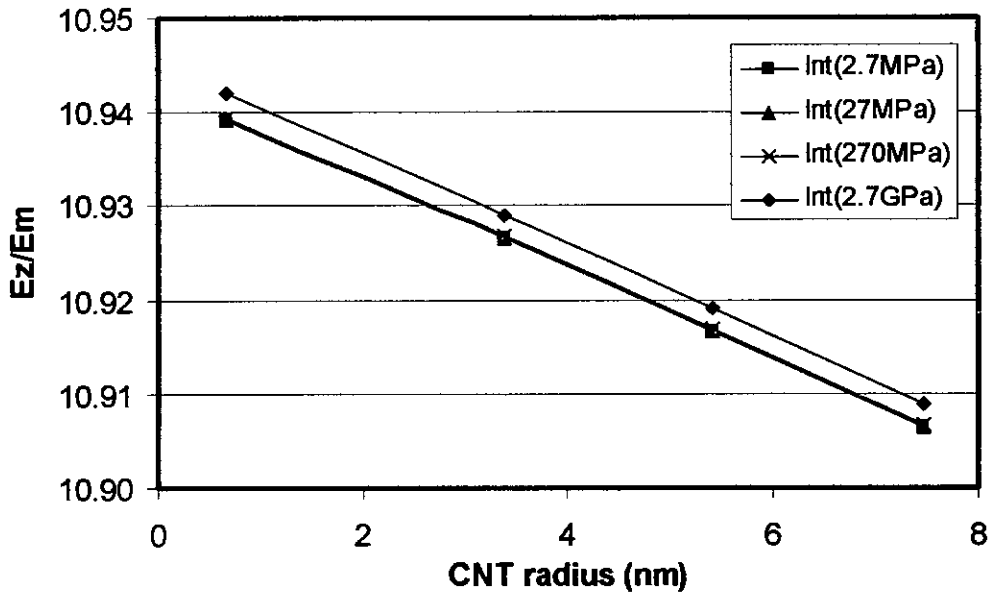


Fig. 4.37:  $E_z/E_m$  versus CNT radius for CNT bundle based composite

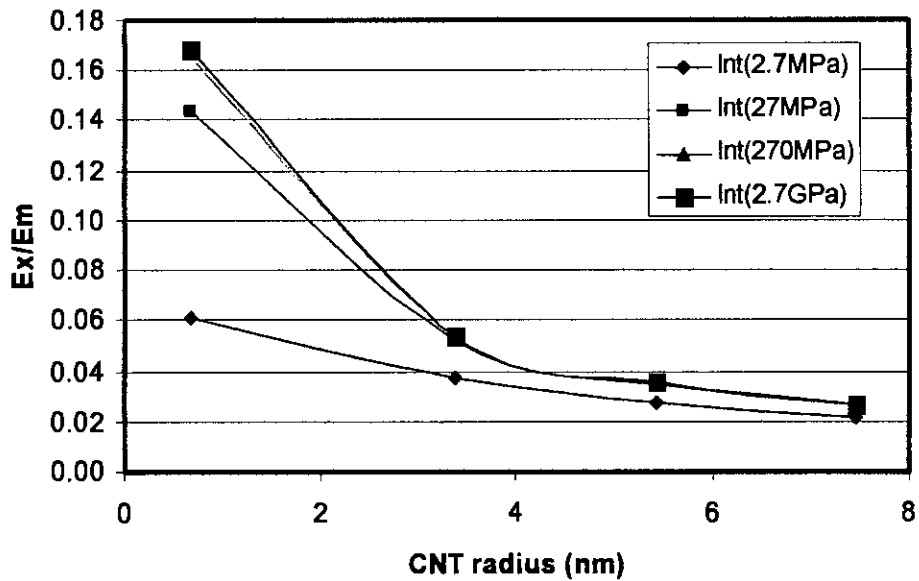


Fig. 4.38:  $E_x/E_m$  versus CNT radius for CNT bundle based composite

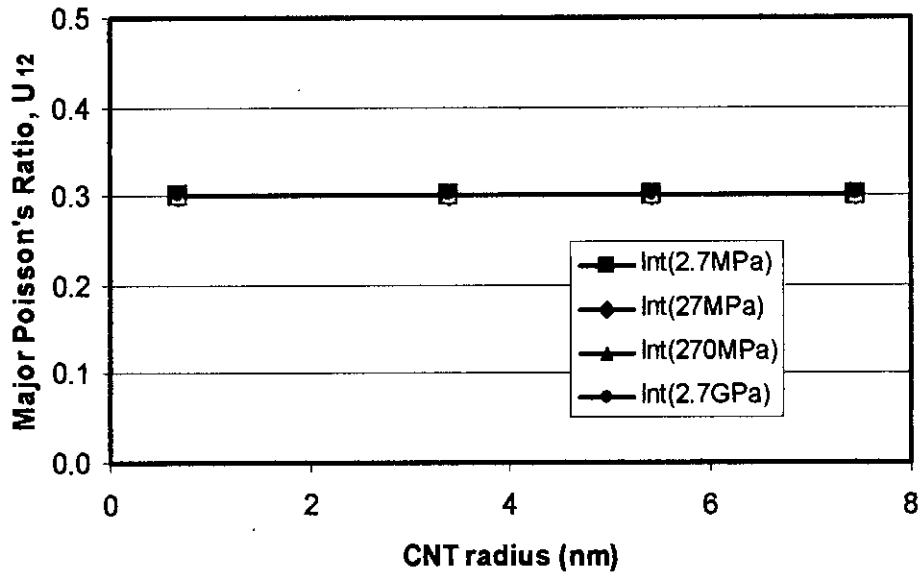


Fig. 4.39: Composite's Poisson's ratio versus CNT radius for CNT bundle based composite

#### 4.5 EQUIVALENT SINGLE SOLID FIBER AS A SUBSTITUTE OF CNT BUNDLE

Equation 3.21 and 3.22 (in chapter 3) are used to calculate the radius and stiffness of the equivalent solid fiber. The comparison of Young's modulus of CNT bundles of four SWNTs and equivalent fiber is shown in Fig. 4.40. In the finite element analysis moduli of matrix and interface are considered 5 GPa and 2.70 MPa respectively, while Poisson's ratio is considered 0.3 for both the matrix and interface. Poisson's ratio of the equivalent solid fiber is considered 0.3 and stiffness of the equivalent fiber is determined from Eq. 3.22.

The variation of longitudinal Young's modulus with fiber diameter is shown in Fig. 4.41 and Fig. 4.42 for long and short fiber respectively. These Figures show that results of equivalent fiber agree well with those of CNT bundle. Here the



RVE is again 100 nm (L) long and cross sectional area (width = 2a) is kept according to the CNT bundle based composite.

But in case of transverse Young's modulus the equivalent solid fiber composite shows much higher stiffness than the CNT bundle composite (Fig. 4.43 and 4.44). This is due to considering the equivalent fiber as an isotropic material.

A typical RVE used in the FEM for evaluating the elastic properties of the equivalent fiber based composite is shown in Fig. 4.45. After axial stretch of 1 nm the stress developed in the RVE is shown in the Fig. 4.46 and 4.47 (cut-plane). It shows uniform stress distribution along the matrix and fiber. The equivalent short solid-fiber composite under axial stretch of 1 nm is shown in Fig. 4.48. It shows that the deformation is maximum in both ends of the RVE and in the mid span it is minimum. The stress developed in the composite is shown in Fig. 4.49 (a & b). It is explicit that the cross section near the end of the short fiber shows more stress concentration (Fig. 4.50). This authenticates the general behavior of short fiber composite.

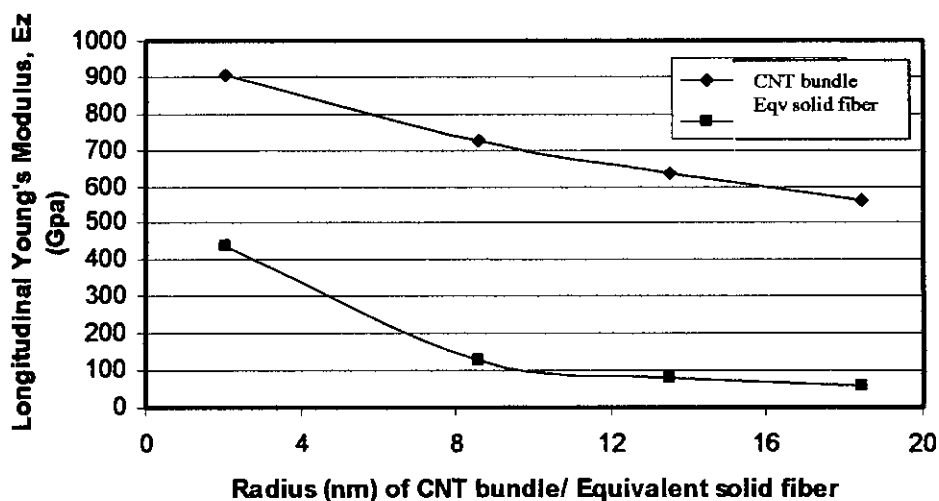


Fig. 4.40: Longitudinal Young's modulus of the CNT bundle and equivalent solid fiber for different radii of them

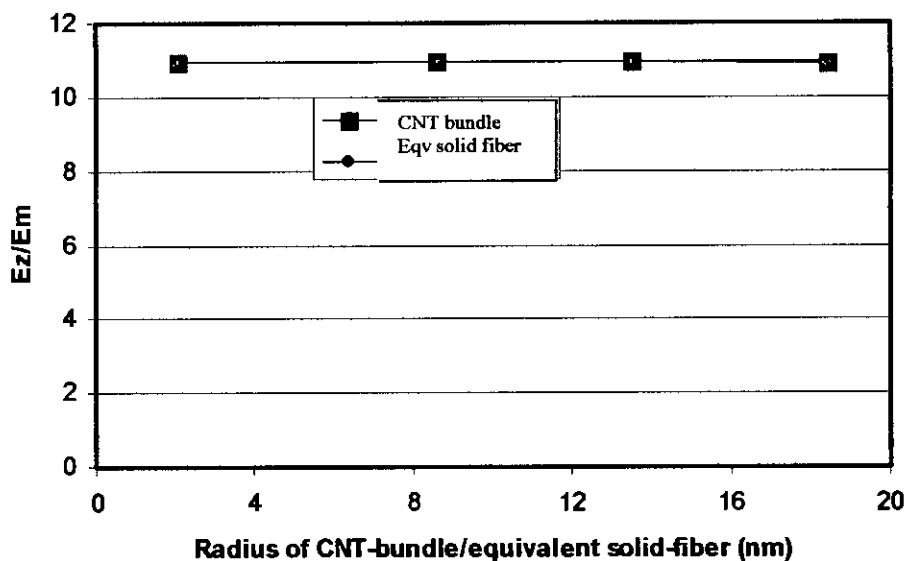


Fig. 4.41: Longitudinal Young's modulus ratio ( $E_z/E_m$ ) of the long CNT bundle composite and equivalent long solid fiber composite for different radii of CNT bundle/ equivalent solid fiber

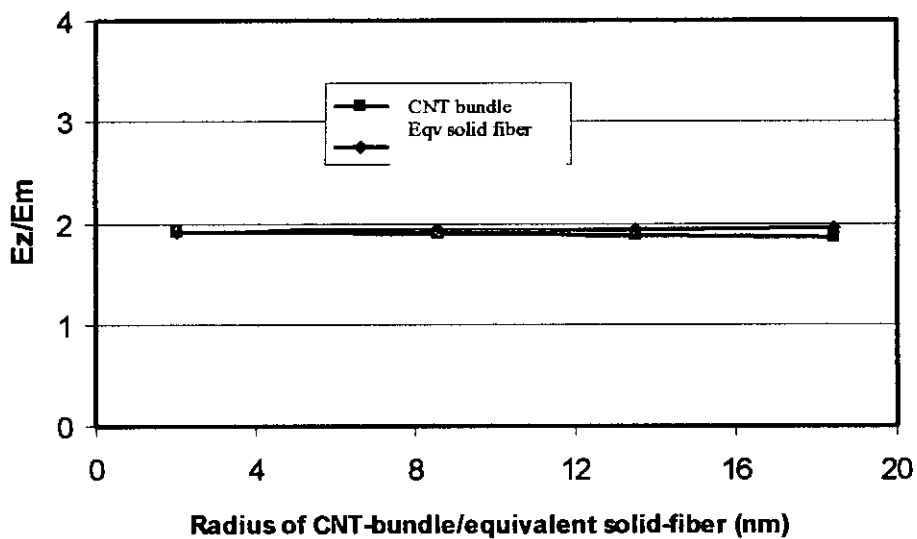


Fig. 4.42: Longitudinal Young's modulus ratio ( $E_z/E_m$ ) of the short CNT bundle composite and equivalent short solid fiber composite for different radii of CNT bundle/ equivalent solid fiber

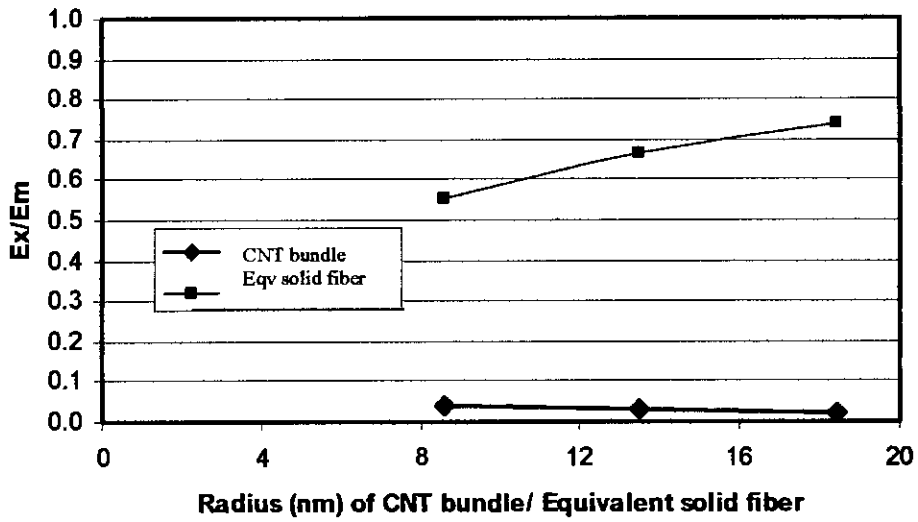


Fig. 4.43: Transverse Young's modulus ratio ( $E_x/E_m$ ) of the long CNT bundle composite and equivalent long solid fiber composite for different radii of CNT bundle/ equivalent solid fiber

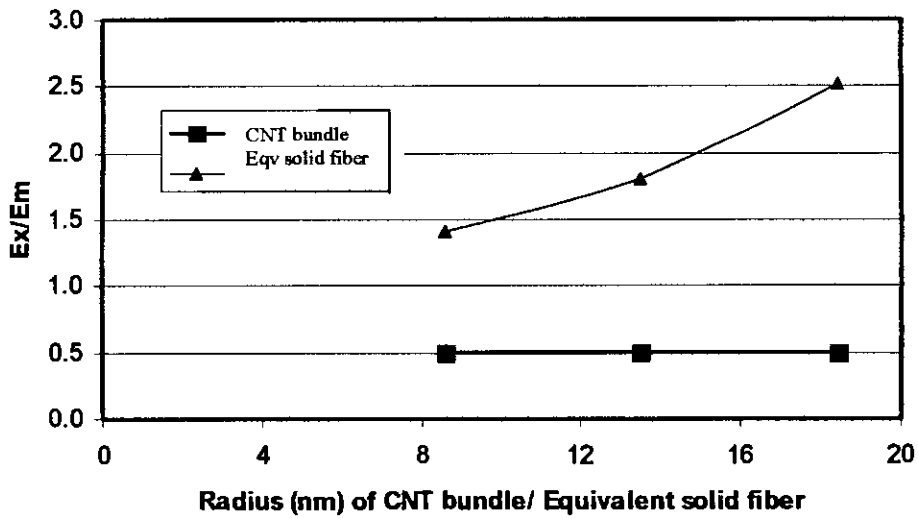


Fig. 4.42: Transverse Young's modulus ratio ( $E_x/E_m$ ) of the short CNT bundle composite and equivalent short solid fiber composite for different radii of CNT bundle/ equivalent solid fiber

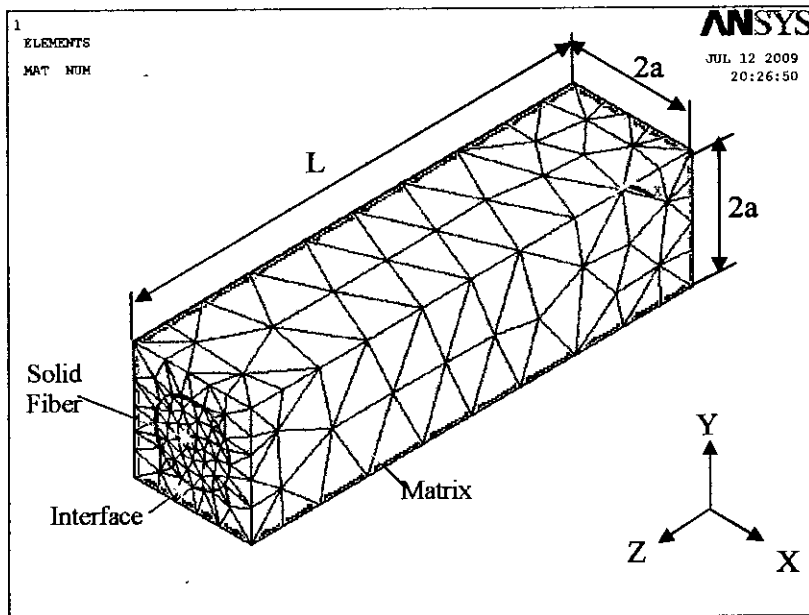


Fig. 4.45: Composite containing a single fiber having equivalent strength of CNT bundle of four

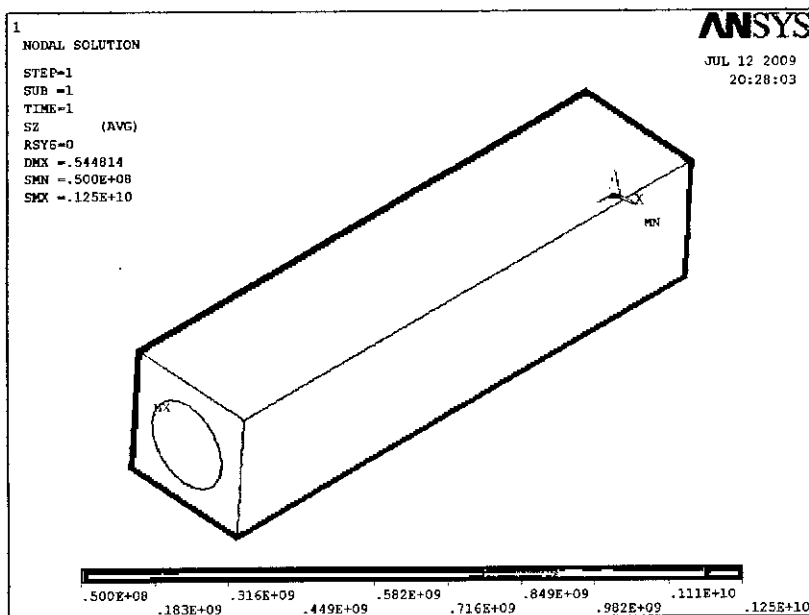


Fig. 4.46: Plot of first principal stress (Z-axis) for long equivalent solid-fiber composite (for axial stretch,  $\Delta L = 1$  nm)

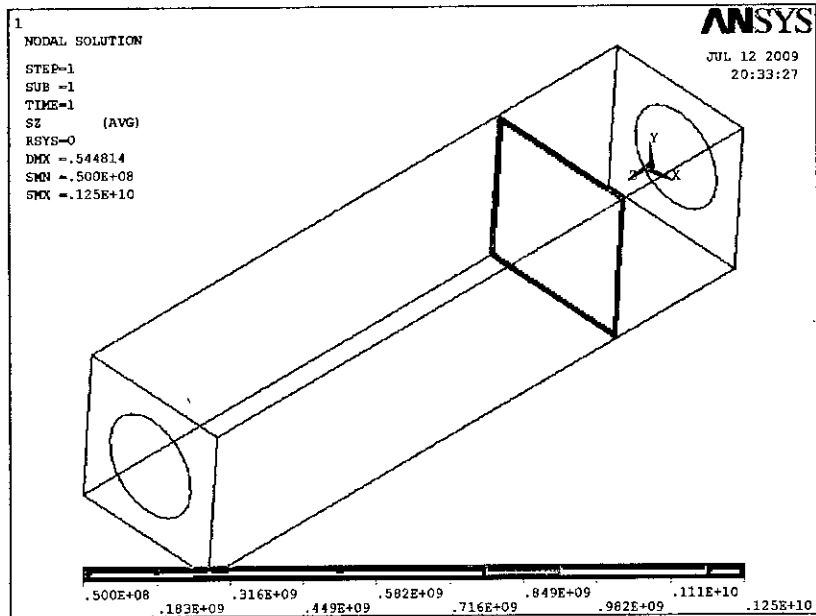


Fig. 4.47: Plot of first principal stress on cut-plane for long fiber composite  
(for,  $\Delta L = 1 \text{ nm}$ )

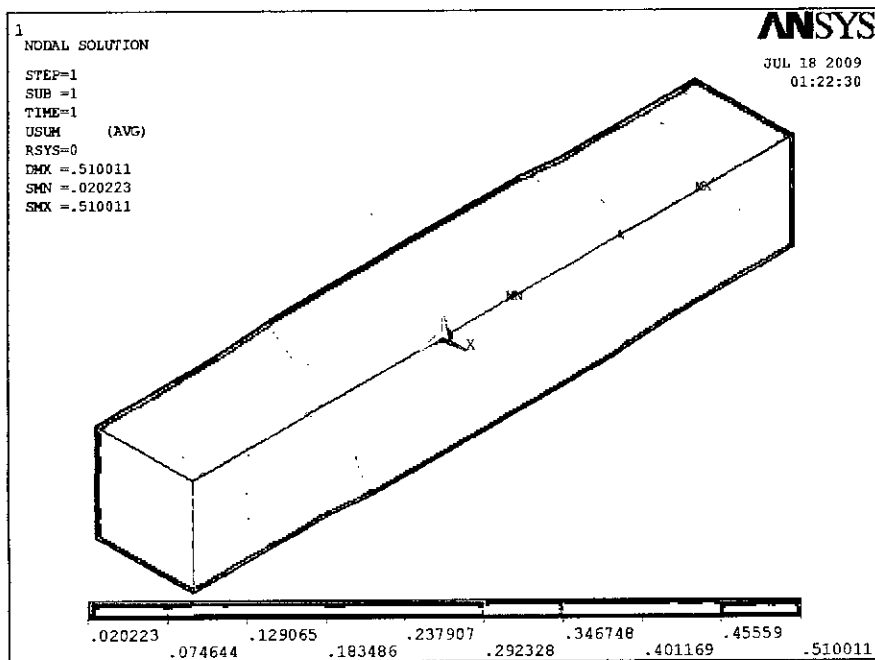


Fig. 4.48: The equivalent short solid-fiber composite under axial stretch of 1 nm  
(i.e.  $\epsilon_z = 0.1$ )

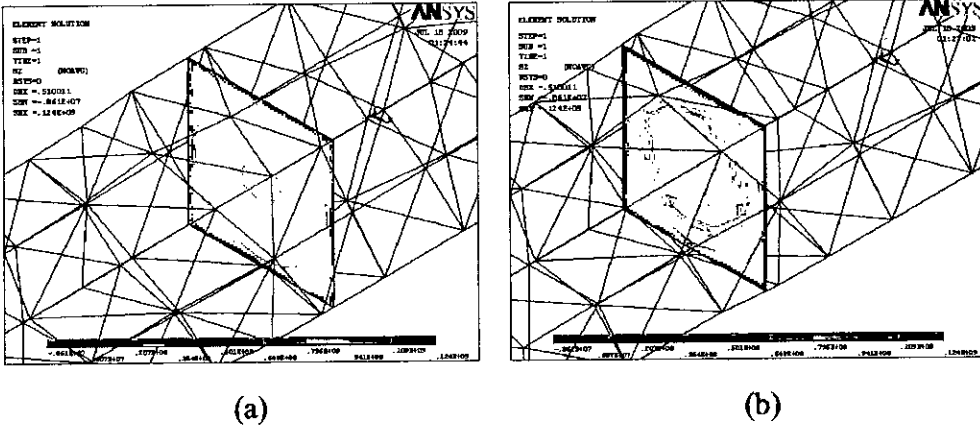


Fig. 4.49: Plot of first principal stress on the cut-plane for The equivalent short solid-fiber composite (for,  $\Delta L = 1$  nm); [(a) The cross section is 15 nm apart from the origin, (b) The section is 24.5 nm apart from the origin]

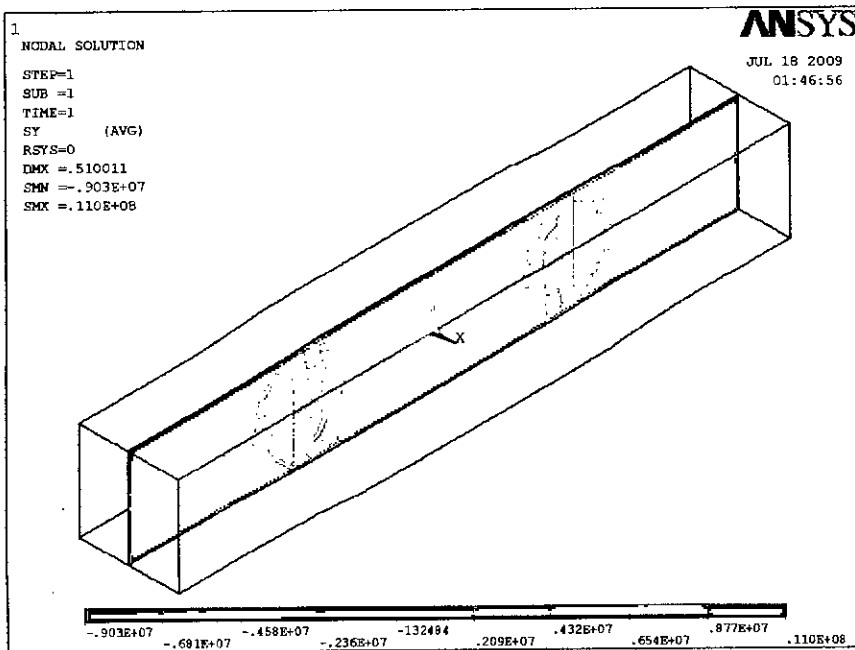


Fig. 4.50: Plot of second principal stress on the cut plane for equivalent solid-fiber composite (for,  $\Delta L = 1$  nm)

## **CHAPTER 05**

---

# **CONCLUSIONS AND RECOMMENDATIONS**

## 5.1 INTRODUCTION

Polymer materials reinforced with CNTs offer potential benefits over traditional reinforcement methods in terms of mechanical behavior. In this research work the effect of the morphology of the CNT bundle on the elastic properties of CNT bundle based composite is investigated. The investigation is done for change of various parameters like bundle diameter, bundle length, bonding between the CNTs within the bundle and bonding (i.e., cross-link) between the bundle and matrix. CNT bundle based polymer composites is studied using representative volume elements (RVEs) by FEM. CNT bundle consisted of four single walled CNTs is considered here. Diameter of the CNT bundle is varied by varying the diameter of the constituent CNTs of the bundle. The diameter is varied according to the CNT chiral indexes of (10, 10), (50, 50), (80, 80) and (110, 110). Regarding the length of the CNT-bundle, both short and long bundles are considered. Short bundle is within the matrix whereas long bundle is through the length of the matrix of the RVE. The cross-link effect is incorporated in this research by changing the interface stiffness between CNT-CNT within the bundle and between CNT-matrix. Then a suitable analytical formula is developed for calculating elastic properties of the composite considering the CNT bundled as an equivalent single solid fiber. In all the above cases CNT volume fraction is considered to be 5%. The results obtained have been discussed in chapter 4. Main findings and recommendations are given in this chapter.

## 5.2 CONCLUSION

The conclusion can be summarized as:

- Change of CNT bundle diameter affects the composite stiffness. With the increase of CNT bundle diameter the longitudinal Young's modulus and transverse Young's modulus of the composite decreases. When the



interface stiffness of CNT-CNT is considered for only van der Waals (vdW) interaction, this stiffness is quite low in comparison to CNT or matrix stiffness. With the increase of CNT bundle diameter this interfacial region increases which results in decrement of composite stiffness. Bundle diameter has no effect on the Poisson's ratio of the CNT bundle based composite.

- Change of CNT bundle length has significant effects on the composite stiffness. The stiffness of CNT bundle based composite increases in longitudinal direction with the increase of CNT bundle length. However, in the transverse direction, composite stiffness decreases with the increase of CNT bundle length. Bundle length has no effect on the Poisson's ratio of the CNT bundle based composite.
- With the increase of cross-link between CNT-CNT within the bundle, the longitudinal Young's modulus increases quite significantly. Effect of cross-link between CNT-CNT on transverse Young's modulus is even higher. This is so as the bundle diameter is higher, the CNT-CNT interface zone increase comprehensively and this interface with higher stiffness strengthens the composite as a whole. However, addition of cross-links between CNT-CNT within the bundle does not have any effect on the Poisson's ratio of the CNT bundle based composite.
- The effect of cross-link between CNT-matrix on longitudinal Young's modulus of the composite is negligible. However, with the increase of cross-link the transverse Young's modulus of the composite increases significantly. Addition of cross-links between CNT-matrix does not have any effect on the Poisson's ratio of the CNT bundle based composite.
- Analytical formula has been developed to determine the elastic properties of the composites considering the CNT bundle as an equivalent single

solid fiber. FEM results with equivalent solid fiber are in well agreement with those obtained for CNT bundle in axial direction. This is due to considering the equivalent fiber as an isotropic material.

### **5.3 RECOMMENDATION**

Many research issues need to be addressed in the modeling and simulations of CNTs in a matrix material for the development of nanocomposites. In the present study, square RVE with CNT bundle consisting of four straight single walled CNTs has been considered. The bundle could be considered with various numbers of CNTs like three, seven. The nanotubes in CNT bundle are usually twisted like ropes. But here for ease of simulation CNTs in the bundle are considered straight. Both long and short CNT bundles are considered to be aligned and equally spaced in the composite. Whereas in practice, they can be irregularly spaced and can also be randomly oriented. These considerations can be done during evaluation of the effective elastic properties of CNT bundle based polymer composite. Finally large multi-scale simulation models for CNT based composites need to be investigated, which can link the models at the nano, micro and macro scales. This can be done with the help of molecular simulation, and experimental work.

## REFERENCES

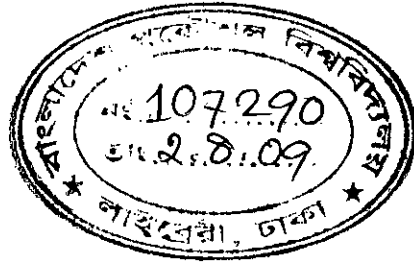
- [1] Kroto H W, Heath J R, O'brien S C, Curl R F, Smalley R E, "C<sub>60</sub>: Buckminsterfullerene", *Nature* 318, 162 (1985).
- [2] Iijima S, "Helical microtubules of graphitic carbon", *Nature* 354, 56 (1991).
- [3] Dresselhaus M S, Dresselhaus G, Avouris P, "Carbon Nanotubes: Synthesis, Structure, Properties and Application", Springer, Berlin, Germany, (2001).
- [4] Nalwa H S, *Handbook of Nanostructured Materials and Nanotechnology*, vol. 5, Academic Press, New York, USA, (2000).
- [5] Schadler L S, Giannaris S C, Ajayan P M, "Load transfer in carbon nanotube epoxy composites", *Applied Physics Letter* 73(26), 3842-4 (1998).
- [6] Dressel M S, Dresselhaus G, Stio R, "Physics of carbon nanotubes", *Carbon* 37(7), 883-891 (1995).
- [7] Thess A, Lee R, Nikolaev P, Dai H, Petit P, Robert J, "Crystalline ropes of metallic carbon nanotubes", *Science* 273, 483-7 (1996).
- [8] Wong E W, Sheehan P E, Liever C M, "Nanobeam mechanics: Elasticity, strength and toughness of nanorods and nano tubes", *Science* 227, 1971-1975 (1997).
- [9] Zhang P, Huang Y, Geubelle P H, Klei P A, Hwang K C, "The elastic modulus of single-wall carbon nanotubes: A continuum analysis incorporating interatomic potentials", *International Journal of Solids and Structures* 39, 3893-3906 (2002).
- [10] Peebles L H, "Carbon Fibers: Formation, Structure and Properties" CRC Press, Boca Raton (1995).
- [11] Baughman R H, Zakhadov A A, Hear W A, "Carbon Nanotubes- the route toward applications", *Science* 297, 787-792 (2002).
- [12] Krishnan A, Dujardin E, Ebbesen T W, Yianilos P N, Treacy M M J, "Young's modulus of single walled nanotubes", *Physical Review B* 58(20), 14013-9 (1998).
- [13] Salvétat J P, Briggs G A D, Bonard J M, Bacsá R R, Kulik A, Stockli, Burnham N A, "Elastic and shear moduli of singlewalled carbon nanotube ropes", *Physical Review Letters* 82(5), 944-7, (1999).

- [14] Thostenson E T, Ren Z, Chou T W, "Advances in the science and technology of carbon nanotubes and their composites: a review", *Composites Science and Technology* 61, 1899-1912 (2001).
- [15] Mintmire J W, Dunlap B I, White C T, "Are fullerene tube metallic?", *Physics Review Letters*, 68, 631-634 (1992).
- [16] Tanaka K, Okahara K, Okada M, Yamabe T, "Electronic properties of bucky-tube model", *Chemical Physics Letters*, 191, 469-472 (1992).
- [17] Hamada N, Sawada S, Oshiyama A, "New one-dimensional conductors: Graphitic microtubules", *Physical Review Letters*, 68, 1579-1581 (1992).
- [18] Iijima S, Brabec C, Maiti A, Bernhole J, "Structural flexibility of carbon nanotubes", *Journal of Physical Chemistry*, 104, 2089-2092 (1996).
- [19] Poulin P, Vigolo B, Launois P, "Films and fibers of oriented single wall nanotubes", *Carbon* 40, 1741-9 (2002).
- [20] Vigolo B, Poulin P, Lucas M, Launois P, Penicaud A, Bernier P, "Improved structure and properties of single-walled carbon nanotube spun fibers", *Applied Physics Letter* 81,1210-2 (2002).
- [21] Vigolo B, Penicaud A, Coulon C, Sauder C, Pailler R, Journet C, "Macroscopic fibers and ribbons of oriented carbon nanotubes", *Science* 290, 331-4 (2000).
- [22] Zhu H W, Xu C L, Wu D H, Wei B Q, Vajtai R, Ajayan P M, "Direct synthesis of long single-walled carbon nanotube strands", *Science* 296, 884-6 (2002).
- [23] Rubaiyat S N, "Study of carbon nanotubes with defects under tensile and compressive loads using molecular dynamics simulation", MS Thesis, March (2009).
- [24] Qian D, Wagner G J, Liu W K, Yu M F, Ruoff R S, "Mechanics of carbon nanotubes", *Applied Mechanical Review* 55, 495-533 (2002).
- [25] Qian D, Dickey E C, Andrews R, Rantell T, "Load transfer and deformation mechanism in carbon nanotube-polystyrene composites", *Applied Physics Letter* 76, 2868-2870 (2000).
- [26] Wagner H D, Lourie O, Feldman Y, Tenne R, "Stress-induced fragmentation of multi-walled carbon nanotubes in a polymer matrix", *Applied Physics Letter* 72(2), 188-190 (1998).

- [27] Cooper C A, Cohen S R, Barber A H, Wagner H D, "Detachment of nanotubes from a polymer matrix", *Applied Physics Letter* 80, 3873-5 (2002).
- [28] Berber A H, Cohen S R, Wagner H D, "Measurement of carbon nanotube-polymer interfacial strength", *Applied Physics Letter* 82, 4140-2 (2003).
- [29] Schadler L S, Giannaris S C, Ajayan P M, "Load transfer in carbon nanotube epoxy composites", *Applied Physics Letter* 73(26), 3842-44 (1998).
- [30] Berber A H, Cohen S R, Kenig S, Wagner H D, "Interfacial fracture energy measurements for multi-walled carbon nanotubes pulled from a polymer matrix", *Composite Science and Technology* 64(14), 2283-2289 (2004).
- [31] Frankland S J V, Harik V M, Odegard G M, Brenner D W, T S Gates, "The stress-strain behavior of polymer-nanotube composites from molecular dynamics simulation", *Composite Science and Technology*, 63, 1655-1661 (2003).
- [32] Griebel M, Hamaeders J, "Molecular dynamics simulations of the elastic moduli of polymer carbon nanotube composites", *Computational Method: Applied Mechanics Engineering* 193, 1773- 1788 (2004).
- [33] Chowdhury S C, Okabe T, "Computer simulation of carbon nanotube pull-out from Polymer by molecular dynamics method", *Composites: Part A* 38, 747-754 (2007).
- [34] Odegard G M, Gates T S, Wise K E, Park C, Siochi E J, "Constitutive modeling of nanotube-reinforced polymer composites", *Composite Science and Technology* 63, 1671-87 (2003).
- [35] Berhan L, Yi Y B, Sastry A M, Munoz E, Selvidge M, Baughman R J, "Mechanical properties of nanotube sheets: Alterations in joint morphology and achievable moduli in manufacturable materials", *Applied Physics* 95(8), 4335-45 (2004).
- [36] Chen X L, Liu Y J, "Square representative volume elements for evaluating the effective material properties of carbon nanotube-based composite", *Computational Materials Science*, 29, 1-11, (2004).
- [37] Lourie O, Wagner H D, "Transmission electron microscopy observation of fracture of single-wall carbon nanotubes under axial tension", *Applied Physics Letter* 73(24), 3527-3529 (1998).

- [38] Ajayan P M, Schadler L S, Giannaris S C, Rubio A, "Single-walled carbon nanotube-polymer composites: strength and weakness", *Advanced Materials* 12(10), 750-753 (2000).
- [39] Ashrafi B, Hubert P, "Modeling the elastic properties of carbon nanotube array/polymer composites", *Composite Science and Technology* 66, 387-396 (2006).
- [40] Thostenson E T and Tsu-Wei Chou, "On the elastic properties of carbon nanotube-based composite: modeling and characterization", *Applied Physics*, 36, 573-582 (2003).
- [41] Kaw K A, "Mechanics of Composite Materials", CRC Press (1997).
- [42] Pipes B R, Frankland S J V, Hubert P, Saether E, "Self-consistent properties of carbon nanotubes and hexagonal arrays as composite reinforcements", *Composites Science and Technology*, 63, 1349-1358 (2003).
- [43] Lau K T, Shi S Q, "Failure mechanisms of carbon nanotube/ epoxy composites pre-treated in different temperature environments", *Carbon* 40, 2965-8 (2002).
- [44] Liao K, Li S, "Interfacial characteristics of a carbon nanotube-polystyrene composite system", *Applied Physics Letter*, 79, 4255-7 (2001).
- [45] Jiang L Y, Huang Y, Jiang H, Ravichandran G, Gao H, Hwang K C, "A cohesive law for carbon nanotube/polymer interfaces based on the vander Waals force", *Mechanical Physics Solids* 54, 2436-52 (2006).
- [46] Kis A, Csányi G, Salvétat J P, Lee T N, Couteaul E, Kulik A J, Benoit W, Brugger J, Forró L, "Reinforcement of single-walled carbon nanotube bundles by intertube bridging", *Nature Materials* 3, 1038-1076 (2004).

## APPENDIX



### Van-der Waals Interaction

Van der Waals (vdW) forces include attractions between atoms, molecules, and surfaces. They differ from covalent and ionic bonding in that they are caused by correlations in the fluctuating polarizations of nearby particles (a consequence of quantum dynamics).

The Lennard-Jones (LJ) potential is often used as an approximate model for the isotropic part of a total (repulsion plus attraction) vdW force as a function of distance. The energy between two atoms of distance  $r$  due to the vdW force can be represented by the following equation.

$$V(r) = 4\epsilon \left[ \left( \frac{\sigma}{r} \right)^{12} - \left( \frac{\sigma}{r} \right)^6 \right]$$

The interaction energy ( $V$ ) is a function of distance ( $r$ ) between two atoms (shown in following figure). Here the parameters  $\epsilon$  and  $\sigma$  depends on atoms under interaction.

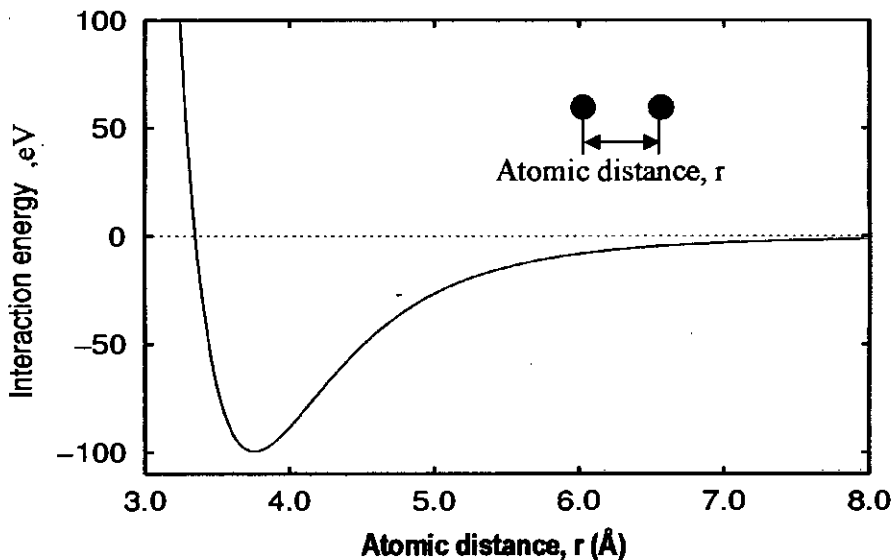


Fig. A.1: Interaction energy versus atomic distance